

Politecnico di Milano

SCHOOL OF INDUSTRIAL AND INFORMATION ENGINEERING
Master of Science – Aerospace Engineering



Thesis Title

Supervisor

Title Name SURMANE

Co-Supervisor

Title Name SURNAME

Candidate
Claudio CACCIA – 820091

Acknowledgements

Thanks

Abstract

This thesis describes bla bla...

Keywords— one, two, three, four

Sommario

In questa tesi bla bla...

Contents

Acknowledgements	iii
Abstract	v
Sommario	vii
Contents	xi
List of Figures	xiv
List of Tables	xv
Listing	xvii
1 Introduction	1
2 Physical aspects of Fluid-Structure Interaction problems	3
2.1 Description of motion	3
2.1.1 Eulerian perspective	3
2.1.2 Lagrangian perspective	4
2.1.3 ALE method	5
2.2 Domains and interface	6
2.2.1 Fluid domain	6
2.2.2 Solid domain	7
2.2.3 Models with reduced dimensionality: beams	8
2.2.4 Interface and interaction	9
2.3 Classification of FSI problems	10
2.3.1 Dimensional analysis	10
2.3.2 Dimensional analysis in fluid domain	11
2.3.3 Dimensional analysis in solid domain	12
2.3.4 Dimensional analysis of coupled problems	12
3 Computational aspects of Fluid-Structure Interaction problems	15
3.1 Monolithic and Partitioned Approach	15
3.2 Coupling Strategies	17
3.2.1 Explicit coupling schemes	17
3.2.2 Implicit coupling schemes	18
3.3 Strong coupling algorithms	20
3.3.1 under-relaxation	20
3.3.2 Quasi-Newton Least Squares schemes	21
3.3.3 Convergence criteria	22

3.4	Interface Mesh and Data Mapping	23
3.4.1	Non-conforming Mesh methods	23
3.4.2	Conforming Mesh methods	24
3.4.3	Data Mapping	24
3.5	Stability: Added Mass Effect	26
3.5.1	AME in compressible regime	26
3.5.2	AME in incompressible regime	26
4	Software Packages used in this work	29
4.1	MBDyn	29
4.1.1	Basic syntax	30
4.1.2	Nodes	31
4.1.3	Elements	31
4.1.4	Beam elements	31
4.1.5	Bodies	33
4.1.6	Joints	33
4.1.7	Forces	33
4.1.8	Simulation output	35
4.2	preCICE	35
4.2.1	Implemented coupling strategies	36
4.2.2	Communication strategies	36
4.2.3	Data mapping	37
4.2.4	Configuration	37
4.2.5	Application Program Interface	38
4.2.6	Official Adapters	38
5	MBDyn Adapter and its integration	39
5.1	Design of the adapter structure	39
5.2	Structure of the code	39
5.2.1	Class MBDynAdapter	41
5.2.2	Class MBDynConnector	43
5.3	Input parameters	44
5.4	Output results	45
6	Validation Test Cases	47
6.1	Introduction	47
6.2	Dummy fluid solver	48
6.3	Vertical flap: incompressible regime	50
6.3.1	Fluid domain	50
6.3.2	Simulation and Coupling parameters	50
6.3.3	Structural Solver: CalculiX	51
6.3.4	Implementation with MBDyn	51
6.3.5	Results	52
6.4	Vertical flap: compressible regime	58
6.4.1	Fluid domain	58
6.4.2	MBDyn model	59
6.4.3	Coupling parameters	59
6.4.4	Results	60
6.5	Square bluff body Benchmark	64
6.5.1	Problem description	64

6.5.2	Fluid domain	64
6.5.3	Solid domain	65
6.5.4	Coupling parameters	66
6.5.5	Results	67
6.5.6	Validation	69
6.6	Turek-Hron FSI2 Benchmark	72
6.6.1	Problem Description	72
6.6.2	Fluid domain	72
6.6.3	Solid domain	73
6.6.4	Coupling parameters	74
6.6.5	Results	74
6.6.6	Validation	75
6.7	Turek-Hron FSI3 Benchmark	81
6.8	Sensitivity analysis of FSI1-FSI3 Benchmarks	82
6.8.1	FSI3 sensitivity Analysis	83
6.8.2	FSI1 sensitivity Analysis	83
6.8.3	Sensitivity Analysis at higher velocity	84
6.8.4	Conclusions	84
7	Conclusions	85
A	preCICE configuration file	87
B	MBDyn adapter configuration file	89
C	preCICE API	91
C.1	preCICE API calls	91
C.2	preCICE adapter structure	92
D	MBDyn input/output file example	95
D.1	MBDyn input file	95
D.2	MBDyn output file structure	103
Acronyms		107
Bibliography		113

List of Figures

Figure 2.1	Eulerian perspective	4
Figure 2.2	Lagrangian perspective	4
Figure 2.3	ALE perspective	5
Figure 2.4	ALE mesh	6
Figure 2.5	beam model, taken from [1]	9
Figure 2.6	fluid solid interface	9
Figure 3.1	monolithic approach: S_f , S_s denote the fluid and the structure solutions	16
Figure 3.2	partitioned approach: S_f , S_s denote the fluid and the structure solutions, while σ and \vec{v} represent coupling data	16
Figure 3.3	Explicit coupling schemes	18
Figure 3.4	Implicit coupling schemes	19
Figure 3.5	non conforming mesh example	23
Figure 3.6	conforming mesh example	24
Figure 3.7	Examples of mapping data between non-coincident meshes: consistent (a) and conservative (b) schemes	25
Figure 4.1	MBDyn beam model, taken from the input manual	32
Figure 5.1	Coupling CFD to CSM via preCICE. The existing solver code, the adapter and the linked library are highlighted (image taken from [2]).	39
Figure 5.2	MBDyn adapter class structure	40
Figure 5.3	Coefficient applied to nodal forces at beginning of simulation	45
Figure 5.4	Output data in VTU format	46
Figure 6.1	cantilever made of 5 beam elements	48
Figure 6.2	body element attached to node 2 of the beam element	49
Figure 6.3	interface points mesh	49
Figure 6.4	model and data exchange test-cases	49
Figure 6.5	vertical flap: fluid domain	50
Figure 6.6	vertical flap: fluid mesh	50
Figure 6.7	vertical flap: CalculiX mesh	52
Figure 6.8	vertical flap: velocity field	53
Figure 6.9	vertical flap: resultant forces	54
Figure 6.10	vertical flap: moment applied at root	55
Figure 6.11	vertical flap: tip displacement x direction	55
Figure 6.12	vertical flap: convergence and iterations	56
Figure 6.13	vertical flap: MBDyn convergence and iterations	57
Figure 6.14	vertical flap (compressible): fluid domain	58
Figure 6.15	vertical flap (compressible): fluid mesh	58
Figure 6.16	vertical flap (compressible): flow solution	60
Figure 6.17	vertical flap (compressible): resultant forces	61

Figure 6.18 vertical flap (compressible): tip displacement	61
Figure 6.19 vertical flap (compressible): convergence and iterations	62
Figure 6.20 vertical flap (compressible): MBDyn internal forces	63
Figure 6.21 square bluff body benchmark: domain	64
Figure 6.22 square bluff body: fluid mesh	65
Figure 6.23 square bluff body: structural interface mesh	66
Figure 6.24 square bluff body: tip displacement	67
Figure 6.25 square bluff body: resultant forces (detail)	68
Figure 6.26 square bluff body: fluid solution	69
Figure 6.27 square bluff body: convergence and iterations	70
Figure 6.28 square bluff body: MBDyn internal forces (detail)	71
Figure 6.29 FSI2: domain	72
Figure 6.30 FSI2: fluid mesh	73
Figure 6.31 FSI2: structural interface mesh	74
Figure 6.32 FSI2: tip displacement	75
Figure 6.33 FSI2: resultant forces (detail)	76
Figure 6.34 FSI2: fluid solution	77
Figure 6.35 FSI2: convergence and iterations	78
Figure 6.36 FSI2: MBDyn internal forces (detail)	79

List of Tables

Table 2.1	fluid matrix of dimension exponents	11
Table 6.1	Vertical flap: fluid properties	51
Table 6.2	Vertical flap: mesh properties	51
Table 6.3	Vertical flap: coupling parameters	51
Table 6.4	Vertical flap: solid properties	51
Table 6.5	Vertical flap: adimensional numbers	52
Table 6.6	Vertical flap (compressible): fluid properties	59
Table 6.7	Vertical flap (compressible): mesh properties	59
Table 6.8	Vertical flap: solid properties	59
Table 6.9	Vertical flap (compressible): coupling parameters	59
Table 6.10	Vertical flap (compressible): adimensional numbers	60
Table 6.11	square bluff body: geometry	64
Table 6.12	square bluff body: fluid properties	65
Table 6.13	square bluff body: mesh properties	65
Table 6.14	square bluff body: solid properties	66
Table 6.15	square bluff body: coupling parameters	66
Table 6.16	square bluff body: adimensional numbers	67
Table 6.17	square bluff body: results	70
Table 6.18	FSI2: geometry	72
Table 6.19	FSI2: fluid properties	73
Table 6.20	FSI2: mesh properties	73
Table 6.21	FSI2: solid properties	74
Table 6.22	FSI2: coupling parameters	74
Table 6.23	FSI2: adimensional numbers	75
Table 6.24	FSI2: comparison of results (displacements)	77
Table 6.25	FSI2: comparison of results (forces)	78
Table 6.26	FSI2-FSI3: different parameters	81
Table 6.27	FSI2-FSI3: adimensional numbers	81
Table 6.28	FSI3 sensitivity analysis: <i>green cells</i> simulation completed with average number of iterations, <i>red cells</i> simulation diverged	83
Table 6.29	FSI1 sensitivity analysis	83
Table 6.30	Re 1000 sensitivity analysis	84

Listings

4.1 MBDyn input file structure	30
5.1 MBDynAdapter simulation execution	42
A.1 preCICE configuration file example	87
B.1 MBDyn adapter configuration file example	89
C.1 preCICE API methods	91
C.2 preCICE adapter structure	92
D.1 MBDyn input file example	95
D.2 MBDyn beam nodes	101
D.3 MBDyn beam elements	102
D.4 MBDyn joints	103

Chapter 1

Introduction

Fluid-Structure Interaction (**FSI**) describes the mutual interaction between a moving or deformable object and a fluid in contact with it, surrounding or internal. It is present in various forms both in nature and in man-made systems: a leaf fluttering in the wind, water flowing underground or blood pumping in an artery are typical examples of fluid-structure interaction in nature. FSI occurs in engineered systems when modeling the behavior of turbomachinery, the flight characteristics of an aircraft, or the interaction of a building with the wind, just to name a few examples.

All the aforementioned problems go under the same category of FSI, even if the nature of the interaction between the solid and fluid is different. Specifically, the intensity of the exchanged quantities and the effect in the fluid and solid domains vary among different problems.

There can be multiple ways to classify FSI problems, based on the flow physics and on the behavior of the body. Incompressible flow assumption is always made for liquid-solid interaction, while both compressible and incompressible flow assumptions are made when a gas interacts with a solid, depending on the flow properties and the kind of simulation. The main application of air-solid interaction considers the determination of aerodynamic forces on structures such as aircraft wings, which is often referred to as *aeroelasticity*. Dynamic aeroelasticity is the topic that normally investigates the interaction between aerodynamic, elastic and inertial forces. Aerodynamic *flutter* (i.e. the dynamic instability of an elastic structure in a fluid flow) is one of the severe consequences of aerodynamic forces. It is responsible for destructive effects in structures and a significant example of FSI problem.

The subject may also be classified considering the behavior of the structure interacting with the fluid: a solid can be assumed rigid or deforming because of the fluid forces. Examples where rigid body assumption may be used include internal combustion engines, turbines, ships and offshore platforms. The rigid body–fluid interaction problem is simpler to some extent, nevertheless the dynamics of rigid body motion requires a solution that reflects the fluid forces. Within the deformable body–fluid interaction, the nature of the deforming body may vary from very simple linear elastic models in small strain to highly complex nonlinear deformations of inelastic materials. Examples of deforming body–fluid interaction include aeroelasticity, biomedical applications and poroelasticity.

The interaction between fluid (incompressible or compressible) and solid (rigid or deformable) can be *strong* or *weak*, depending on how much a change in one domain influences the other. An example of weakly coupled problem is aeroelasticity at high Reynolds number, while incompressible flow often leads to strongly coupled problems. This distinction can lead to different solution strategies, as briefly described below.

Physical models aren't the only way in which FSI problems can be classified. The solution

procedure employed plays a key role in building models and algorithms to solve this kind of problems. The two main approaches are: the *monolithic approach* in which both fluid and solid are treated as one single system and the *partitioned approach* in which fluid and solid are considered as two separated systems coupled only through an interface. This latter approach is often preferred when building new solution procedures as it allows to use solvers that have been already developed, tested and optimized for a specific domain. The solvers only need to be linked to a third component, which takes care of all the interaction aspects.

The partitioned approach can be further classified considering the coupling between the fluid and solid: the solution may be carried out using a *weakly coupled approach*, in which the two solvers advance without synchronization, or a *strongly coupled approach*, in which the solution for all the physics must be synchronized at every time step. Although the weakly coupled approach is used in some aerodynamic applications, it is seldom used in other areas due to instability issues. A strongly coupled approach is generally preferred, even though this leads to more complex coupling procedures at the interface between fluid and solid.

This work describes the implementation and the validation of what is called an *adapter*, that is the "glue-code" needed to interface a solver to a coupling software library, thus adopting a *partitioned approach* to solve FSI problems. The *adapter* presented here connects the software code *MultiBody Dynamics analysis software (MBDyn)* to the multiphysics coupling library *precise Code Interaction Coupling Environment (preCICE)*.

Interfacing MBDyn with preCICE has multiple advantages: on one side it extends the capabilities of MBDyn to be used in FSI simulations by connecting it with a software library which has been already connected to widely used CFD solvers; on the other side, it allows to describe and simulate FSI problems with a suite of lumped, 1D and 2D elements (i.e. rigid bodies, *beams*, *membranes*, *shells*, etc.) decoupling the shape of the object (the interface with the fluid) from its structural properties, which can be described by different models and constitutive laws.

The thesis is structured as follows:

- Section 2 introduces the reader to FSI problems and their complexity, with particular attention to the physical description of the fluid and solid domains and the interface.
- Section 3 focuses on numerical methods, describing how to computationally deal with these kind of problems: details regarding the different coupling approaches are given here.
- Section 4 explains the features of preCICE that the adapter needs to support and gives a short introduction to MBDyn, explaining the main functionalities of interest.
- Section 5 presents the adapter developed in this work, its most important features and how to configure a FSI simulation with it.
- Section 6 describes the successful validation of the adapter, the comparison of the results with some well-known benchmarks **and an example of real world application**.
- Section 7 summarizes the findings and outcome of this work and gives an outlook to future work on this topic.
- Finally XX appendices give further information on...

Chapter 2

Physical aspects of Fluid-Structure Interaction problems

Dynamic models of solids or fluids aim at describing the evolution of an initial configuration through time. Structural mechanics and fluid dynamics use different perspectives when describing the motion of respectively a solid or a fluid particle. When dealing with FSI problems the two approaches need to be combined in order to obtain a suitable description of the two domains and their interface: this aspect is treated in 2.1.

As outlined in the introduction, the fluid and the solid domain of a FSI problem might be described by means of many different models: some of them are outlined in section 2.2. *Dimensional analysis* and the use of dimensionless numbers is a powerful tool used to classify fluid dynamics problems: some of the principles used there can be applied to FSI problems in order to classify them: this can help define and classify FSI problems, as described in section 2.3.

2.1 Description of motion

In a FSI model, the fluid in motion deforms the solid because of the forces exerted to the structure. The change in the shape of the solid modifies the fluid domain, causing a different flow behavior. For this reason it is necessary to describe formally the kinematics and the dynamics of the whole process. Classical continuum mechanics considers the motion of particles by means of two different perspectives [3]: the *Eulerian description*, briefly described in section 2.1.1, and the *Lagrangian description*, outlined in section 2.1.2. Those two perspectives are typically combined into the *arbitrary Lagrangian-Eulerian (ALE)* method, described in section 2.1.3.

2.1.1 Eulerian perspective

The *Eulerian perspective* observes the change of quantities of interest (e.g. density, velocity, pressure) at spatially fixed locations. In other words: the observer does not vary the point of view during different time steps. Thus, quantities can be expressed as functions of time at fixed locations. This is represented by the following notation:

$$\Theta = \tilde{\Theta}(x, y, z, t) \quad (2.1)$$

where Θ is a quantity of interest and $\tilde{\Theta}$ denotes the same quantity from an Eulerian point of view; (x, y, z) represent a fixed location in the Euclidean space.

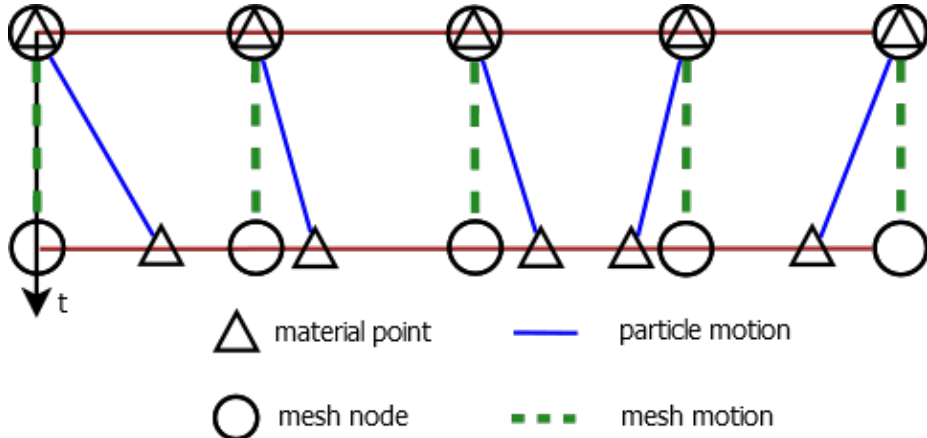


Figure 2.1. Eulerian perspective

A computational mesh can be interpreted as a number of observers distributed across the domain of interest and connected to each other in order to form a grid with nodes. If the particles of the domain move, a purely Euclidean mesh does not move and the position other nodes remain fixed at any instance of time [4]. This behavior is represented in Figure 2.1 (adapted from [4]). The mesh is independent of particles movement, resulting in a convenient choice for Computational Fluid Dynamics (CFD) problems, where fluid flows throughout the whole computational domain. Within this approach, proper mesh refinement is crucial for computational accuracy as it defines to what extent small scale movement can be modeled and resolved [5].

2.1.2 Lagrangian perspective

A *Lagrangian observer* focuses on a single particles and follows it throughout the motion, as depicted in Figure 2.2. Changes in the quantities of interest are observed at different spatial locations.

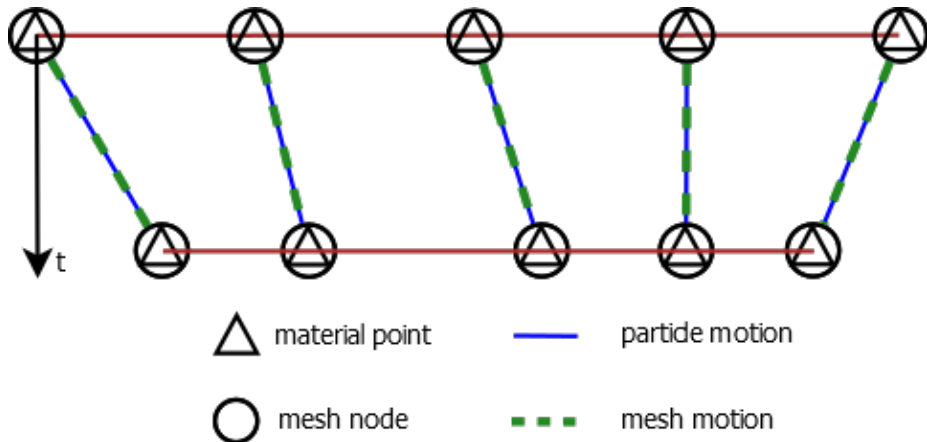


Figure 2.2. Lagrangian perspective

The motion of the particle and the other quantities of interest can be described by reference coordinates (or *material coordinates*) in Euclidean space (X, Y, Z), uniquely identifying the observed particle at a reference configuration [6]. Usually $t = 0$ is chosen as reference but this

is not mandatory. The Lagrangian observer only registers changes concerning one specific particle as time advances. Thus, quantities of interest can be described as:

$$\Theta = \hat{\Theta}(X, Y, Z, t) \quad (2.2)$$

In contrast to the Eulerian perspective (Equation 2.1), the obtained information is strictly limited to a single material particle (implied by the usage of the capital reference coordinate variables). Information about a fixed point in space is not directly available and no convective fluxes appear in a Lagrangian description.

This perspective is again translated into computational meshes: at a reference instance of time, mesh nodes are attached to material particles. As these move, the mesh nodes move with them causing the mesh to deform. Figure 2.2 describes the situation. The mesh nodes always coincide with their respective particles.

In this situation large-scale and irregular motions and more importantly deformation lead to distortions of the computational mesh, which yields smaller accuracy in simulations requiring to apply techniques to keep the desired accuracy [7].

Lagrangian perspective is the usual method of choice for Computational Solid Mechanics (**CSM**) simulations.

Eulerian and Lagrangian descriptions are related [8]. A mapping between them can be described by the *motion* function ϕ such that:

$$\vec{x}(t) = \phi(\vec{X}, t) \quad (2.3)$$

Equation 2.3 tells that the Eulerian, spatial position \vec{x} of a particle at time t is the mapping of the particle at its reference configuration \vec{X} : the mapping must be bijective.

2.1.3 ALE method

As outlined above, CSM and CFD problems adopt different perspectives. The **ALE** approach, a combination of the two points of view, is used for FSI problems. As the name implies, an ALE observer moves arbitrarily with respect to a specific material particle. Figure 2.3 depicts such a situation.

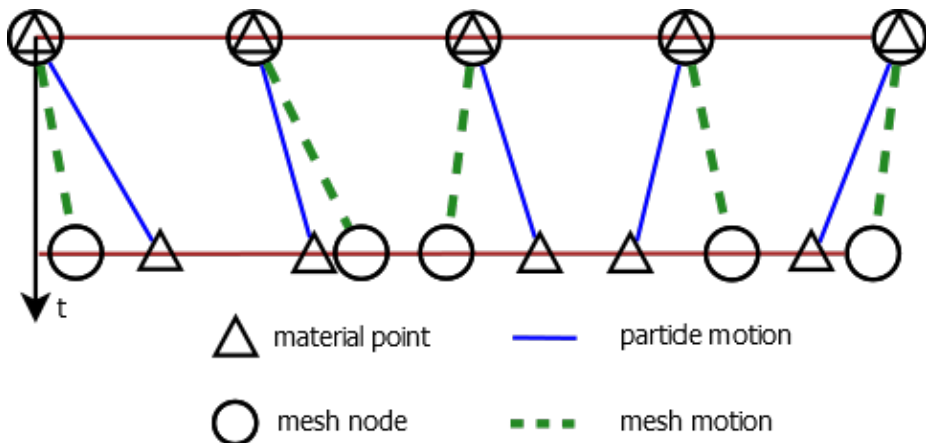


Figure 2.3. ALE perspective

When dealing with computational meshes, an ALE mesh is considered as it can move almost arbitrarily with respect to the motion of the underlying particles, as shown in Figure 2.4. The only constraint is that node movements should not distort the mesh too much

as this leads to computational inaccuracy. Many algorithm exist to implement suitable quality criteria and keep the mesh motion reasonable and to allow the nodes to follow moving particles up to a certain extent [9].

Since the mesh motion and material particle motion are not directly linked, a new unknown is introduced: the relative movement between the ALE mesh and the material domain. This approach is particularly useful in FSI problems: fluid and solid must follow the moving interface between them for physical reasons. Since the solid domain is usually described in a Lagrangian perspective, the solid mesh is kept attached to the FSI interface. However, also the fluid domain must deform to avoid formation of gaps between the meshes. Therefore, in ALE methods the fluid mesh nodes at the interface move with it. Fluid mesh nodes follow the fluid particles sticking to the interface (for viscous flows), while the rest of the fluid mesh is allowed to move in such way that mesh distortions are kept minimal, to preserve computational accuracy [10].

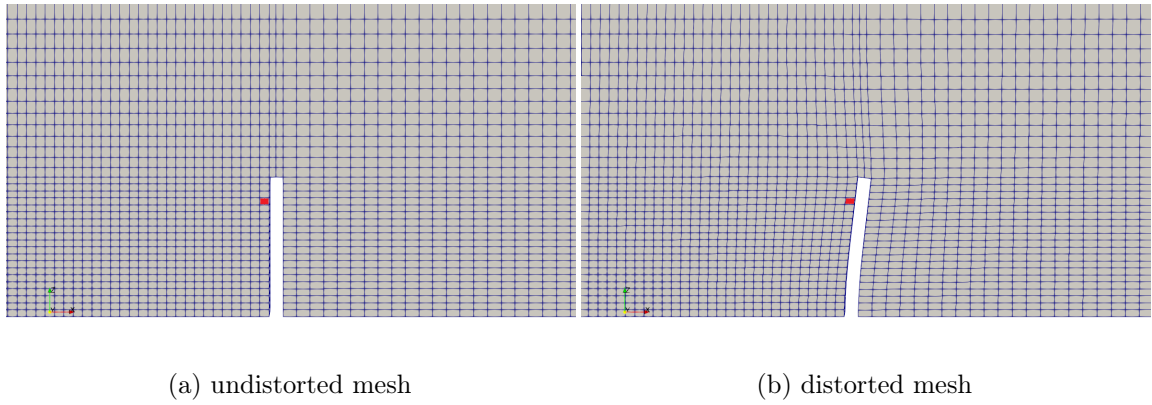


Figure 2.4. ALE mesh

2.2 Domains and interface

Fluid-structure interaction implies that the overall model is determined by models defining the fluid behavior and the solid behavior, briefly described in sections 2.2.2 and 2.2.1. A short overview of beam models is given in section 2.2.3 as it is relevant for the model developed in this work. Finally a formal definition of the interface is given in section 2.2.4, as it is necessary to define suitable coupling conditions at the common boundary of the solid and the fluid.

2.2.1 Fluid domain

An exhaustive description of all possible fluid models is far beyond the scope of this work. A quite general model is the viscous compressible one described by the Navier Stokes Equations ([NSE](#)).

$$\frac{\partial \rho}{\partial t} + \nabla \cdot (\rho \vec{v}) = 0 \quad (2.4a)$$

$$\frac{\partial}{\partial t} (\rho \vec{v}) + \nabla \cdot (\rho \vec{v} \otimes \vec{v}) + \nabla p - \nabla \cdot \tau - \rho \vec{g} = 0 \quad (2.4b)$$

$$\frac{\partial}{\partial t} (\rho e_0) + \nabla \cdot (\rho e_0 \vec{v}) + \nabla \cdot (\vec{v} p + \vec{q} - \vec{v} \cdot \boldsymbol{\tau}) - \vec{v} \cdot \rho \vec{g} = 0 \quad (2.4c)$$

where:

- ρ denotes density
- \vec{v} is flow velocity in all dimensions
- p denotes pressure
- τ is the viscous stress tensor
- \vec{g} represents the sum of all body forces
- e_0 is the total energy per unit mass
- \vec{q} is the heat flux by conduction

They consist in the mass conservation equation (2.4a), the conservation of momentum equation (2.4b) and the energy conservation equation (2.4c). For a Newtonian fluid, the viscous stress tensor is given by:

$$\tau = -\frac{2}{3}\mu(\nabla \cdot \vec{v})I + 2\mu S \quad (2.5)$$

with μ being the dynamic viscosity and S the rate of deformation tensor (i.e. the symmetric part of the velocity gradient $\nabla \vec{v}$):

$$S = \frac{1}{2}(\nabla \vec{v} + \nabla \vec{v}^T) \quad (2.6)$$

A detailed derivation of such equations and the theory beyond can be found for example in [11] and [12] or in [13].

The set of equations above, even with a Newtonian fluid model, lack some other information in order to form a closed set of Partial Differential Equations (PDE). A conductive heat flux model is needed (e.g. Fourier's Law), the caloric and thermodynamic equations of state have to be chosen, a proper turbulence model if needed (see [13]) and finally, the appropriate initial and boundary conditions for the problem [14] must be defined.

Simplifications can be done to obtain less sophisticated models such as: adiabatic, inviscid, incompressible, and many others. Dimensional Analysis is a powerful tool to determine to what extent some reduced models are meaningful, and it is widely used in fluid dynamics, as described in section 2.3.1. Most CFD software codes allow to set up simulations with the most suitable model which can be coupled with a solid model to build a FSI problem. Some further details are given in section 3.1.

2.2.2 Solid domain

In solid mechanics, particles do not travel as much as they do in fluid dynamic problems, as described in 2.1.2. For this reason, a Lagrangian perspective is generally used.

The de-Saint Venant-Kirchhoff model [15] is very commonly used when describing the movement of a solid: it is also often used in FSI problems ad it is capable of handling large deformation. The material is considered:

- *homogeneous*: the material properties do not depend on the position of the particle
- *linear elastic*: the stress-strain relationship is linear
- *isotropic*: the stress-strain relationship is independent from the direction of the load

A general expression of the dynamic equation can be derived from the Virtual Work Principle (**VWP**) applied to an arbitrary control volume:

$$\frac{\partial^2 \vec{u}}{\partial t^2} = \nabla \cdot \mathbf{T} + \rho \vec{f} \quad (2.7)$$

In equation 2.7:

- ρ : is the material density
- \vec{u} : is the particle displacement
- \mathbf{T} : is the *second Piola-Kirchhoff* stress tensor
- \vec{f} : is the sum of body forces

In order to close the dynamic equation, a constitutive law which must be considered to relate stress and strain:

$$\mathbf{T} = \lambda \text{I} \text{tr} [\boldsymbol{\varepsilon}_G] + 2\mu \boldsymbol{\varepsilon}_G \quad (2.8)$$

where $\boldsymbol{\varepsilon}_G$ is the Green-Lagrange strain tensor:

$$\boldsymbol{\varepsilon}_G = \frac{1}{2} (\mathbf{F}^T \mathbf{F} - \mathbf{I}) \quad (2.9)$$

and \mathbf{F} is the deformation gradient. λ and μ are material properties and are named Lamé constants. These relate to the Young modulus E and the Poisson ratio ν which are more commonly used in practice. The relationship among the various parameters is the following:

$$E = \frac{\mu(3\lambda + 2\mu)}{\lambda + \mu} \quad (2.10)$$

$$\nu = \frac{\lambda}{2(\lambda + \mu)} \quad (2.11)$$

The set of parameters (E, ν) or (λ, μ) , together with the density ρ fully define the material, under the assumptions of linear elasticity, isotropy and homogeneity.

The set of PDEs is completed when suitable initial and boundary conditions are defined.

2.2.3 Models with reduced dimensionality: beams

The equations introduced in section 2.2.2 may be a tough task to solve even of the case of isotropic hyperelasticity, when considering a 3-D domain. Even with today's computers and using finite elements techniques, it is not always feasible or convenient to treat a solid as a three-dimensional continuum. Body with particular geometric features can be seen as lower dimension bodies, with respect to the governing equations [16]. Such bodies are called *beams* (one dimension), *plates* or *shells* (two dimensions).

The *beam* model splits the description of the geometry into two subproblems:

1. a beam is defined by its *reference line* and the movement (displacement and rotation) of the solid is completely defined by it (see Figure 2.5),

2. the beam *cross section* is considered as a whole, its movement depends on the movement of the reference line, stresses are generalized into *resultants* (axial, bending, shear, torsional) which represent the aggregate effect of all of the stresses acting on the cross section. The constitutive properties of the section (axial, shear, torsion and bending stiffness) allow to relate stresses and deformations (by means of VWP) and close the problem.

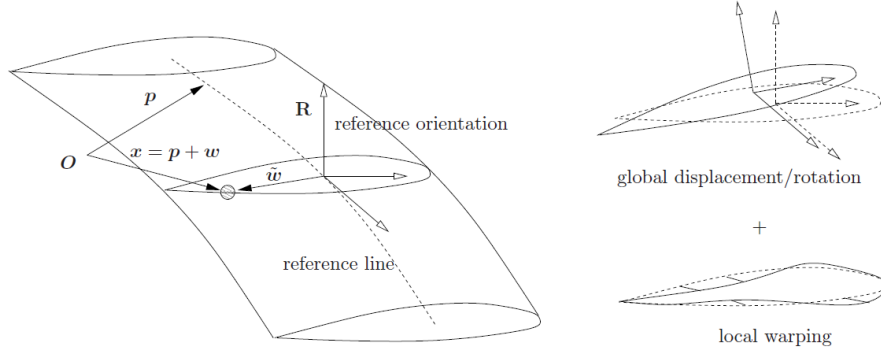


Figure 2.5. beam model, taken from [1]

The beam model can be used to build elements of a Finite Element Method (**FEM**). For example, the beam element can be modeled by means of a Finite Volume approach, as described in [17], which computes the internal forces as functions of the straining of the reference line and orientation at selected points along the line itself, called evaluation points.

This approach is particularly interesting for FSI problems in which slender structures are involved. A mapping is needed between the fluid-solid interface and the reference line movement, which will be described in Sections 4.1.4 and 4.1.7.

2.2.4 Interface and interaction

Since FSI problems are centered on the interaction of the fluid and solid domain, their common interface needs to be described properly. A simple representation of the situation at the so called *wet surface* is shown in Figure 2.6. Quantities related to the solid use S subscript, while fluid domain and the interface are labeled with F and FS, respectively.

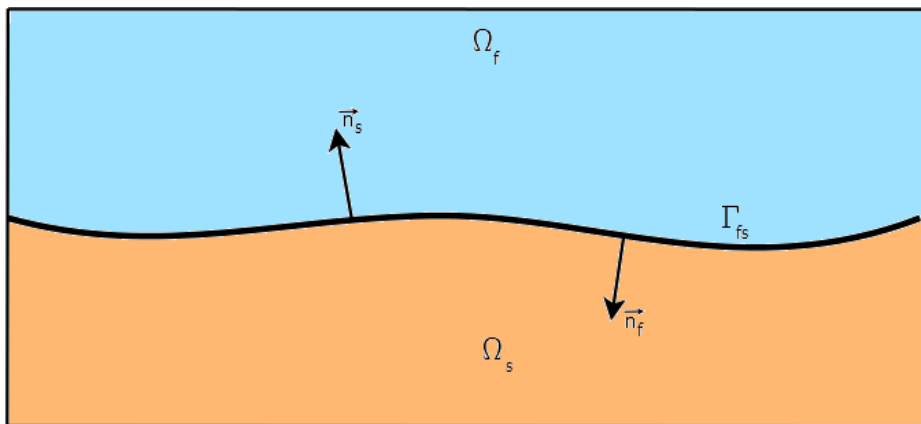


Figure 2.6. fluid solid interface

In order to have a physically correct behavior, some conditions have to be met [18]:

- solid and fluid domains should not overlap nor separate,
- for a viscous fluid model, the flow velocity at the interface must equal the boundary velocity (*no-slip* condition),
- for an inviscid fluid model, only velocity components normal to the wet surface have to be equal to the structural velocity as the fluid may slip freely in tangential direction at any boundary,
- forces exchanged at the interface must be at equilibrium.

The first conditions result in the *kinematical requirement* that the displacements of fluid and solid domains, as well as their respective velocities have to be equal at the wet surface (denoted by Γ_{FS}):

$$\Delta \vec{x}_F = \vec{u}_S \quad (2.12)$$

$$\vec{v}_F = \frac{\partial \vec{u}_S}{\partial t} \quad (2.13)$$

The last condition results in the equilibrium requirement. Force vectors are computed from the stresses at the interface and the outward normal vectors of fluid and solid domain, respectively. They have to be equal and opposite leading to the dynamic coupling condition:

$$\boldsymbol{\sigma}_F \cdot \vec{n}_F + \boldsymbol{\sigma}_S \cdot \vec{n}_F = 0 \quad (2.14)$$

$\boldsymbol{\sigma} \in \mathbb{R}^{3 \times 3}$ represents the stress tensor (note that for the fluid it comprises pressure and viscous stresses), while $\vec{n} \in \mathbb{R}$ is the outward normal unit vector.

2.3 Classification of FSI problems

In the previous chapters we have seen that there exist a lot of models that can describe fluid flow and solid mechanics. In FSI problems we need to couple two of them: the variety of coupled problems seems to be so large that single FSI model that is applicable to every problem appears to be unfeasible. For this reason it is useful to classify FSI problems and look for specific properties in each class. The first step is to switch from dimensional quantities to dimensionless ones.

2.3.1 Dimensional analysis

We use the principle that a physical law should only relate to dimensionless quantities. There exist a rather general theorem called the Π Theorem or the *Vaschy-Buckingham Theorem* [19], which tells how many dimensionless quantities are needed to rewrite a model in dimensionless fashion. This theorem states that the number of dimensionless quantities, P , is equal to that of the dimensional ones describing the problem, N , minus R , which is the rank of the matrix of dimension exponents. This matrix is formed by the columns of the dimension exponents of all variables [20]. An example is given in the following Section 2.3.2, Table 2.1.

2.3.2 Dimensional analysis in fluid domain

Dimensional analysis is widely used in fluid dynamics. In order to keep the analysis simple, we consider the adimensionalization of the incompressible Navier-Stokes momentum equation for a Newtonian fluid [21]:

$$\frac{\partial \vec{v}}{\partial t} + (\vec{v} \cdot \nabla) \vec{v} = -\frac{\nabla p}{\rho} + \nu \nabla^2 \vec{v} + \vec{g} \quad (2.15)$$

The variables involved in equation 2.15 are the following:

- t : time
- \vec{x} : coordinates
- \vec{v} : velocity field
- p : pressure field
- ρ : fluid density
- ν : fluid kinematic viscosity
- \vec{g} : gravity
- L : reference dimension
- V_0 : reference velocity

	t	\vec{x}	\vec{v}	p	ρ	ν	\vec{g}	L	V_0
L	0	1	1	-1	-3	2	1	1	1
M	0	0	0	1	1	0	0	0	0
T	1	0	-1	-1	0	-1	-2	0	-1

Table 2.1. fluid matrix of dimension exponents

The rank of the above matrix is 3 so 6 dimensionless parameters are needed to rewrite the equation 2.15:

- *length*: $\vec{x}^* = \frac{\vec{x}}{L}$
- *velocity*: $\vec{v}^* = \frac{\vec{v}}{V_0}$
- *time*: $t^* = \frac{V_0 t}{L} = \frac{t}{T_{fluid}}$
- *pressure*: possible choices: $p^* = \frac{p}{\rho V_0^2}$ or, if viscous forces are dominant, $p^* = \frac{p L}{\rho \nu V_0}$
- *Reynolds number*: $Re = \frac{V_0 L}{\nu}$. It defines the ratio between inertia and viscous forces.
- *Froude number*: $Fr = \frac{V_0}{\sqrt{gL}}$. It defines the ratio between the flow inertia to the body field forces

The adimensionalized momentum equation becomes:

$$\frac{\partial \vec{v}^*}{\partial t^*} + (\vec{v}^* \cdot \nabla) \vec{v}^* = -\nabla p^* + \frac{1}{Re} \nabla^2 \vec{v}^* + \frac{1}{Fr^2} \vec{g} \quad (2.16)$$

From Equation 2.16 a lot of models might be derived: from *Stokes regime* when viscosity is dominant, to *Euler regime* when viscosity is negligible with respect to inertia forces.

2.3.3 Dimensional analysis in solid domain

Even if it is seldom used, Dimensional Analysis can be made also for the solid domain [22].

The variables involved in a solid dynamics equation are:

- t : time
- \vec{X} : coordinates
- \vec{u} : displacement field
- ρ_S : solid density
- E : elastic modulus
- \vec{g} : gravity
- L : reference dimension
- U_0 : reference displacement

From the variables above the following parameters can be derived:

- *length*: $\frac{\vec{X}}{L}$: dimensionless coordinate
- *displacement*: $\frac{\vec{u}}{L}$: dimensionless displacement
- *time*: $\frac{t\sqrt{\frac{E}{\rho_S}}}{L} = \frac{t}{T_{solid}}$ dimensionless time
- entity of displacements: $\frac{U_0}{L} = \delta$: *displacement number*
- gravity: $\frac{\rho_S g L}{E}$: *elastogravity number*

T_{solid} can be seen as $\frac{L}{c}$ with $c = \sqrt{\frac{E}{\rho_S}}$ which is the scale of elastic wave velocity. The displacement number δ tells how big the structure displacement are related to the overall dimension, and defines the *large displacements* region. Finally, the *elastogravity number* combines gravity (or body forces in general), density and stiffness: when large the deformation induced by body forces in the solid are large.

2.3.4 Dimensional analysis of coupled problems

It is now possible to undertake the dimensional analysis of a fully coupled fluid and solid interaction problem. Some of the parameters are only defined in the fluid side or in the solid side (e.g. viscosity or stiffness). Some parameters are common to both domains (e.g. length scale or gravity). The variables of interest are now the velocity in the fluid and the displacements in the solid. Each of them can be related to all the parameters without separation. For example, the fluid velocity relationship is of the kind:

$$g(\vec{v}; \vec{x}, t; \rho, \mu, V_0; \rho_S \cdot E; \vec{g}, L) = 0 \quad (2.17)$$

Equation 2.17 is composed of 11 dimensional parameters. Applying π theorem, the total number of independent dimensionless parameter expected is 8. Starting from the ones derived in the previous sections:

1. $\vec{x}^* = \frac{\vec{x}}{L}$: dimensionless coordinates
2. $\vec{v}^* = \frac{\vec{v}}{V_0}$: dimensionless fluid velocity
3. $t^*_f = \frac{V_0 t}{L}$: dimensionless time
4. $Re = \frac{V_0 L}{\nu}$: Reynolds number
5. $Fr = \frac{V_0}{\sqrt{gL}}$: Froude number
6. $\delta = \frac{U_0}{L}$: displacement number
7. $\frac{\rho_S g L}{E}$: elastogravity number

The 7 quantities above derive from the separated problem. The last one necessarily mixes things from the fluid and the solid side otherwise it would have been found in one uncoupled case. There is no unique choice for this parameter, the following are the most common ones.

Mass number

The simplest, but arguably most important parameter is the ratio of the two densities: the *Mass Number* M.

$$M = \frac{\rho}{\rho_S} \quad (2.18)$$

This can range from $\mathcal{O}(10^{-4})$ in air-steel interaction to $\mathcal{O}(1)$ when both media have about the same density. This parameter is particularly significant for the so called *added mass* stability problem, described in Section 3.5.

Reduced velocity

Another possible choice is the reduced velocity:

$$U_R = \frac{V_0}{\sqrt{\frac{E}{\rho_S}}} \quad (2.19)$$

It is the ratio between the fluid free velocity and the velocity of elastic waves in a solid, c . It contains information on the way the two dynamics are related and it can range different orders of magnitude.

Cauchy number

Another possible parameter combines stresses or stiffness: the Cauchy number, as defined in [23]:

$$C_Y = \frac{\rho V_0^2}{E} \quad (2.20)$$

It is the ratio between the fluid inertial forces, quantified by the dynamic pressure and the stiffness of the solid E. The higher it is, the more the solid is elastically deformed by the flow.

These are actually the most important parameters involving FSI problems. Among them, there is no universally better choice. But there are efficient choices, that would be more helpful in solving a given problem.

Chapter 3

Computational aspects of Fluid-Structure Interaction problems

This section deals with the computational aspects of FSI problems. The first possible categorization of solution techniques distinguishes between monolithic and partitioned approach, as discussed in Section 3.1. This work is based on the latter approach, so the two different coupling strategies, namely strong and weak, are discussed in Section 3.2. As strong coupling is generally needed for accurate solution, an overview of strong coupling algorithms is given in Section 3.3. Section 3.4 focuses on aspects concerning the interface mesh, and how the solid and the fluid exchange data between them. Finally 3.5 briefly describes a common issue arising in strongly coupled problems: the added mass effect ([AME](#)).

3.1 Monolithic and Partitioned Approach

Analytical solutions are impossible to obtain for the large majority of FSI problems; on the other hand, laboratory experiments may be costly, unfeasible or limited. For those reasons, numerical simulations may be employed to analyze the physics involved in the interaction between fluids and solids. With the current capabilities of computer technology, simulations of scientific and engineering models have become increasingly detailed and sophisticated.

The numerical methods used to solve FSI problems may be roughly classified into two classes: the *monolithic approach* and the *partitioned approach*. There is no exact distinction between the two approaches, as they might be seen differently among fields of applications. The idea here is to consider how many solvers are used to find a solution.

In the *monolithic approach*, the whole problem is treated as a unique entity and solved simultaneously with a specialized ad hoc solver (see Figure 3.1). The fluid and structure dynamics form a single system of equations for the entire problem, which is solved simultaneously by a unified algorithm. The interface conditions are implicit in the solution procedure [24], [25].

This approach can potentially achieve better accuracy, as they solve the system of equations exactly the interface conditions are implicit in the model [26], but it may require more resources and expertise to develop from scratch a specialized code (it solves a very specific model) that can be cumbersome to maintain.

On the other hand, in the *partitioned approach*, the fluid and the solid domains are treated as two distinct computational fields, with their respective meshes, that have to be solved separately (see Figure 3.2: how data are passed between solvers is detailed in Section 3.2). The interface conditions are used explicitly to communicate information between the

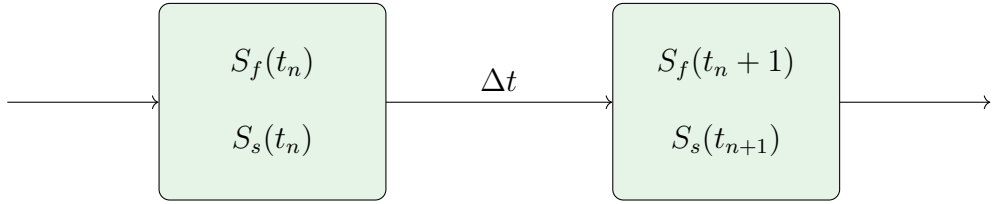


Figure 3.1. monolithic approach: S_f , S_s denote the fluid and the structure solutions

fluid and structure solutions. This implies that the flow does not change while the solution of the structural equations is calculated and vice versa [27]. The partitioned approach thus requires a third software module (i.e. a coupling algorithm) to incorporate the interaction aspects. It communicates the boundary conditions described in Section 2.2.4: that is forces or stresses (dynamic data) calculated by the fluid solver at the wet surface are passed to the solid component and displacements or velocities (kinematic data) computed by the solid solver at the interface are sent to the fluid component in return. Finally, fluid and structural solutions together yield the FSI solution.

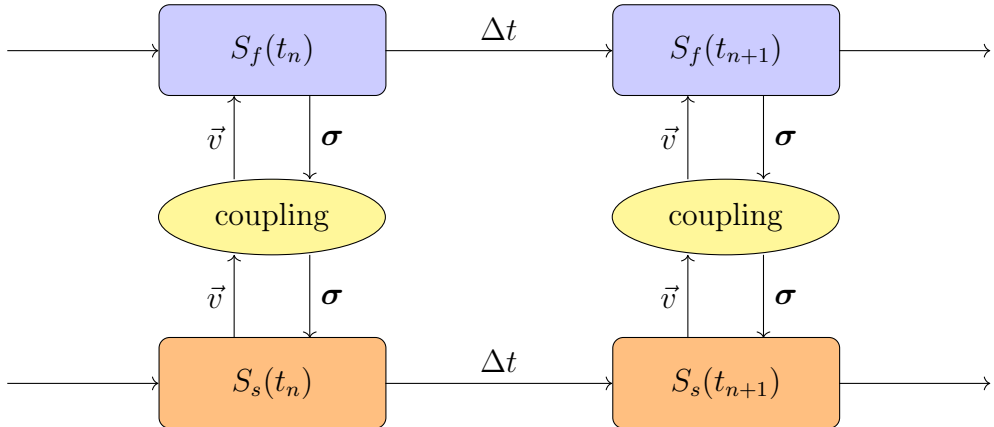


Figure 3.2. partitioned approach: S_f , S_s denote the fluid and the structure solutions, while σ and v represent coupling data

A big advantage of this approach is that software modularity is preserved: different and efficient solution techniques can be used for the flow equations and structural equations. Provided that they can exchange data, existing solvers for the fluid and solid problem can be reused, ranging from commercial to academic and open-source codes. Those solvers are usually well-validated. Besides, compared to monolithic procedures, the programming efforts are lower for partitioned approaches, as only the coupling of the existing solvers has to be implemented rather than the solvers themselves. The challenge of this approach is, however, to define and implement algorithms to achieve accurate and efficient fluid-structure interaction solution with minimal code modification. Particularly, the interface location that divides the fluid and the structure domains changes in time. The partitioned approach requires that the fluid solver has ALE capabilities, as introduced in Section 2.1.3. More detailed and practical explanations about the coupling component used in this work are given in Section 4.2.

3.2 Coupling Strategies

Because of the modularity, the partitioned approach has gained much attention in research. The structure sketched in Figure 3.2 needs to be detailed and specialized in function of the coupling strategies.

In an interface multi-physics coupling like FSI, the boundary surface is in common between the two sides of the simulation. The results make sense and are numerically stable only if the two sides of the interface are in agreement, since the output values of the one simulation become input values for the other (and vice-versa). The solution strategies can be roughly divided into weakly and strongly coupled approaches. They are often referred to as *explicit* and *implicit* methods in the literature. When the fluid and solid solutions are computed iteratively until some convergence criteria within the same time step, the scheme is called *implicit coupling*. The faster, simpler but less precise *explicit coupling* consists in executing a fixed number of iterations (typically one per time step) and exchange coupling values without convergence checks.

3.2.1 Explicit coupling schemes

As in the previous Section, S_f represents the fluid solver, which computes the pressures (named d_f here) at the deformable boundary and S_s is the structure solver, which uses these forces to compute the displacement and velocity of the boundary (named d_s). In a *serial-explicit* (or *conventional staggered*) coupling scheme, the solver S_f uses the old time step boundary values $d_s^{(n)}$ to compute the values of $d_f^{(n+1)}$ for the next time step:

$$d_f^{(n+1)} = S_f(d_s^{(n)}) \quad (3.1)$$

When the fluid solver completes the time step, data are passed to the structural solver:

$$d_s^{(n+1)} = S_s(d_f^{(n+1)}) \quad (3.2)$$

Note that Equation 3.1 uses values computed at t^n , while Equation 3.2 uses values computed at $t^{(n+1)}$. The order of execution might be inverted.

In order to reduce execution time, the solvers might run in parallel, using data from the same time step (*parallel-explicit coupling*):

$$d_f^{(n+1)} = S_f(d_s^{(n)}) \quad (3.3a)$$

$$d_s^{(n+1)} = S_s(d_f^{(n)}) \quad (3.3b)$$

The two explicit schemes are shown schematically in Figures 3.3a and 3.3b.

In general, an explicit coupling is not enough to regain the exact (as in the monolithic approach) solution of the problem as the matching coupling conditions between the solvers is not enforced within each time step: no balance between fluid and structural domain with respect to forces and displacements at the interface can be guaranteed ([18], [27]). Nevertheless, explicit coupling yields good results if the interaction between fluid and solid is weak as in aeroelastic simulations, where in general the simulations show small displacements of the structure within a single time step and the flow field isn't much influenced by the structural displacements [28].

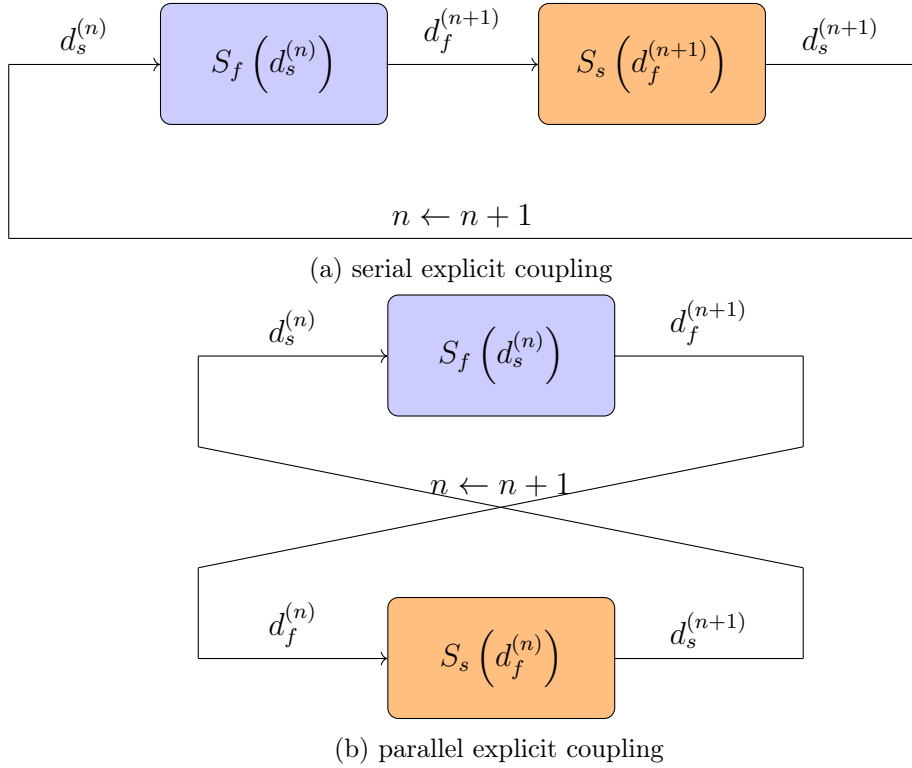


Figure 3.3. Explicit coupling schemes

3.2.2 Implicit coupling schemes

On the other hand, strongly (implicit) coupling techniques require an iterative method to solve the fixed-point equation that derives from enforcing the agreement of the interface variables. The coupling conditions at the wet surface are enforced in each time step up to a convergence criterion. If the criterion is not met, another subiteration within the same time instance is computed. Therefore, the solution can approximate the monolithic solution to an arbitrary accuracy.

As in the explicit case, solvers may run in a sequential mode: the coupling is then named *serial* (or staggered) and the solvers wait for each other.

$$d_f^{(n+1),i+1} = S_f(d_s^{(n+1),i}) \quad (3.4a)$$

$$d_s^{(n+1),i+1} = S_s(d_f^{(n+1),i+1}) \quad (3.4b)$$

Equations 3.4 show that, in contrast with explicit coupling, both solvers use interface values at time step $n+1$, but one of them uses data from previous iteration. If run in parallel mode [29], the system becomes:

$$d_f^{(n+1),i+1} = S_f(d_s^{(n+1),i}) \quad (3.5a)$$

$$d_s^{(n+1),i+1} = S_s(d_f^{(n+1),i}) \quad (3.5b)$$

At convergence, the following relation holds of serial (or *Gauss-Seidel*) coupling:

$$d_s^{(n+1)} = S_s \left(S_f \left(d_s^{(n+1)} \right) \right) \quad (3.6a)$$

$$d_s^{(n+1)} = S_s \circ S_f \left(d_s^{(n+1)} \right) \quad (3.6b)$$

and the following relation holds for parallel (or *Jacobi*) coupling:

$$\begin{pmatrix} d_s^{(n+1)} \\ d_f^{(n+1)} \end{pmatrix} = \begin{pmatrix} 0 & S_f \\ S_s & 0 \end{pmatrix} \begin{pmatrix} d_s^{(n+1)} \\ d_f^{(n+1)} \end{pmatrix} \quad (3.7)$$

Acceleration techniques are necessary to bring fixed point equation 3.6b or 3.7 to convergence. Those techniques are described in Section 3.3.

The two implicit schemes are shown schematically in Figures 3.4a and 3.4b: *accel* refers to the post-processing step implemented to speedup convergence. After every non-converged iteration, the latest stored state of the solver (*checkpoint*) is reloaded and coupling iteration i for the current time step is incremented. When the solution converges, the time step n is incremented.

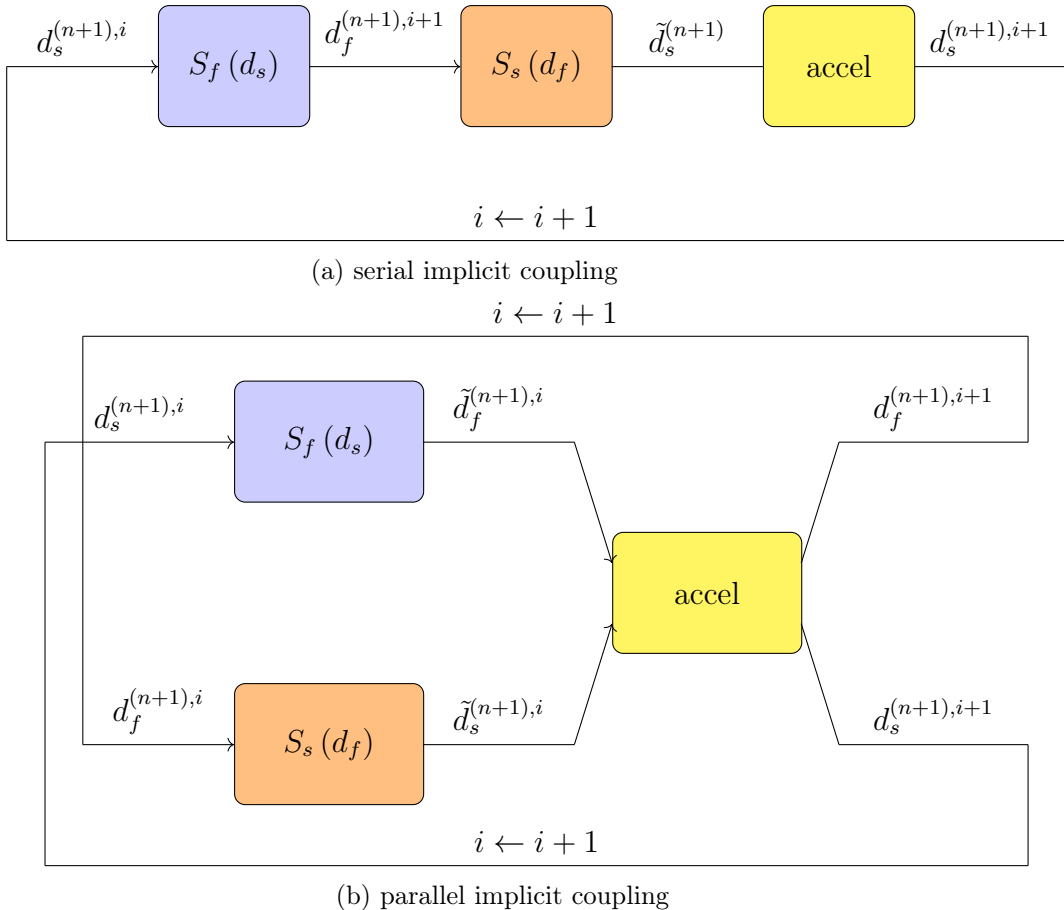


Figure 3.4. Implicit coupling schemes

Implicit methods are generally applicable to any kind of FSI problems, in contrast with explicit methods. When fluid and structure are strongly coupled, explicit coupling can be

subject to numerical instabilities, a problem that cannot always be solved by reducing the coupling time step size [30]. These instabilities can be overcome by implicit methods, even if several coupling iterations may be executed every time step, until the values on both sides of the interface converge.

3.3 Strong coupling algorithms

As mentioned in the previous section, implicit methods require some post-processing (generally called *acceleration*) techniques to make the solution of the single time step of the coupled partitioned FSI problem converge. This requires to solve a *fixed-point equation*, in fact:

$$H(d_s) := S_s \circ S_f(d_s) \quad (3.8a)$$

$$d_s = H(d_s) \quad (3.8b)$$

$$R(d) := H(d) - d = 0 \quad (3.8c)$$

Equation 3.8a represents the composition of the solid and the fluid solution, while Equation 3.8b represents the resulting fixed point equation. As the order of execution can be switched, in Equation 3.8c, where the *residual* is defined, the input data d_s is generically substituted with d .

The basic approach to solve the fixed point equation is to perform the corresponding fixed point iteration (**FPI**):

$$x_{i+1} = H(x_i) \quad i = 1, 2, \dots \quad (3.9)$$

which is known to converge if the mapping H is a contraction, but this is not the general case in FSI computations [29].

3.3.1 under-relaxation

The way to stabilize the iterations is to perform a FPI with *under-relaxation* as illustrated in the following algorithm:

Algorithm 1: FPI with relaxation

```

Result:  $d_k$ 
1 initialization of  $d_0$ ;
2  $k = 0$ ;
3  $\tilde{d}_1 = S_s \circ S_f(d_0)$ ;
4  $r_0 = \tilde{d}_1 - d_0$ ;
5 while  $\|r_k\| > \varepsilon$  do
6   | compute  $d_k$  by relaxation;
7   |  $k = k + 1$ ;
8 end
```

The under-relaxation is defined by:

$$d_{k+1} = d_k + \omega (H(d_k) - d_k) \quad (3.10)$$

Where ω in Equation 3.10 is the *relaxation factor*. The relaxation parameter has to be small enough to keep the iteration from diverging, but as large as possible in order to use as

much of the new solution as possible [31]. The optimal ω value is problem specific and not known a priori. A suitable dynamic relaxation parameter, is a better choice, like the *Aitken under-relaxation* [32] which adapts the factor at each iteration with the following relation:

$$\omega_i = -\omega_{i-1} \frac{r_{i-1}^T (r_i - r_{i-1})}{\|r_i - r_{i-1}\|^2} \quad (3.11)$$

Aitken under-relaxation can be a good choice for strong interaction with a fluid solvers that does not fully converge in every iteration or for compressible fluid solvers.

3.3.2 Quasi-Newton Least Squares schemes

Under-relaxation is a good choice for easy stable problems, but is outperformed by more sophisticated quasi-Newton coupling schemes. Equation 3.8c could be solved iteratively with a Newton method [33]:

$$R(d_k) := r_k \quad (3.12a)$$

$$R(d_k) + \left. \frac{\partial R}{\partial d} \right|_{d_k} (d_{k+1} - d_k) = 0 \quad (3.12b)$$

$$d_k + \left(\left. \frac{\partial R}{\partial d} \right|_{d_k} \right)^{-1} (-r_k) = d_{k+1} \quad (3.12c)$$

The *residual* at iteration k is defined in Equation 3.12a, if the Jacobian matrix of the equation is known, a Newton iteration can be performed as in Equation 3.12b. The updated values can be computed using Equation 3.12c.

In situations where:

- *black-box* systems are considered (i.e. the Jacobian is unknown),
- the cost of a function evaluation is sufficiently high that numerical estimation of the Jacobian is prohibitive,

there exist a number of matrix-free methods that use only information derived from the consecutive iterates and that build an approximation based on those values. This approach is known as *quasi-Newton method* [34]. Input and output data of H and R are used to approximate the solution of 3.12c. Algorithm 12 (taken from [35]) shows the basics steps to

estimate data at next step using the *Quasi Newton Least Squares Method*:

Algorithm 2: Quasi Newton Least Squares method

Result: d_{k+1}

- 1 initial value d_0 ;
- 2 $\tilde{d}_0 = H(d_0)$ and $R_0 = \tilde{d}_0 - d_0$;
- 3 $d_1 = d_0 + \omega r_0$;
- 4 **for** $k = 1 \dots$ **do**
- 5 $\tilde{d}_k = H(d_k)$ and $r^k = \tilde{d}_k - d_k$;
- 6 $V^k = [\Delta r_0^k, \dots, \Delta r_{k-1}^k]$ with $\Delta r_i^k = r^i - r^k$;
- 7 $W^k = [\Delta \tilde{d}_0^k, \dots, \Delta \tilde{d}_{k-1}^k]$ with $\Delta \tilde{d}_i^k = \tilde{d}_i - \tilde{d}_k$;
- 8 decompose $V^k = Q^k U^k$;
- 9 solve the first k lines of $U^k \alpha = -Q^{k^T} R^k$;
- 10 $\Delta \tilde{d}^k = W^k \alpha$;
- 11 $d_{k+1} = \tilde{d}_k + \Delta \tilde{d}_k$;
- 12 **end**

In algorithm 12 the matrices V^k and W^k are constructed from the previous iterations and the known values of d_0, \dots, d_k and $\tilde{d}_0, \dots, \tilde{d}_k$. $\Delta \tilde{d}^k$ is constructed in the column space of W^k (line 10). For this reason a least squares problem is solved:

$$\alpha = \underset{\beta \in \mathbb{R}^k}{\operatorname{argmin}} \|V^k \beta + R(d_k)\| \quad (3.13)$$

The least squares problem is solved computing the decomposition of V^k into an orthogonal matrix $Q^k \in \mathbb{R}^{k \times k}$ and an upper triangular matrix $U^k \in \mathbb{R}^{n \times k}$ (line 8). Then α is computed in line 9.

When building matrices V^k and W^k (lines 6-7), it is possible to use information from previous time steps.

Finally, to ensure linear independence of columns in the multi-secant system for Jacobian estimation, a filter can be used [36], in order to drop nearly dependent columns of Q^k and avoid singularity of the approximated Jacobian.

The above algorithm is usually denominated in FSI interface quasi Newton with inverse Jacobian from a least squares model (**IQN-ILS**) (or Anderson acceleration). There exist other algorithms, like generalized Broyden (**IQN-IMVJ**) or manifold mapping to solve the problem. A complete description of those methods goes beyond the scope of this work: a description of the most common algorithms can be found in [37], while a comparison of the performances can be found in [38].

3.3.3 Convergence criteria

At each time step, the coupling algorithm enforce matching conditions at the wet surface up to a convergence criterion. If not sufficiently met, another iteration within the same time step is performed. The fixed point formulation itself induces a criterion based on the residual itself r_{k+1} .

A scalar, *absolute convergence criterion* can be defined as in Equation 3.14: it is useful for close to zero values of the coupling quantities, when rounding errors become important:

$$\|r_{k+1}\| \leq \epsilon_{abs} \quad (3.14)$$

A more common *relative convergence criterion*, defined in Equation 3.15 is particularly useful when different quantities (e.g. forces and displacements) are compared together to evaluate convergence:

$$\frac{\|r_{k+1}\|}{\|\tilde{d}_{k+1}\|} \leq \epsilon_{rel} \quad (3.15)$$

3.4 Interface Mesh and Data Mapping

FSI methods can also be classified considering how the fluid and solid meshes are treated. The *conforming mesh methods* consider the interface as a physical boundary condition (see Section 3.4.2), while *non-conforming mesh methods* treat the boundary location as a constraint imposed on the model equations (see Section 3.4.1) [18].

3.4.1 Non-conforming Mesh methods

In non-conforming mesh strategies all interface conditions are imposed as constraints on the flow and structural governing equations. It is possible to use non-conforming meshes for fluid and solid domains as they remain geometrically independent from each other (see Figure 3.5).

This approach is mostly used in *immersed boundary* methods [39]. Coupling is imposed by means of additional force terms appearing in the model equations of the fluid, which impose the kinematic and dynamic conditions. The forces represent the effects of a boundary or body being immersed in the fluid domain. A purely Eulerian mesh (see Section 2.1.1) can be used for the whole computational domain, since the force terms are dynamically added at specific locations to represent the structure.

The fluid forces applied on the solid at the wet surface are computed and used as input for the structural solver, which employs a standard Lagrangian mesh (see Section 2.1.2).

Immersed boundary methods are particularly innovative and are useful to overcome some issues in CFD computations, on the other hand most of the current implementations of FSI problem implement a conforming mesh strategy.

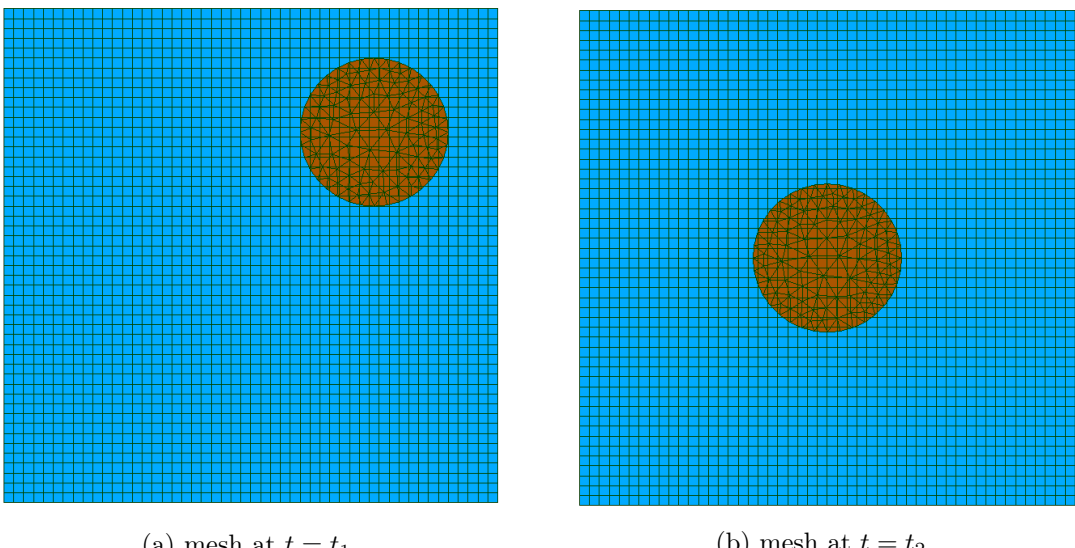


Figure 3.5. non conforming mesh example

3.4.2 Conforming Mesh methods

Conforming mesh methods adapt very well to the partitioned approach described in Section 3.1 as they usually consists in the computational steps described above, namely: computation in the fluid, computation in the solid, enforcing of interface condition and mesh movement (see Figure 3.6).

Fluid and structure meshes need share the boundary of the wet surface, as the coupling conditions are enforced by applying kinematic or dynamic conditions to those boundaries. Node-to-node matching of fluid and structure meshes at the interface is not required, as long as a suitable mapping between the interface nodes is performed (see Section 3.4.3).

The match between the interfaces must hold at each time step: this implies that both solid and fluid domains need to deform. Deformation is easily expressed in the solid domain as the structural mesh is usually represented in Lagrangian perspective (see Section 2.1.2). ALE perspective (Section 2.1.3) for the fluid domain becomes necessary in this case.

Mesh deformation can turn out to be a complicated task as in general the fluid mesh is deformed during motion (see Figure 2.4). Mesh smoothing techniques need to be applied in order to keep a good mesh quality in terms of distorted elements which can lead to accuracy loss in simulations. (the following video shows highly distorted fluid elements during FSI motion: [video](#)).

Mesh smoothing is generally applied to keep the fluid mesh as uniform and undistorted as possible during movement. There is a wide variety of mesh updating procedures [40]. The *torsional spring analogy* [41] is a fairly simple technique that computes mesh movement considering mesh edges as springs and solving the subsequent Laplace equation that derives from the mesh movement.

Some other references about mesh motion alternatives can be found in [42].

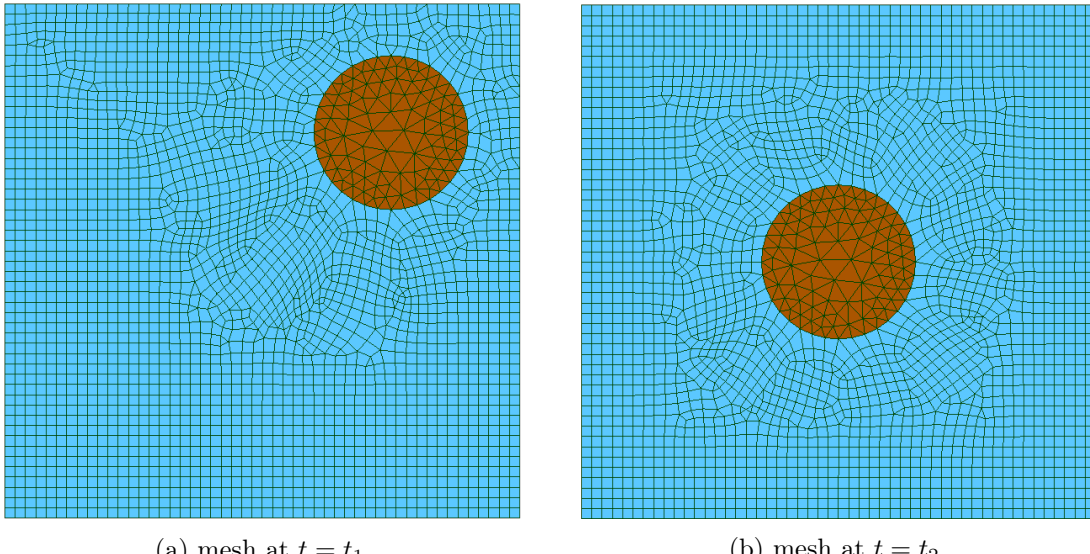


Figure 3.6. conforming mesh example

3.4.3 Data Mapping

When partitioned coupling is involved and the meshes are conforming but not node-to-node coincident, the challenge is to correctly map the data between the solid and the fluid sides.

This is a common situation as fluid and solid require a different mesh refinement at the interface.

The mapping procedure needs not only to find the closest available mesh point (or points) on the opposite mesh, but also to preserve mass and energy balance. Variables are basically mapped in two ways: *consistent* and *conservative* forms.

In the *consistent mapping* a value on a node of one grid has the same value of the corresponding node on another grid: that is, it reproduces the values on both meshes. In the *conservative form*, integral values are preserved between meshes. In an FSI problem, nodal forces are mapped in conservative form, while velocities or displacements are mapped in consistent form. An example is shown in Figure 3.7.

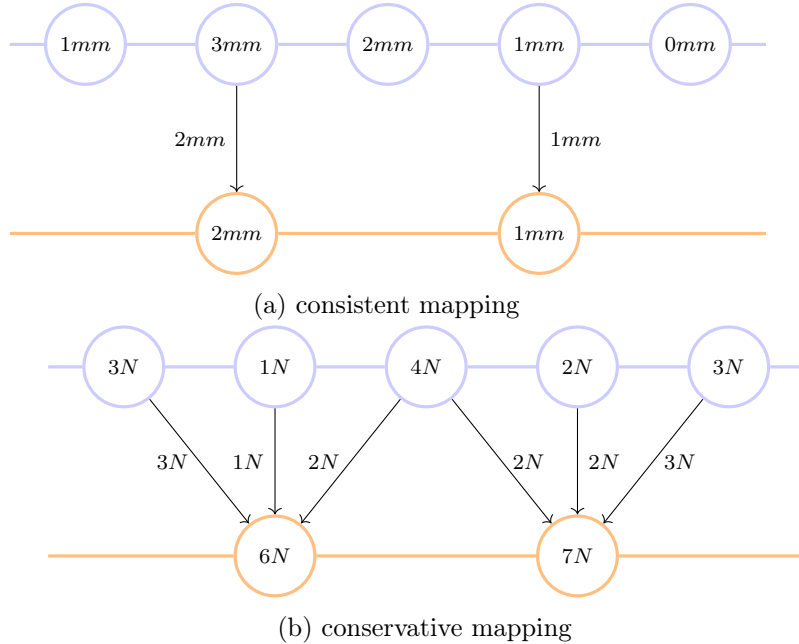


Figure 3.7. Examples of mapping data between non-coincident meshes: consistent (a) and conservative (b) schemes.

different mapping strategies can be implemented [43]:

- *Nearest Neighbor*: finds the closest point on the source mesh and uses its value for the target mesh. It does not require any topological information and is first-order accurate. It is the computationally easiest implementation and it is useful when interface meshes are coincident.
- *Nearest Projection*: projects the points of the target mesh on the source mesh, interpolates the data linearly and assigns the values to the target mesh. It requires topology information for the source mesh. The interpolation on the mesh elements is second order accurate.
- *Radial Basis Function (RBF)*: this method does not require topological information and works well on general meshes. The mapping uses radial basis functions centered at the grid points of the source mesh [44].

3.5 Stability: Added Mass Effect

When a solid moves or vibrates in a fluid domain, the interaction changes the way in which the structure behaves. There exist a vast variety of literature (e.g.: [45], [46], [47], [48]) describing the effects of FSI in terms of *added mass*, *added damping* or even *added stiffness* on a vibrating structure in function of fluid properties (e.g. density or viscosity), or flow properties (e.g. velocity), or geometry.

Besides the physical aspects of the interaction, some numerical issues arise when trying to simulate this kind of problems.

The numerical issue named **AME** is introduced here, as it is relevant for both strongly and weakly coupled partitioned approaches in the solution of FSI problems.

Weakly coupled algorithms give good results in aeroelasticity studies, but they are known to become unstable under certain conditions, in particular when fluid and structure densities are comparable ($M \approx 1$, see Section 2.3.4) and when the structure is particularly slender [49]. Under the same conditions, strongly coupled algorithms exhibit convergence problems.

For this reason, the mass ratio M is a suitable indicator to determine the kind of interaction between solid and fluid: when $M \ll 1$ (i.e. when the solid is much denser than the fluid), the interaction is weak, while when densities are comparable the interaction is strong and imposes some limits on the partitioned solution techniques.

The problem has been analyzed in literature by means of “toy FSI models” (in [49], [50] or [29]). Even though the number of parameters affecting stability is large and not completely understood in complex scenarios, all of the studies point out the mass-ratio M as the most relevant parameter.

A simplistic explanation of the phenomenon stems from the idea that at the interface, fluid and structure have no gaps (Section 2.2.4). For this reason, if the structure moves, also the fluid particles around it have to move: the acceleration of the surrounding fluid results in greater inertial forces and the structure appears more inert.

Added mass effect appears both in incompressible and in compressible fluid models, but with slightly different effects and implications.

3.5.1 AME in compressible regime

In compressible regime, using a weakly coupled algorithm which does not enforce mass and energy balance at the interface (see Section 3.2.1) imposes a limit to the mass ratio above which the simulation becomes unstable and the algorithm fails to find a solution [51].

A strongly coupled algorithm (Section 3.2.2) does not become unstable, but converges slowly: many subiterations are needed at each time step in order to reach the required convergence criteria (Section 3.3.3).

It can be shown that, in the compressible case, changing the time step of the partitioned simulation can be beneficial to the solution. The time step reduction to an arbitrarily small value cannot stabilize a weakly coupled algorithms when the stability criterion on the mass ratio is not met, but has an effect on strongly coupled ones [30].

A step size reduction can compensate a higher mass-ratio value [52]: the convergence of a strongly coupled algorithm improves proportionally to the time step reduction. At the theoretical limit of vanishing time step, the monolithic solution could be found.

3.5.2 AME in incompressible regime

AME is a much greater issue in incompressible regime than in compressible flows. A simple physical explanation of this fact could be as follows: a deformation of the structure results

in a perturbation of the fluid domain close to the structure, which then propagates through the rest of the fluid domain. In compressible models, the speed at which a perturbation propagates (speed of sound) has a finite value. For this reason the effect of a perturbation is spatially limited during a time step. In contrast, in an incompressible model, the speed at which the aforementioned perturbation propagates through the domain is infinitely large. A change in the geometry affects the whole domain without delay and impacts the whole domain at each time step [49].

It has been observed that loose coupling of fluid and structural part in the context of incompressible flow and slender structures frequently yields unstable computations [52]. However, strict stability limits exist also for strongly coupled algorithms. Those limits have a different relation to the time step with respect to compressible models.

Simulations show that reducing the time step may result in increased instability. The AME is inherent in the coupling itself: in sequentially staggered schemes the fluid forces depend upon predicted structural interface displacements rather than the correct ones and thus contain a portion of incorrect coupling forces. This contribution yields the instability [50].

Provided that the stability limit is not exceeded, implicit methods behave differently in incompressible regime: the number of subiterations required to reach convergence during a single time step increases when the time step decreases. Besides, achieving the monolithic solution limit is not guaranteed ([52], [30]).

These observations are consistent with the aforementioned physical explanation.

Chapter 4

Software Packages used in this work

This chapter illustrates the main software tools used in this work. First, the multibody dynamics solver *MBDyn* is shortly presented in Section 4.1. Then, the coupling library *preCICE* is introduced in Section 4.2.

4.1 MBDyn

MBDyn is free and open-source¹ general purpose Multibody Dynamics analysis software developed at the *Dipartimento di Scienze e Tecnologie Aerospaziali* of the University Politecnico di Milano.

Most of the information concerning MBDyn is taken from the official documentation given in the software website² and from the input manual³.

MBDyn allows to build a simulate multibody system, which⁴ is the study of the dynamic behavior of interconnected rigid or flexible bodies, each of which may undergo large translational and rotational displacements.

MBDyn can simulate linear and non-linear dynamic of rigid and flexible bodies (including geometrically exact and composite-ready beam and shell finite elements, component mode synthesis elements, lumped elements) subjected to kinematic constraints, external forces and control subsystems [55]. MBDyn has been developed to serve as an analysis tool for rotorcraft research and can simulate essential fixed-wing and rotorcraft aerodynamics.

As explained more in detail later, MBDyn is open to be connected to other software components to perform multiphysics simulations. In particular, it is possible to pass externally computed forces and to steer the multibody simulation from an external API: this feature has been particularly useful in building and *adapter* to couple MBDyn with the library preCICE (see Chapter 5).

In this section we give a short introduction to some of the relevant features of MBDyn, starting form basic information on the input file syntax (Section 4.1.1), and the output files (Section 4.1.8). Then some of the elements relevant for the description of the models used in the this work are presented: nodes (Section 4.1.2), beam elements (Section 4.1.4), bodies (Section 4.1.5) and forces (Section 4.1.7).

¹the software is available through a public git repository gitlab.polimi.it/Pub/mbdyn

²MBDyn website: mbdyn.org

³a copy can be found at the following link [[input manual](#)] or in the code repository

⁴see Wikipedia entry: [Multibody system](#)

4.1.1 Basic syntax

MBDyn is a command line tool and can be generally started from a terminal passing an input file containing all the information required to perform a simulation.

The input files is structured in blocks and each block has a syntax described in Backus Naur form in the input manual.

```

1 begin : data ;
2     # select a problem
3     problem : initial value ;
4 end : data ;
5
6 begin : initial value ;
7     # problem-specific data
8 end : initial value ;
9
10 begin : control data ;
11     # model control data
12 end : control data ;
13
14 begin : nodes ;
15     # nodes data
16 end : nodes ;
17
18 begin : elements ;
19     # elements data
20 end : elements ;

```

Listing 4.1. MBDyn input file structure

As illustrated in listing 4.1, statements are logically divided in blocks. Each block is opened by a `begin` statement and it is closed by an `end` statement.

The sequence of relevant valid blocks is:

- `data`: defines the kind of problem to be solved by the analysis. The most significant one is `initial value` and is already defined in the example.
- `type of problem`: block takes the name of the problem defined in the data block (`initial value` in this case) and contains all the information required by the integration method to perform the desired simulation (e.g. simulation type, time step, number of iterations, tolerance ...).
- `control data`: mostly contains information about the problem that is required to ensure that a consistent model will be generated (i.e. the number of nodes, elements, forces...).
- `nodes`: The nodes block contains all the nodes required by the simulation. They are defined as the entities that make degrees of freedom available to the simulation, so they must exist before any element is generated.
- `elements`: contains all the elements. They are defined as the entities that generate equations using the degrees of freedom provided by the nodes.

We focus now on the main entities of a MBDyn simulation, namely nodes and elements. A detailed example of the input file used in most simulations in this work can be found in Appendix D.1.

4.1.2 Nodes

Nodes are the basic blocks of a model: they instantiate kinematic degrees of freedom and the corresponding equilibrium equations. There can be different type of nodes in MBDyn, we focus here on **structural nodes**.

Structural nodes can have 3 degrees of freedom, thus describe the kinematics of point mass motion in space (position) or 6 DoFs (position and orientation), and thus describe the kinematics of rigid-body motion in space.

Each node has a unique label and can be specified in different ways:

- **static**: this keyword instantiates only equilibrium equations (force for 3 DoF nodes or force and moment for 6 DoF nodes)
- **dynamic**: this also instantiates momentum (3 and 6 DoFs) and momenta moment (6 DoFs)

Also **modal** and **dummy** nodes exist, but are beyond the scope of this work.

Nodes are the starting point to define the elements of a simulation.

4.1.3 Elements

Elements constitute the components of the multibody model. Each has a unique numerical label and is connected to one or more nodes. They write contributions to nodes equations and represent *connectivity* and *constitutive properties*.

There exist many types of elements in MBDyn, we focus here on the ones used in the FSI simulation: beams, bodies, joints and forces.

4.1.4 Beam elements

As briefly introduced in Section 2.2.3, when simulations involve slender bodies, it is particularly interesting to use a 1D finite element model together with a form of mapping between the interface (wet surface) and the model to exchange kinematics and dynamics information. This can be performed in MBDyn using **beam** elements (described in this section) and the **external structural mapping** element (described in Section 4.1.7).

MBDyn models slender deformable components by means of finite volume **beam** elements with a high level of flexibility.

The beam element is defined by its nodes and a reference line; although 2 and 3 nodes beam elements are implemented, only **beam3** are considered here (Figure 4.1). Each node of the beam is related to a **structural node** (node 1 to 3 in Figure 4.1) by an offset (o_1 to o_3) and a relative orientation.

The Finite Volume approach described [17] is used to model the beam element. It computes the internal forces as functions of the reference line strain and as functions of the orientation at the *evaluation points* (i.e. integration points, point I and II in Figure 4.1) that are between nodes 1 and 2, and between nodes 2 and 3 (at $\xi = -1/\sqrt{3}$ and $\xi = 1/\sqrt{3}$ of a non-dimensional abscissa $-1 \leq \xi \leq 1$ ranging from node 1 to node 3).

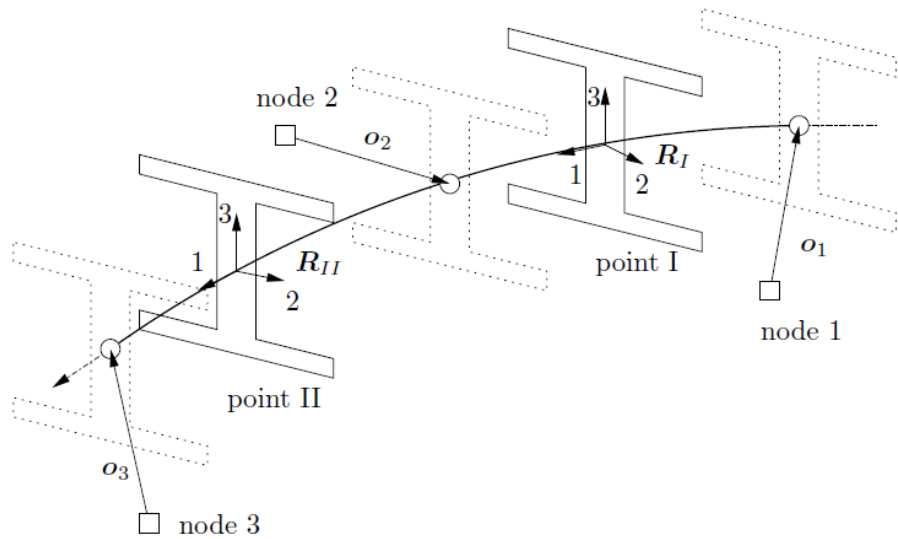


Figure 4.1. MBDyn beam model, taken from the input manual

A 6D constitutive law is defined at each evaluation point: it relates the strains and the curvatures of the beam (and their time derivatives) to the internal forces and moments at the evaluation points in the form:

$$\begin{Bmatrix} F_x \\ F_y \\ F_z \\ M_x \\ M_y \\ M_z \end{Bmatrix} = f \left(\begin{Bmatrix} \epsilon_x \\ \gamma_y \\ \gamma_z \\ \kappa_x \\ \kappa_y \\ \kappa_z \end{Bmatrix}, \begin{Bmatrix} \dot{\epsilon}_x \\ \dot{\gamma}_y \\ \dot{\gamma}_z \\ \dot{\kappa}_x \\ \dot{\kappa}_y \\ \dot{\kappa}_z \end{Bmatrix} \right) \quad (4.1)$$

Using the convention of *x-axis* as beam axis we have:

- F_x : axial force component,
- F_y and F_z : shear force components,
- M_x : torsional moment component,
- M_y and M_z : bending moment components,
- ϵ_x : axial strain component,
- γ_y and γ_z : shear strain components,
- κ_x : torsional curvature component,
- κ_y and κ_z : bending curvature components,
- f : constitutive law.

Beam section Constitutive Law

In dynamic simulations, linear elastic or viscoelastic laws are generally used, even though nonlinear laws can be used. Focusing on linear laws, MBDyn allows the user to define every constitutive laws, going from an isotropic beam section to a fully anisotropic one: in fact the entire 6×6 constitutive matrix can be provided. It is up to the user to define a valid law as the matrix must satisfy some constraints, e.g. it must be symmetric. The simplest case of linear elastic constitutive law is represented in Equation 4.2, in which a diagonal matrix relates internal forces to strain and curvature of the beam.

$$f = \begin{bmatrix} EA & 0 & \dots & 0 \\ \chi GA & \chi GA & & \\ & GJ_p & \vdots & \\ sym. & EJ_y & 0 & \\ & & EJ_z & \end{bmatrix} \cdot \begin{Bmatrix} \epsilon_x \\ \gamma_y \\ \gamma_z \\ \kappa_x \\ \kappa_y \\ \kappa_z \end{Bmatrix} \quad (4.2)$$

The simplest case of linear viscoelastic law uses a proportional factor to be applied to the stiffness matrix of Equation 4.2 such that: *viscosity* = *factor* · *stiffness*.

In the context of FSI simulations, this feature allows the user to define a section constitutive law that is independent from the shape of the beam itself. Thus the aerodynamic aspects and the structural aspects are handled by two distinct elements of the model: i.e. the interface mesh defines the aerodynamic forces and the beam constitutive law defines the structural properties.

Some studies about the definition of general beam section constitutive properties (*composite beam section characterization*) are available in the literature: an early work can be found in [56], a review in [57] or an application to wind turbine blades in [58].

4.1.5 Bodies

The **body** element describes a lumped rigid body when connected to a regular, 6 DoF structural node, or a point mass when connected to a rotationless, 3 DoF structural node. It can be used in connection with a structural element to give inertial properties: for example, in a **beam** element (see Section 4.1.4), 2 bodies are added to the evaluation points of the beam to account for lumped inertia of each portion in which the beam is divided.

4.1.6 Joints

structural nodes can be constrained by means of **joint** elements. Many different joints are available. In the FSI model the following types of joints are used:

- **clamp**: grounds all 6 DoFs of a node in an arbitrary position and orientation
- **total joint**: allows to arbitrarily constrain specific components of the relative position and orientation of two nodes [59]

4.1.7 Forces

The **force** element is a general means to introduce a right-hand side to the equations. Structural forces are specific to structural nodes and have three components that may depend on arbitrary parameters and a location in space.

MBDyn allows to communicate with an external software that computes forces based on information on the kinematics of the model. This feature is at the basis of the development of the *adapter*. The following elements can be used.

External Structural

The **External Structural** element allows to communicate with an external software that computes forces applied to a pool of **nodes** and may depend on the kinematics of those nodes. In this case forces are applied directly to the nodes. In a FSI model, this would require that each interface mesh node has a correspondent MBDyn structural node.

External structural mapping

This element is similar to the previous one, but the nodes where forces are applied and the kinematics is computed depend on structural nodes through a linear mapping. This element has been used in building the adapter. In order to use the **external structural mapping** elements, the following steps have to be performed:

1. a set of points is defined for each **structural node** according to a specified offset. Those points are used to compute the kinematics of the interface points, originating from the rigid-body motion of the structural nodes
2. before the simulation, a linear mapping matrix H is generated starting from the position of the above points and the interface mesh points (this is performed by means of an **Octave** script which is part of MBDyn). The matrix is stored in sparse form
3. the mapping matrix is used during simulation to map forces and kinematics between the interface nodes and the structural nodes

The constant matrix mapping allows to compute the position and the velocity of the *interface* points as function of the points rigidly offset from structural nodes:

$$x_{\text{interf}} = Hx_{\text{mbdyn}} \quad (4.3a)$$

$$\dot{x}_{\text{interf}} = H\dot{x}_{\text{mbdyn}} \quad (4.3b)$$

The same matrix is used to map back the forces onto structural nodes based on the preservation of the work done in the two domains:

$$\delta x_{\text{mbdyn}}^T \cdot f_{\text{mbdyn}} = \delta x_{\text{interf}}^T \cdot f_{\text{interf}} = \delta x_{\text{mbdyn}}^T \cdot H^T \cdot f_{\text{interf}} \quad (4.4)$$

which implies

$$f_{\text{mbdyn}} = H^T f_{\text{interf}} \quad (4.5)$$

When performing an FSI simulation with strong coupling (see Section 3.3), MBDyn may need to compute multiple iterations of the same time step in order to reach global convergence. This is performed by using the keyword **tight** in the coupling of the **external structural mapping**. The computation and the communication pattern is the following:

1. MBDyn sends the predicted kinematics for time step k
2. MBDyn receives a set of forces sent by the external peer; those forces are computed based on the kinematics at iteration j

3. MBDyn continues iterating until convergence using the last set of forces until, while reading the forces, it is informed that the external peer converged. this implies that MBDyn solves the kinematics for time step k at iteration j using the forces evaluated by the external solver for iteration $j - 1$

The communication with the external software, in our case the adapter itself, is performed by means of a local unix socket.

4.1.8 Simulation output

There are a bunch of output files regarding a simulation performed with MBDyn. the name of those files is specified with the option `-o` (otherwise the name is the same as the input file) and the extensions are:

- `.out`: for miscellaneous output
- `.mov`: for kinematic output of the nodes
- `.ine`: for the dynamic output of the nodes
- `.frc`: for the output of force elements
- `.act`: for the output of beam elements
- `.jnt`: for the output of joint elements

The `.out` file contains information regarding the simulation iterations residuals while other files are described in more detail in Appendix D.2.

4.2 preCICE

The main information concerning preCICE is taken from the official documentation: that is [53] and [43]. The preCICE website is also a source of documentation⁵.

The open-source⁶ software library preCICE provides the components to connect traditional single-physics solvers and create a partitioned multi-physics simulation (e.g. fluid-structure interaction, conjugated heat transfer, solid-solid interaction, etc.). It aims at coupling existing solvers in a partitioned black-box manner (see Section 3.2): only minimal information about the solver is available and connection involves just interface nodes. In order to be flexible and easily implemented, the impact on the solvers should be as minimal as possible: for this reason, preCICE offers a high level application programming interface (API) (Section 4.2.5) different languages, such as C/C++, Fortran and Python. The ability to switch among different solvers is advantageous as it provides a lot of flexibility in developing and testing new coupled components.

In a nutshell, preCICE simply affects the input and observes the output of the solvers (called *participants*). The required data and control elements are accessed using an *adapter*, i.e. a “glue code” that is attached to the corresponding solver and communicates the information with the library.

preCICE performs all the actions required to perform a coupled simulation: implements the coupling strategy and convergence criteria (Section 4.2.1), the communication between the participants (Section 4.2.2), the mapping of data between meshes (Section 4.2.3). preCICE is configured by means of an extensible markup language (XML) file (Section 4.2.4).

⁵www.precice.org

⁶The code can be accessed via Github: github.com/precice/precice

4.2.1 Implemented coupling strategies

The *partitioned approach* (Section 3.2) is obviously the coupling strategy adopted by preCICE. It allows both *explicit* (Section 3.2.1) and *implicit* coupling (Section 3.2.2). The possible variants are four:

- **serial-explicit**: a serial, weakly coupled algorithm (Figure 3.3a). The first solver uses the second solver solution at the last time step to compute its current solution. In contrast, the second solver needs the current first solution to compute its solution at the same time instance. The order of execution is user defined.
- **parallel-explicit**: both solvers advance in parallel (Figure 3.3b) and exchange data at the end of each time step, resulting in a less stable procedure. The bottleneck of this procedure is related to the most time consuming solver.
- **serial-implicit**: a serial strongly coupled algorithm (Figure 3.4a). The user can define the order of execution, the coupling algorithm (basically all the algorithms described in Section 3.3) and its parameters in a section of the configuration file named `acceleration`.
- **parallel-implicit**: again both solvers execute in parallel (Figure 3.4b). An implicit scheme modifies the result of the fixed-point iteration on both data [29].

4.2.2 Communication strategies

All the participants need to communicate with each other, in order to share coupling data. Each solver might be executed in multiple processes or on different nodes of a cluster (*intrafield parallelism*). This form of parallelization requires efficient forms of communication between the solver in order to avoid that data transfer becomes a bottleneck during a simulation.

preCICE implements a fully parallel process-to-process communication approach [54] using:

- *message passing interface (MPI)*: available on most scientific computers, it may be necessary to adapt/change the MPI versions of the respective single-physics solvers or of preCICE.
- *Transmission Control Protocol/Internet Protocol (TCP/IP)*: popular means of network communication and free of incompatibilities between versions.

As to performances, MPI is the best technique especially when a high numbers of nodes is present. Anyway, socket communication is quite as fast, such that both techniques are very well-suited for larger-scale simulations [53].

In each solver, executed in parallel, one "master" process is defined to manage the progress of the simulation. No central node is required. The participating processes use asynchronous point-to-point (M:N) communication. The channels are static and defined in the beginning of the simulation. This sets a limit in using preCICE with dynamically adaptive meshes or immersed boundaries.

4.2.3 Data mapping

Even if volume coupling is possible, preCICE is mainly designed to couple simulations that share a common surface boundary (namely *conforming meshes*, in the terminology used in Section 3.4.2). The meshes don't need to be node-to-node coincident, so it is necessary to map variables at the interface, preserving the geometry (i.e. no gaps or superpositions at the interface) and the mass and energy balances.

The user defines which data are shared by each *participant* (i.e. solver) and the way data is shared in the configuration section named `mapping`. As described in Section 3.4.3, two kinds of mapping are available:

- **consistent**: the value of a node at the one grid is the same as the value of the corresponding node (or nodes) at the other grid. In general the number of fluid nodes is at least the same or, more often, exceeds the nodes of the structure, so a single structural node is associated to several fluid nodes. The mapping of displacements is consistent: in the simplest case, all fluid nodes experience the same displacement of a single solid node, otherwise an interpolation is performed (see Section 3.4.3 for a detailed explanation and Figure 3.7a for an example).
- **conservative**: in the same conditions as before, forces are mapped from multiple fluid nodes to a single solid node in an additive manner (see Section 3.4.3 and Figure 3.7b for an example).

Along with the mapping strategy, a method must be defined: `nearest-neighbor`, `nearest-projection`, `rbf` (see Section 3.4.3). For the latest method, preCICE implements a wide variety of basis functions, with Gaussian and thin plate splines being the most widely used.

4.2.4 Configuration

In order to run a multi-physics simulation with preCICE, all the participating, *adapted* solvers have to be started (the order is irrelevant). Some configuration files are needed:

- each adapter in general needs its own configuration file. It normally contains information about the boundaries (wet-surface) used for the coupling, names of exchanged data, mesh and the name of the common preCICE configuration file, plus other parameters, specific to the adapter. The one for the MBDyn adapter will be described in more detail in Chapter 5 and in Appendix B.
- preCICE configuration file: This is an XML file and each participant points at it. It defines all the information relevant to the simulation:
 - type and name of exchanged data and meshes over which those data are passed
 - which solvers participate in the simulation, which data produce or consume, and how the mapping is performed
 - how solvers communicate among each other
 - coupling scheme and all the necessary information

The structure of a preCICE configuration file is illustrated in Appendix A.

4.2.5 Application Program Interface

A solver, in order to be coupled to preCICE, must either provide a way to access its core functions (e.g. initialize, set input data, read output, advance...) from outside the code (via API, socket, etc...) or it has to be slightly modified in order to perform all the operations required by the preCICE library.

The result is an *adapter*, which can be the modified and recompiled original solver, or a standalone piece of code that communicates with the original unmodified solver on one side and with the preCICE library on the other. The adapter groups together all the calls to the preCICE methods from its API (a list of the API calls, taken from the official documentation, can be found in Appendix C.1).

While preCICE is written in C++, there exist APIs also for other languages, so that the adapter can be written also in C, Fortran or Python.

A coupling consists of a configuration and an initialization phase, multiple coupling advancements and a finalization phase: the general structure of an adapter can be found in C.2.

4.2.6 Official Adapters

This work introduces an adapter to preCICE for MBDyn. It is based on previous MBDyn adapters and on the examples given on the preCICE website⁷. Official adapters are currently available for several free solvers, e.g. CalculiX, Code-Aster and SU2. Also some closed-source software packages are supported. A (maybe outdated) list of official adapters can be found in [2], while the current status of coupled codes can be found at the following link: [preCICE adapters](#).

⁷github.com/precice/precice/wiki/Adapter-Example

Chapter 5

MBDyn Adapter and its integration

To prepare an existing simulation code for coupling, preCICE has to be integrated with the solver, using API described in Section 4.2.5 and in Appendix C.1. The "glue-code" required for this operation is called *adapter*, as depicted in Figure 5.1.

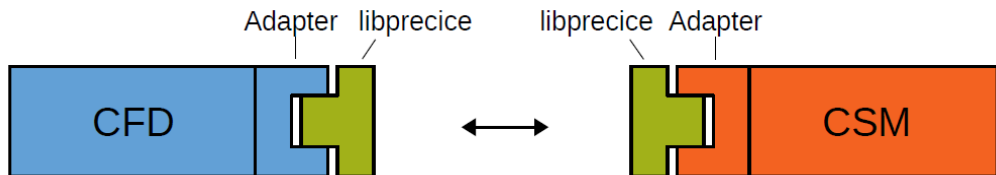


Figure 5.1. Coupling CFD to CSM via preCICE. The existing solver code, the adapter and the linked library are highlighted (image taken from [2]).

5.1 Design of the adapter structure

In order to couple MBDyn with preCICE a C++ adapter has been implemented within the scope of this work. The *adapter* needs to be integrated with both the MBDyn solver and the coupling library. The two connections are distinct but strictly interconnected. The adapter has the advantage of being completely independent from both the preCICE library and MBDyn. The first connection is achieved via the API given by the library `libprecice.so`, the second connection exploits the API given by MBDyn through its library `libmbc.so`.

5.2 Structure of the code

The code for the adapter is available through a public git repository¹. The code is conceptually divided in two classes, as illustrated in Figure 5.2.

The main class is `MBDynAdapter`, which implements the functions given by the preCICE interface. It has access to the class `MBDynConnector` which takes care of all the aspects regarding MBDyn. Attributes, methods and operations of each class are briefly described in the following sections.

¹[mbdyn-beam-adapter](#)

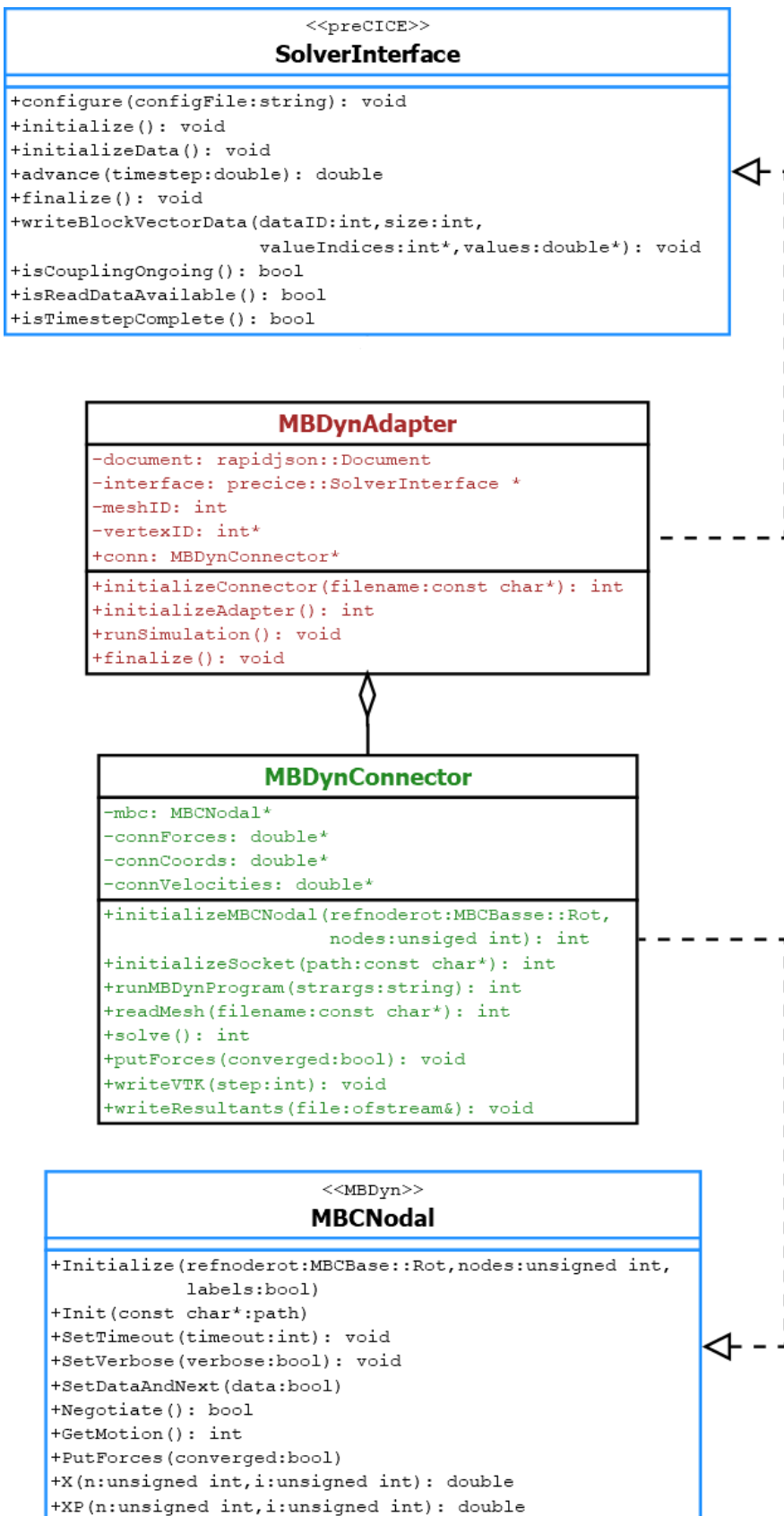


Figure 5.2. MBDyn adapter class structure

5.2.1 Class MBDynAdapter

The file `MBDynAdapter.h` and its source file `MBDynAdapter.cpp` implements all the methods required to perform and FSI simulation with MBDyn as the solid solver. The basic steps are:

1. prepare the MBDyn solver,
2. prepare the interface,
3. provide access to the mesh and initialize the coupling data,
4. steer the coupled simulation,
5. finalize the simulation.

Initialization

In the initialization phase, the instance of `MBDynAdapter` gets a `json` file (see Section 5.3) that contains all the parameters useful for the simulation. Then it instantiates the `MBDynConnector` (see Section 5.2.2) which takes care of all the operations concerning MBDyn: in particular starting the simulation the creating an instance of `MBCNodal` in order to have access to the simulation.

In the next step an instance of `precice::SolverInterface` is initialized and configured with all the relevant information data:

- preCICE configuration file (see Section 4.2.4 and Appendix A).
- *participant* (i.e. solver) name
- information regarding the data to be read and written

The next initialization step concerns the definition of the interface mesh. The data concerning the vertices is stored in the `MBDynConnector` to be used to plot the output and is passed to the `SolverInterface` to define the wet surface nodes. The mesh nodes are stored in the same text file that is used by MBDyn to build the `external structural mapping` information (see Section 4.1.7). This means that the MBDyn mapped points coincide with the interface mesh on the structural side (note that it doesn't have to be the same mesh of the fluid side, as preCICE can map non identical meshes, as described in 4.2.3). The suitable size of memory is then initialized to contain the coupling information: mainly *displacements*, to be written on the preCICE interface, and *forces*, to be read from the interface.

Execution

The simulation phase of the adapter follows the steps briefly described in Section 4.2.5 and in Appendix C. The most important elements of the code are illustrated in listing 5.1.

The main execution phases include:

1. read initial checkpoint (i.e. reload state if previous iteration did not converge) [line 6]
2. read *forces* from interface (i.e. get the current available fluid solution) [line 10]
3. copy forces to MBDyn: this step is performed as forces can be scaled by a user specified coefficient during the initial part of the simulation, see Section 5.3 [line 14]
4. make MBDyn connector solve the current simulation time step [lines 16-18]

5. make MBDyn connector compute force and moment resultants [line 22]
6. write the *displacements* computed at the current iteration of the current time step to preCICE in order to perform coupling [line 25]
7. get the interface time step (this would be mandatory in case of different time steps between fluid and solid) [line 28]
8. check if the current time step converged [line 31]: notify MBDyn [lines 35 and 38]. If converged, update time, iterations and write output data (see Section 5.4).

```
1 void MBDynAdapter::runSimulation(){
2     // Start coupling:
3     while (interface->isCouplingOngoing()){
4
5         if(interface->isActionRequired(cowic)){
6             interface->fulfilledAction(cowic);
7         }
8
9         // read forces from interface
10        interface->readBlockVectorData(forceID, vertexSize, vertexIDs, forces);
11
12        // copy forces to connector with coefficient
13        conn->computeForces(forces,coeff);
14
15        // MBDyn solves the current iteration
16        if(conn->solve()){
17            conn->writeVTK(iteration);
18            break;
19        }
20
21        // compute force and moment resultants on the structure
22        conn->computeResultants(true, root);
23
24        // write data to interface
25        interface->writeBlockVectorData(displID, vertexSize, vertexIDs,
26                                         displacements);
27
28        // advance time step
29        precice_dt = interface->advance(precice_dt);
30
31        // Checkpoint
32        if(interface->isActionRequired(coric)){
33            // timestep not converged
34            interface->fulfilledAction(coric);
35            // tell MBDyn that time step not converged
36            conn->putForces(false);
37        }else{
38            // timestep converged
39            conn->putForces(true);
40            iteration++;
41        }
42    }
43}
```

```

40     t += precice_dt;
41     conn->writeVTK(iteration);
42 }
43 }
44 }
```

Listing 5.1. MBDynAdapter simulation execution

Finalization

In the finalization phase all the objects used during the simulation are closed and memory is released.

5.2.2 Class MBDynConnector

The class `MBDynConnector` takes care of all the operations related to MBDyn and the structural side of the simulation.

Initialization

The instance of `MBDynConnector` is initialized within the `MBDynAdapter` and some different tasks are performed in this phase.

The first task is to read the mesh of interface points. The mesh file location is passed through the input file: to avoid too much duplication, it is the same file used by MBDyn to build the mapping matrix before the simulation (see Section 4.1.7). The mesh file contains information concerning the interface points and the connectivity. The (x, y, z) coordinates are passed to preCICE to build the structural part of the interface mesh. The same points, together with the connectivity, are stored in the `MBDynConnector` and are used to write the output in *VTK* format during the simulation (see Section 5.4).

The following task consists in starting MBDyn. The input file location is passed through the input file and a separated process is spawned with the parameters required to run an MBDyn program. Upon a correct initialization, the MBDyn simulations hangs waiting for an external connection (i.e. the `external structural mapping`).

Finally, an instance of `MBCNodal` is created to take care of the communication with MBDyn: a socket is opened and the communication is initialized.

Execution

During the execution phase, `MBDynConnector` steers the simulation on the MBDyn side. Some of the actions have been already introduced in listing 5.1:

- send *forces* to the `external structural mapping` points
- perform the simulation step
- retrieve *displacements*
- inform MBDyn that the time step has converged or not

If the time step has converged and at a user defined interval, the simulation data are saved.

5.3 Input parameters

Some input data are needed in order to perform a simulation. Such data are stored in a json file². The file is given as input in the form:

¹ `mbdyn-beam-adapter -f config.json`

An example of input file is given in Appendix B. The type of data can be related to different aspects of the simulation:

1. preCICE

- `precice-config`: the interface must be initialized with the *preCICE configuration file* (see Section 4.2.4 and Appendix A)
- `readDataName`: label of the data to be read from the interface (typically forces)
- `writeDataName`: label of the data to be written (typically displacements)
- `participantName`: label the participant in the FSI simulation
- `meshName`: label of the interface mesh in the FSI simulation

2. MBDyn

- `mesh`: location of the file containing the points mapped in MBDyn
- `mbdyn-input`: input file name to be passed to MBDyn
- `node-socket`: name of the socket to exchange data between the adapter and MBDyn (the name has been made configurable to allow different simulations to run in parallel using different sockets: the user must take care to use the same name in the MBDyn input file)
- `mbdyn-output`: location and prefix of all MBDyn related output files (see Section 4.1.8 and Appendix D.2).

3. Simulation

- `displacement-delta`: Boolean value that tells the adapter whether to pass the relative displacement between two consecutive iterations or the displacement from the initial configuration. This is mainly due to compatibility with different fluid adapters (e.g. the current version of the *SU2 adapter* requires delta displacements)
- `iterstart`: the following four parameters are used to give progression to the forces applied to the structure (Figure 5.3 gives an example of the behavior). The purpose is to ease the beginning of the simulation, letting the flow settle and avoiding initial spikes in the application of the forces that could result in a diverging simulation. The current parameter tells `MBDynConnector` how many iterations to perform with a reduced starting coefficient (200 in the example)
 - `coeff0`: this value is the initial coefficient (0.1 in the example)
 - `period`: this value is the number of iterations to reach 1 (600 in the example)
 - `ramp-type`: label defining the type of ramp. A linear law or a $1/2 \cdot (1 - \cos)$ law can be used

²see for example json.org for some information about the syntax

4. Output (see Section 5.4 for some more details)

- **write-interval**: value that defines how often the `MBDynConnector` writes output data
- **resultant-file**: location of the file containing the resultant and moment of the fluid forces applied to the structure.
- **root-coords**: vector containing the coordinates of the point about which the resultant moment has to be computed
- **vtk-output**: location and prefix of the output file.

5. Some parameters are used for debug purposes and might be removed in future releases

- **pre-iteration**: number of simulation iterations performed by MBDyn before coupling with the fluid solver. This can ease the initial coupling in case the definition of the structural model isn't in equilibrium
- **read-coords**: Boolean value used to read the mapped points coordinates back in the adapter from MBDyn instead of reading the mesh file.
- **every-iteration**: Boolean value used to force the adapter to write output data at each coupling iteration

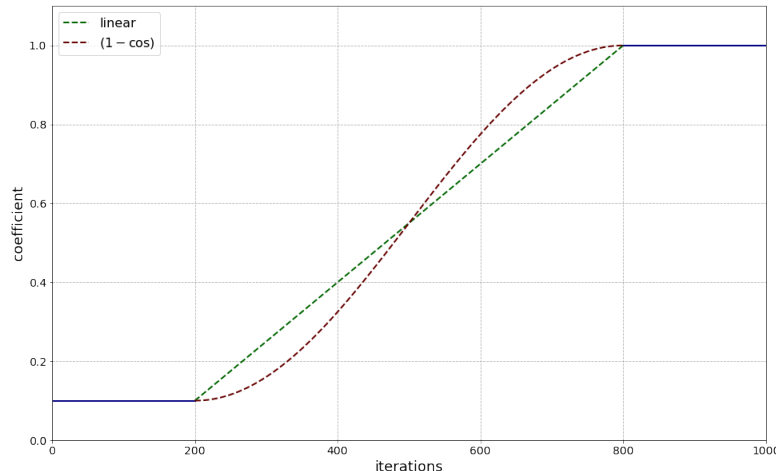


Figure 5.3. Coefficient applied to nodal forces at beginning of simulation

5.4 Output results

Besides the output strictly related to preCICE, concerning information about convergence and number of iterations, or the output strictly related to the MBDyn solution (see Appendix D.2), the adapter gives two types of output.

The information concerning the interface mesh points is saved in `vtu` file format, which is a binary XML VTK file format used to store data on unstructured grids of points. A sequential number corresponding to the current iteration is appended to the name of the file

so that any visualization software (e.g. *ParaView*³) can load the whole dataset as a time series. Each file contains the following vector data:

- displacement
- displacement delta
- velocity
- nodal force

for each node. An example of visualization is given in Figure 5.4. For debug purposes also the area and the normal of each cell can be saved.

output: VTK and resultants

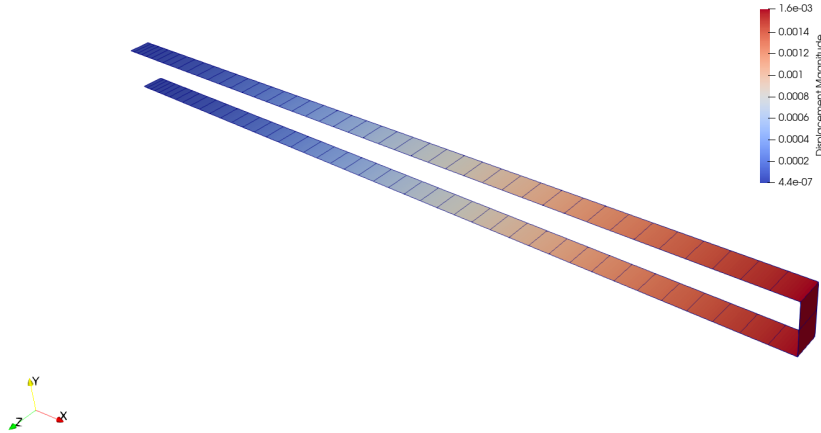


Figure 5.4. Output data in VTU format

The second output file contains the resultant and the moment applied to the structure by the fluid forces.

Each line of the file has the form:

$t \cup F_x \cup F_y \cup F_z \cup M_x \cup M_y \cup M_z \cup c$

where t is the current time step, F_x, F_y, F_z are the components of the resultant, M_x, M_y, M_z are the components of the moment (the point is defined in the input file) and finally c is the coefficient applied to the nodal forces (see Figure 5.3).

³paraview.org

Chapter 6

Validation Test Cases

6.1 Introduction

In order to validate the coupling adapter developed in this work, a set of test cases have been simulated, which are supposed to qualitatively and quantitatively confirm the physically correctness of the implementation.

The validation has been carried out in different steps: the first task (section 6.2) consisted in validating the MBDyn model that has been used throughout the simulations and verifying that the implementation of the coupling works as expected.

The second step aimed at comparing the results obtained performing an FSI simulation with MBDyn with another structural solver, both in compressible and in incompressible regime (Sections 6.3 and 6.4).

Then, some results obtained from FSI simulations coupling MBDyn with OpenFOAM, have been compared with some benchmarks present in literature. At first, the problem described in [10] has been considered (see Section 6.5): it is composed of a square bluff body with a trailing flap. It is characterized by a mass ratio (see Section 2.3.4) of $1.18 \cdot 10^{-3}$, this turned out to be a fundamental parameter for the convergence of simulations, and has been extensively analyzed in the subsequent sections.

One set of well-known benchmarks in FSI literature are the three Turek-Hron FSI test cases described in [60]. Those cases are characterized by the same domain (a round cylinder with a trailing flap) and the same fluid properties. Changes impact only fluid velocity and structural properties (in particular ρ, E).

At first, the so-called FSI2 benchmark (characterized by a mass number of 0.1) has been considered (Section 6.6). This benchmark, together with the previous one, shows the validity of the adapter and its potential use in FSI simulations.

Finally, the FSI3 benchmark has been extensively analyzed (Section 6.7). It has a mass number of 1 and, up to now, it hasn't been possible to find a suitable set of coupling parameters that can make this case converge when coupled with MBDyn.

It appears that the added mass effect (see Section 3.5), plays a dominant role in the convergence of a FSI problems with MBDyn. For this reason, a sensitivity analysis has been performed on the FSI3 problem setup (Section 6.8). In particular, flow velocity, fluid density and solid stiffness have been varied in order to gain some insight about the range of parameters, and adimensional numbers that must be considered to understand how critical a simulation can be.

Each section starts with a short description of the test case, including the most relevant parameter: e.g. the fluid domain geometry and discretization, structural and coupling parameters. Finally some results are presented, together with the coupling performances.

The meshes for all test cases have been generated with the free software *Salome*¹. Files for MBDyn interface points have been generated by a Python script running within the *Salome* environment. The script is part of the software made for this work.

6.2 Dummy fluid solver

The first task implemented to validate the adapter consisted in developing a simple *dummy fluid solver*: i.e. a software component connected to the coupling library preCICE with the simple task to apply forces to user-defined nodes on the structure and read back the displacements of the interface nodes.

This approach allowed first to validate the MBDyn model with the `external_structural_mapping` component (see Section 4.1.7) and the correct data exchange between preCICE and the adapter.

The *dummy solver* has been written in Python and it is part of the software package in this work.

A MBDyn cantilever beam model composed of 5 `beam3` elements (see Section 4.1.4) has been written to perform this test, as depicted in Figure 6.1. This requires a total of 11 `node` elements to define the structure.

The beam section is uniform and rectangular ($w \times h$) and the physical properties (eg. ρ, E, ν) are constant throughout the beam length.

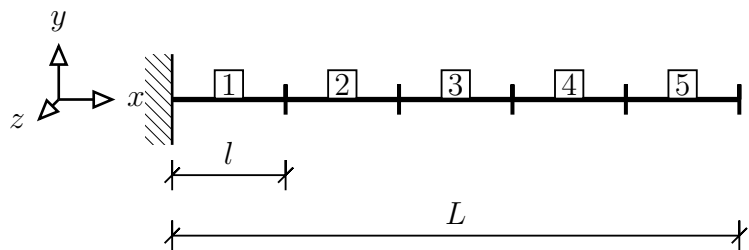


Figure 6.1. cantilever made of 5 beam elements

The inertia of the structure is provided by 2 `body` elements (see Section 4.1.5 attached to the second and third nodes of each beam (see Figure 4.1). The center of gravity of each body is offset by $-l/4$ in x-direction (where l is the length of the single beam element). Each body has the following inertial properties (see Figure 6.2):

$$m = \rho w h \frac{l}{4} \quad I = \frac{m}{12} \begin{bmatrix} h^2 + w^2 & 0 & 0 \\ 0 & \frac{l^2}{16} + w^2 & 0 \\ 0 & 0 & \frac{l^2}{16} + h^2 \end{bmatrix} \quad (6.1)$$

The first node of the structure is clamped (to implement the cantilever constraint), while all other joints are constrained to move in the $x - y$ plane and rotate only around the $x - axis$ so that the structure can move only in the $x - y$ plane. The interface mesh is represented in Figure 6.3. Only the connectivity elements belonging to the $x - z$ and $y - z$ plane are represented, but it does not affect the behavior of the structure.

The model has been loaded by a concentrated load on two tip nodes (Figure 6.4a) and with an equivalent distributed load on the nodes belonging to the upper surface (Figure 6.4b).

¹salome-platform.org/

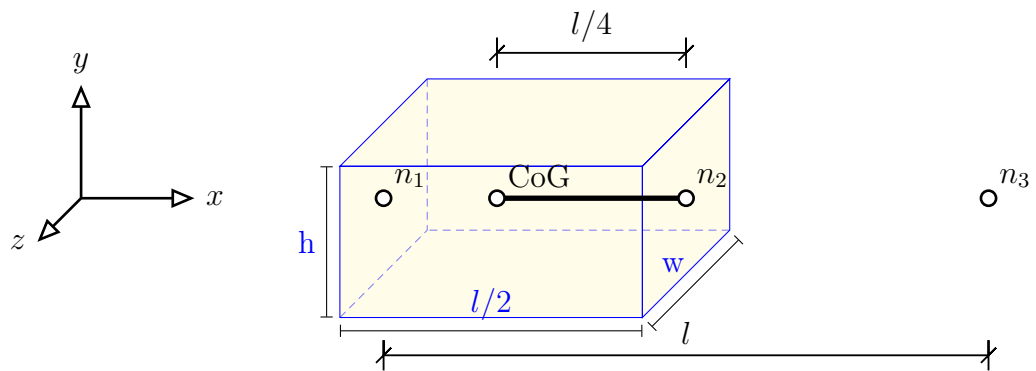
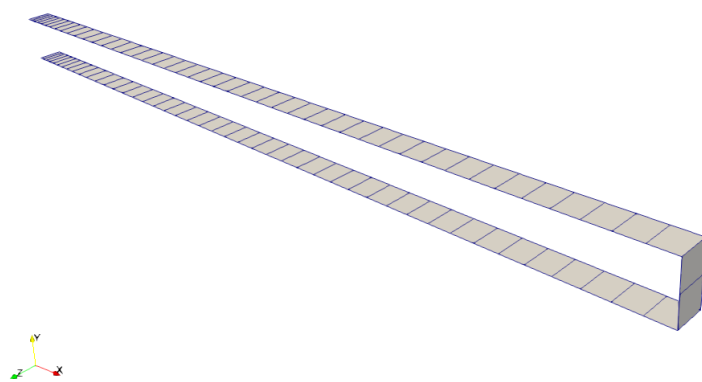
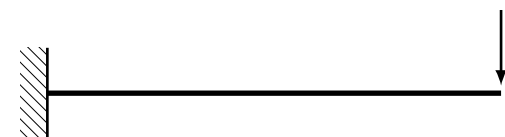
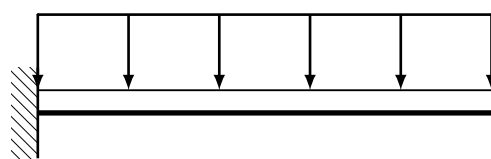

 Figure 6.2. `body` element attached to node 2 of the `beam` element


Figure 6.3. interface points mesh



(a) cantilever with tip load



(b) cantilever with distributed load

Figure 6.4. model and data exchange test-cases

The results have been compared the expected theoretical values in terms of tip displacement at steady state and in terms of frequency of the tip movement when the system has been loaded with a step load.

When both the MBDyn model and the data exchanged through the preCICE interface have been validated, the model has been coupled to a CFD solver.

6.3 Vertical flap: incompressible regime

The first validation step consisted in comparing the results obtained with MBDyn with the ones given by another structural solver with the same fluid model.

For this purpose a simple case of a vertical flap immersed in a flow in incompressible regime, has been considered, borrowing an example given in the preCICE website.

6.3.1 Fluid domain

The fluid domain is represented in Figure 6.5. The inlet is on the left with uniform flow velocity, the outlet is on the right, while all other boundaries are *no-slip* walls.

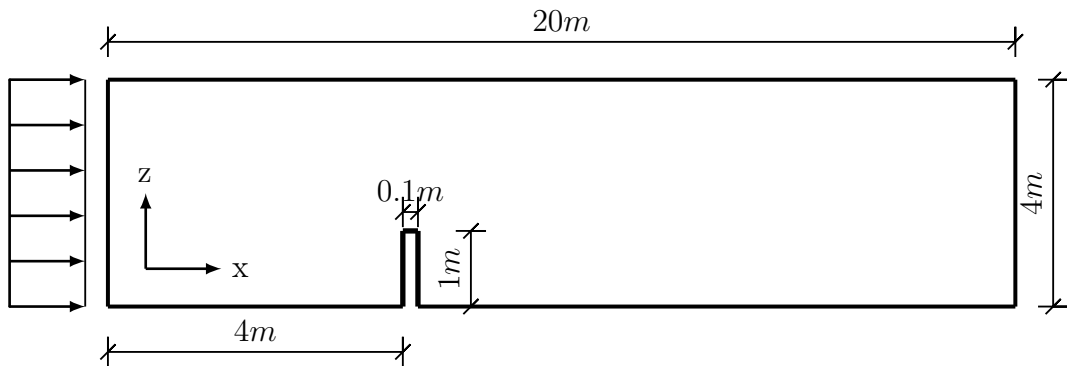


Figure 6.5. vertical flap: fluid domain

The fluid domain is discretized in an structured hexaedral mesh as depicted in Figure 6.6. The main fluid and mesh values are given in Table 6.1 and 6.2.

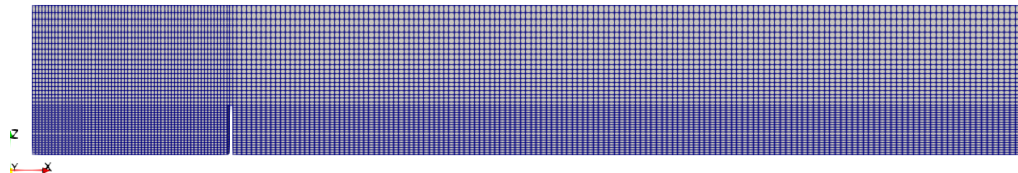


Figure 6.6. vertical flap: fluid mesh

6.3.2 Simulation and Coupling parameters

The coupling between the fluid solver and the structural solver is the same for the MBDyn and the CalculiX simulation. The main data are given in Table 6.3:

parameter		value
fluid density	ρ	kg m^{-3}
kinematic viscosity	ν	$\text{m}^2 \text{s}^{-1}$
flow velocity	\vec{v}	m s^{-1}
flow type		laminar

Table 6.1. Vertical flap: fluid properties

parameter		value
number of mesh points	n_{dof}	17344
number of cells	n_c	8400
number of interface cells	n_{int}	42

Table 6.2. Vertical flap: mesh properties

parameter		value
simulation time	t	s
step size	Δt	s
coupling scheme		serial implicit $S \rightarrow F$
coupling algorithm		IQN-ILS
displacement rel. convergence limit		10^{-4}
force rel. convergence limit		10^{-3}
interface mesh mapping		RBF

Table 6.3. Vertical flap: coupling parameters

6.3.3 Structural Solver: CalculiX

The structural model built in CalculiX is composed of 40 **C3D8**² as represented in Figure 6.7.

The properties of the solid are reported in Table 6.4.

parameter		value
solid density	ρ	kg m^{-3}
Elastic modulus	E	Pa
Poisson coefficient	ν	

Table 6.4. Vertical flap: solid properties

6.3.4 Implementation with MBDyn

The MBDyn model uses the same solid properties of Table 6.4 and is composed of 10 **beam3** elements. Apart from the different orientation, the setup is the same as the one briefly

²general purpose linear brick element with 8 nodes

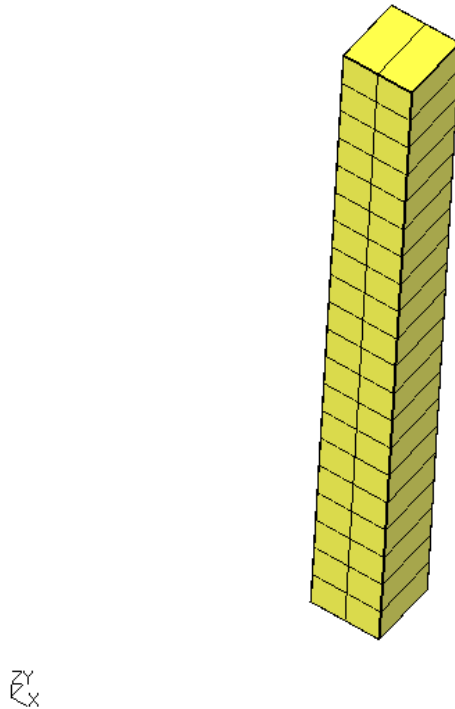


Figure 6.7. vertical flap: CalculiX mesh

described in Section 6.2. The only relevant parameter that can be explicitly set up in MBDyn in comparison to CalculiX, consists in the structural damping of the beam elements (see Section 4.1.4), which is set to be proportional to stiffness matrix of the element with a coefficient of $2 \cdot 10^{-3}$.

The interface mesh is divided into 20 faces for the front and back surfaces of the flap. The upper surface is divided into 2, so that the interface is identical to the one obtained in CalculiX.

6.3.5 Results

The problem considered is characterized by the adimensional parameters given in Table 6.5 and its solution is represented in Figure 6.8.

parameter		value
mass number	M	$3.3 \cdot 10^{-4}$
reduced velocity	U_R	0.274
Cauchy number	C_Y	$2.5 \cdot 10^{-5}$

Table 6.5. Vertical flap: adimensional numbers

The solutions between CalculiX and MBDyn are first compared in terms of resultants applied to the structure during the simulation (Figures 6.9 and 6.10), then the tip displacement in x direction is considered in Figure 6.11. The forces and moments applied to the structure in the two cases are very close. The tip displacement shows that both structures exhibit the same damping and the oscillating frequency is very close: CalculiX shows a slightly

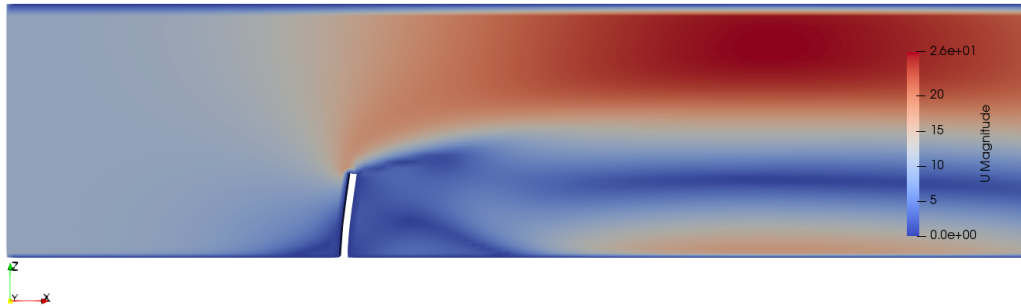


Figure 6.8. vertical flap: velocity field

higher frequency and a more visible second order frequency. The MBDyn structure looks a little more flexible: after 50 seconds of simulation tends to 58mm of tip displacement in x direction, while the same structure in CalculiX tends to 53mm of displacement.

As to convergence and number of iterations between the two solvers, Figure 6.12a and 6.12b show that, in general, MBdyn and CalculiX require 2 iterations to converge. This can be explained by the small mass number of this case. At some iterations MBDyn requires more iterations: this is due to the fact, for some reasons due to the coupling not completely understood at the moment, a force unbalance arises in the y -direction (out of the plane of the model) which produces a moment around x -axis. This moment is absorbed by the rotation constraints at the nodes and it does not affect the behavior of the resultant in x and z directions.

Finally, MBDyn allows to analyze the internal forces of each beam, as represented in Figure 6.13.

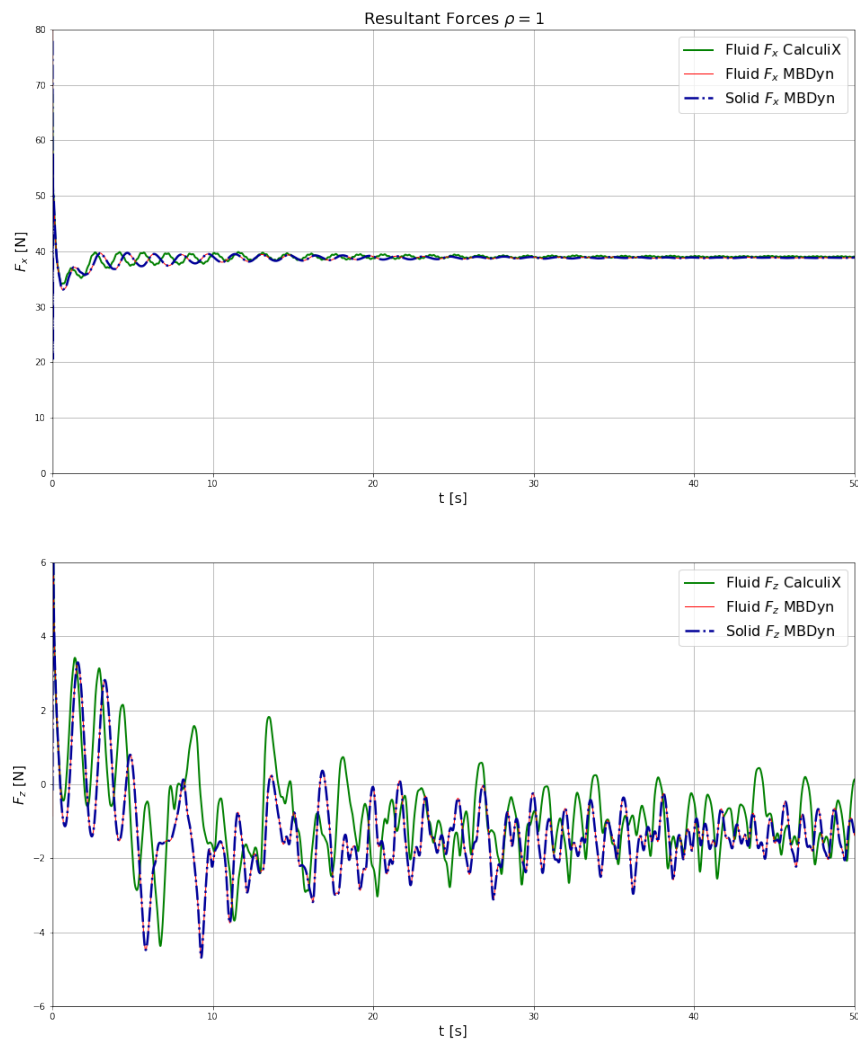


Figure 6.9. vertical flap: resultant forces

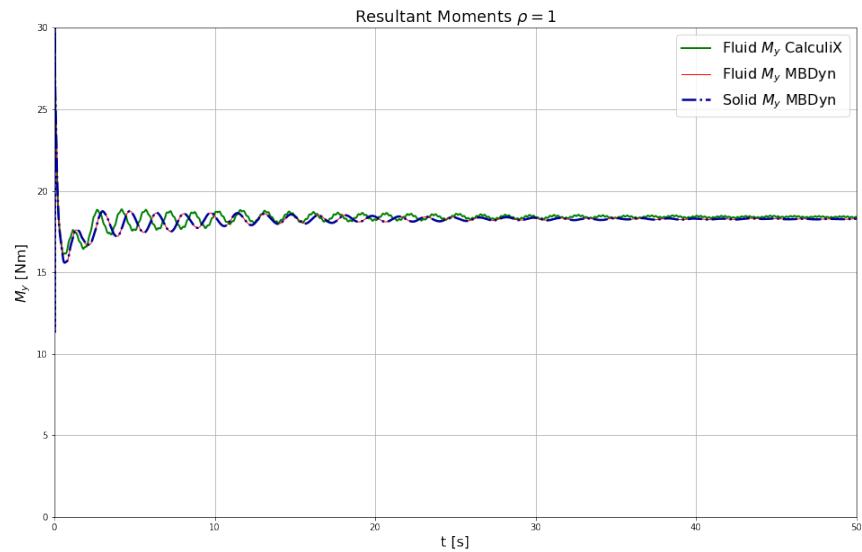


Figure 6.10. vertical flap: moment applied at root

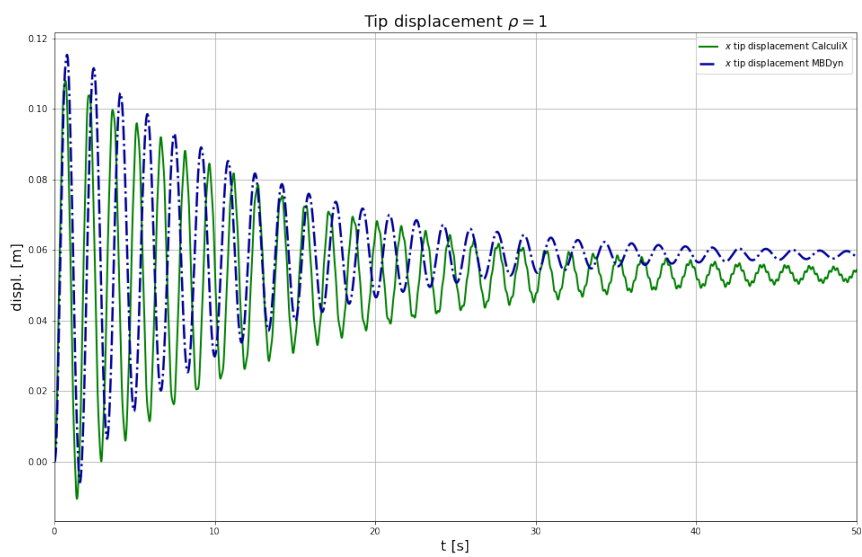


Figure 6.11. vertical flap: tip displacement x direction

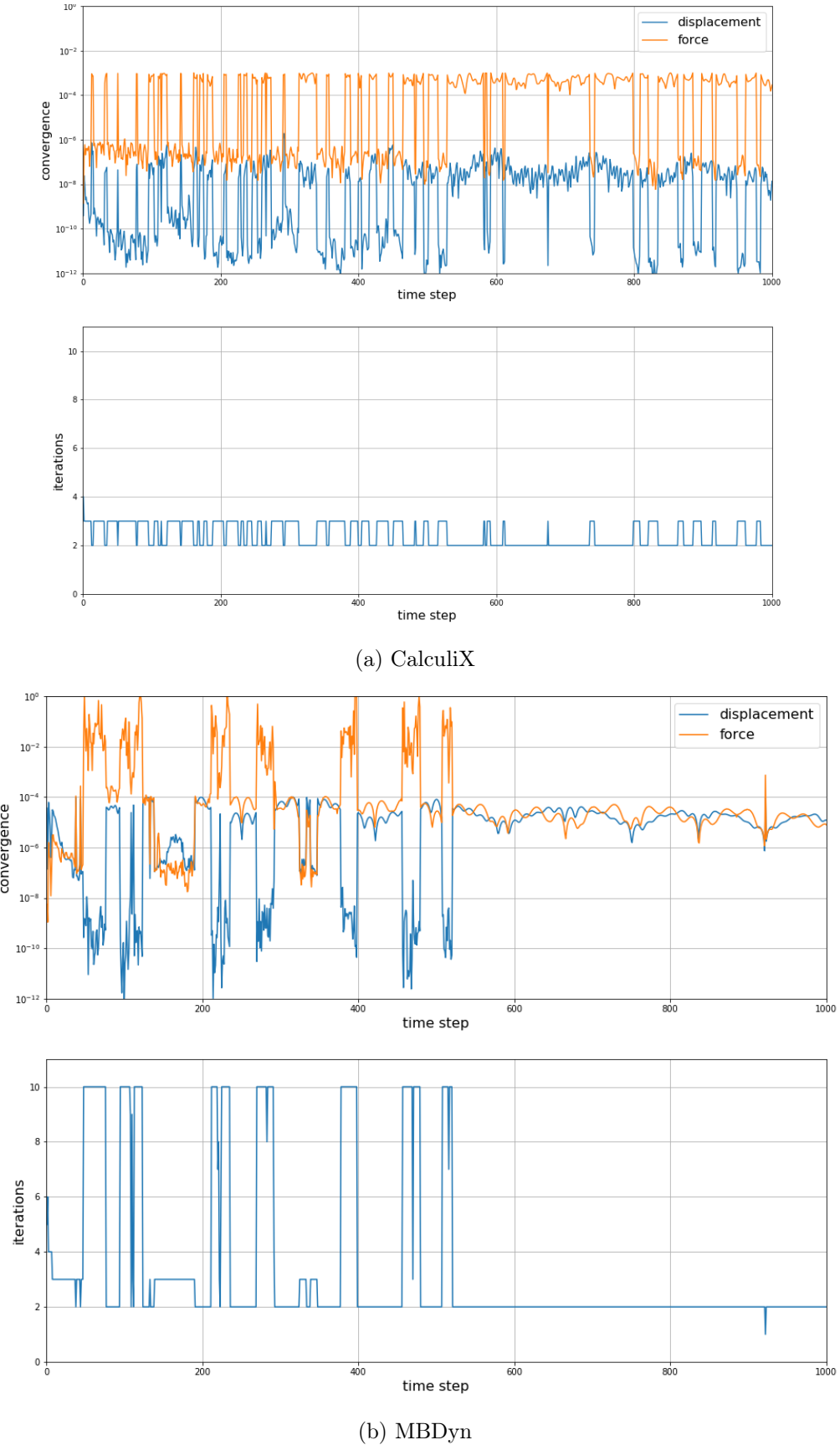


Figure 6.12. vertical flap: convergence and iterations

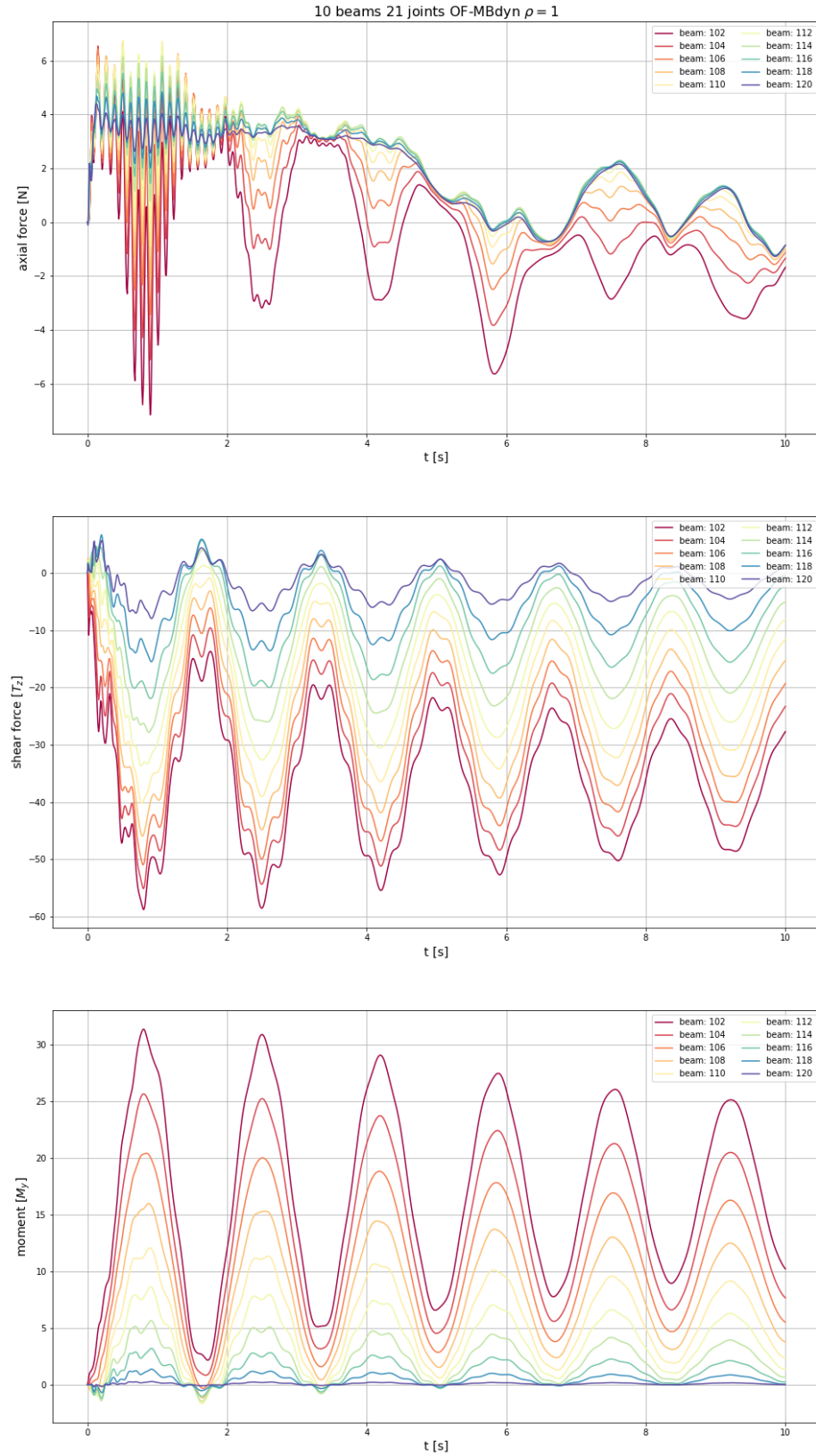


Figure 6.13. vertical flap: MBDyn convergence and iterations

6.4 Vertical flap: compressible regime

A model similar to the one described in the previous section has been used to test the coupling capabilities of the adapter with a different fluid solver: SU2³. The coupling adapter between SU2 and preCICE allows to build FSI simulations in compressible regime. Besides, SU2 allows to define strictly bidimensional domains, while OpenFOAM and MBDyn are strictly tridimensional. Bidimensionality is enforced in OpenFOAM using *empty* boundary conditions, while in MBDyn is enforced through constraints on nodes. For those reasons a similar model has been built.

6.4.1 Fluid domain

The fluid domain is represented in Figure 6.14. The inlet is on the left with uniform flow velocity, the outlet is on the right, while all other boundaries are *slip* walls.

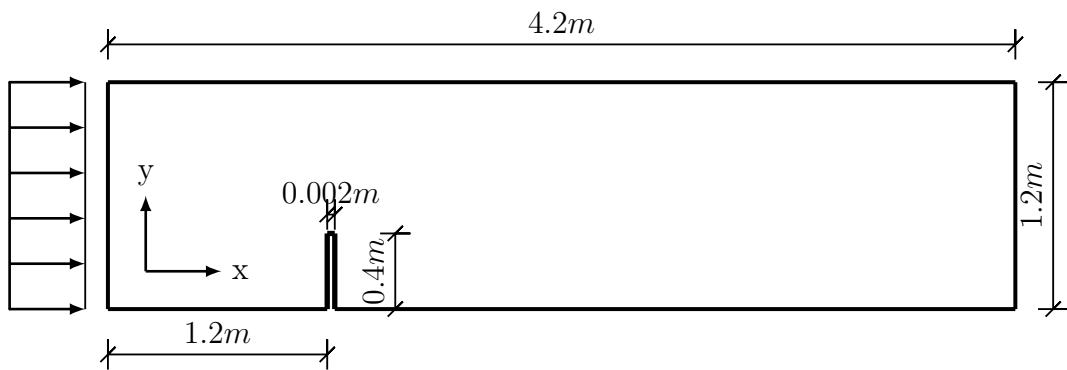


Figure 6.14. vertical flap (compressible): fluid domain

The fluid domain is discretized in an unstructured triangular mesh as depicted in Figure 6.15. The main fluid and mesh values are given in Table 6.6 and 6.7.

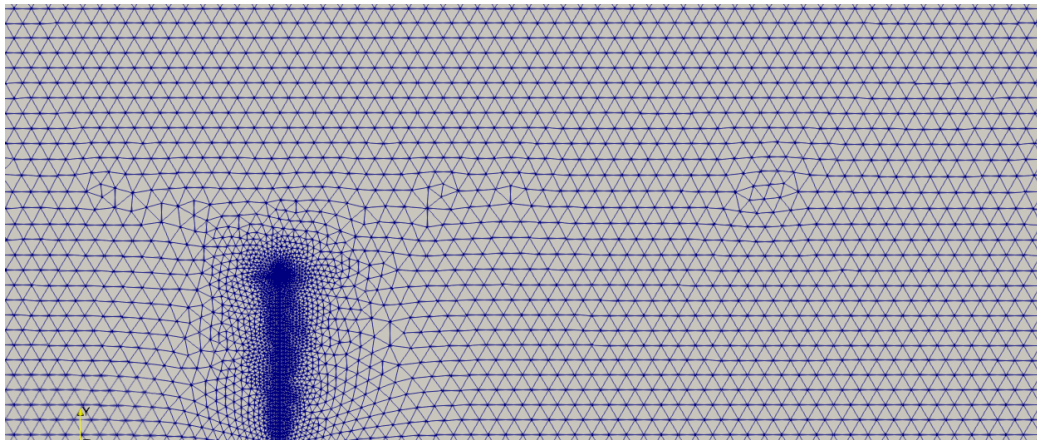


Figure 6.15. vertical flap (compressible): fluid mesh

³su2code.github.io

parameter				value
fluid properties				standard air
outlet pressure	p	Pa		101300
inlet temperature	T	K		288
inlet Mach number	Ma			0.1
flow type				euler

Table 6.6. Vertical flap (compressible): fluid properties

parameter				value
number of mesh points				n_{dof} 5580
number of cells				n_c 10709
number of interface points				n_{int} 162

Table 6.7. Vertical flap (compressible): mesh properties

6.4.2 MBDyn model

The MBDyn model uses solid properties defined in Table 6.8 and is composed of 5 `beam3` elements.

parameter				value
solid density	ρ	kg m ⁻³		1000
Elastic modulus	E	Pa		$5.6 \cdot 10^9$
Poisson coefficient	ν			0.4
structural damping				$1 \cdot 10^{-3}$

Table 6.8. Vertical flap: solid properties

6.4.3 Coupling parameters

The main data concerning the coupling between MBDyn and SU2 are given in Table 6.9:

parameter				value
simulation time	t	s		1
step size	Δt	s		10^{-3}
coupling scheme				serial implicit $S \rightarrow F$
coupling algorithm				IQN-ILS
displacement rel. convergence limit				10^{-5}
force rel. convergence limit				10^{-3}
interface mesh mapping				RBF

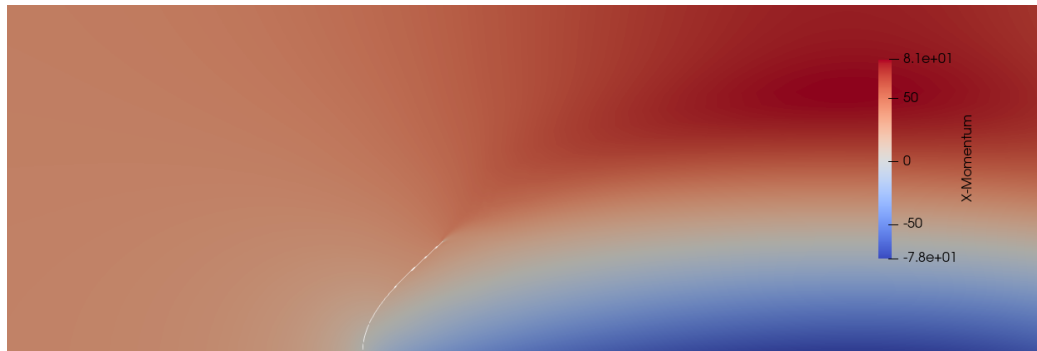
Table 6.9. Vertical flap (compressible): coupling parameters

6.4.4 Results

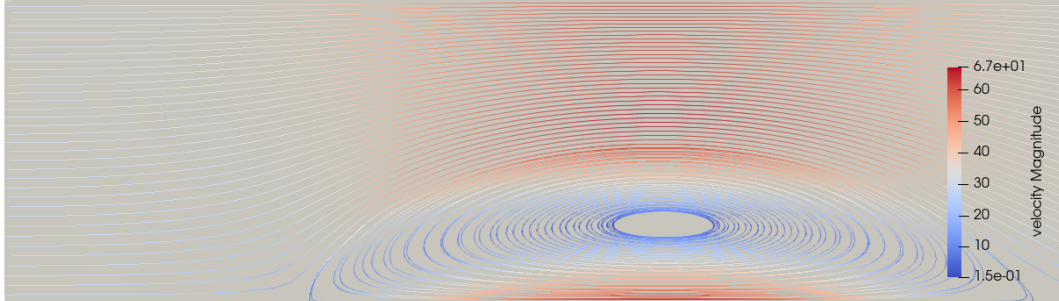
The problem considered is characterized by the adimensional parameters given in Table 6.10: in particular the mass number remains in the order of $\mathcal{O}(10^{-3})$. A sketch of the flow solution is represented in Figure 6.16.

parameter		value
mass number	M	$\approx 1.2 \cdot 10^{-3}$
reduced velocity	U_R	$\approx 1.44 \cdot 10^{-2}$
Cauchy number	C_Y	$\approx 2.53 \cdot 10^{-7}$

Table 6.10. Vertical flap (compressible): adimensional numbers



(a) vertical flap (compressible): x-momentum



(b) vertical flap (compressible): streamlines

Figure 6.16. vertical flap (compressible): flow solution

The combination of parameters considered in this test case aimed at considering a very thin flexible element surrounded by a low-Mach flow, so that large displacements are involved. The structure reaches a steady deformed shape after around 1 second as shown in Figure 6.18, concerning tip displacement.

The fluid flow has been initialized with a steady solution obtained considering a rigid structure, then the FSI problem has been simulated applying the aerodynamic load to the flap progressively: a linear ramp starting at 1% of the load with a duration of 0.2 seconds (see Section 5.3 for the adapter input parameters).

Resultant forces (R_x, R_y) and moment (M_z) computed at the root of the flap are shown in Figure 6.17.

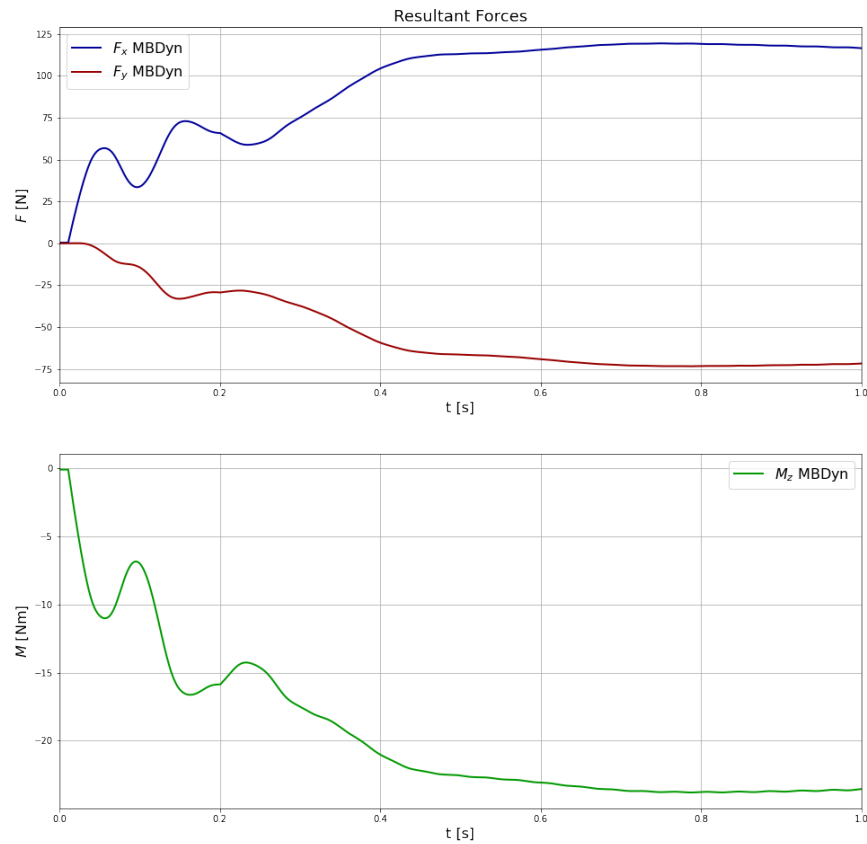


Figure 6.17. vertical flap (compressible): resultant forces

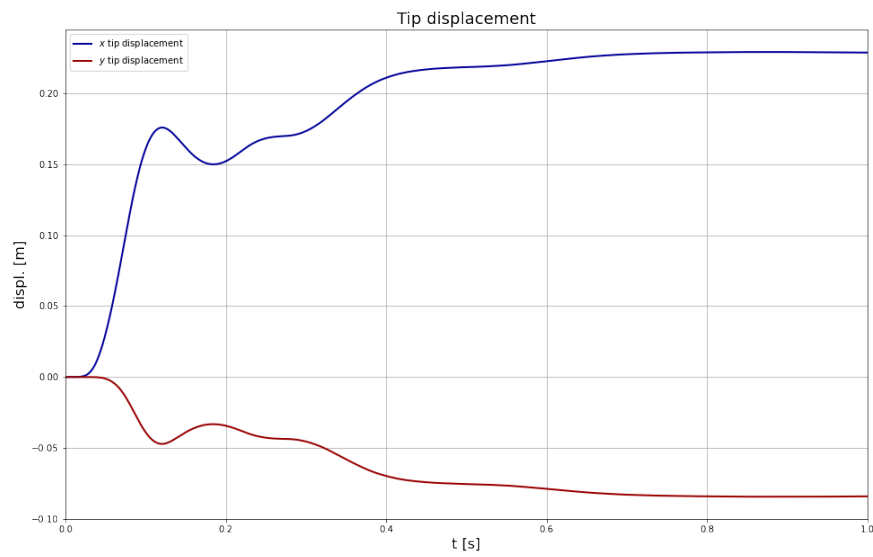


Figure 6.18. vertical flap (compressible): tip displacement

Each time step of the problem converges quite rapidly, requiring 5 iterations in most cases (see Figure 6.19). This outcome agrees with the fact that a low mass number and a high fluid velocity make the problem loosely coupled (see section 3.3 for some details). Nevertheless an explicit simulation diverges immediately.

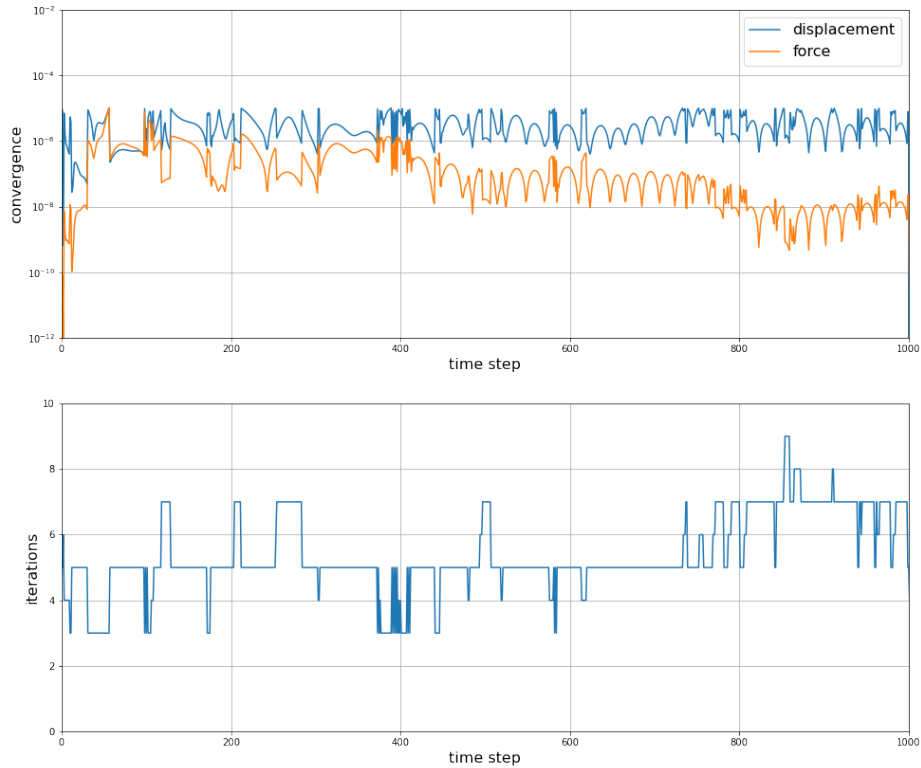


Figure 6.19. vertical flap (compressible): convergence and iterations

Axial, shear and bending moment in each of the MBDyn elements are plotted in Figure 6.20.

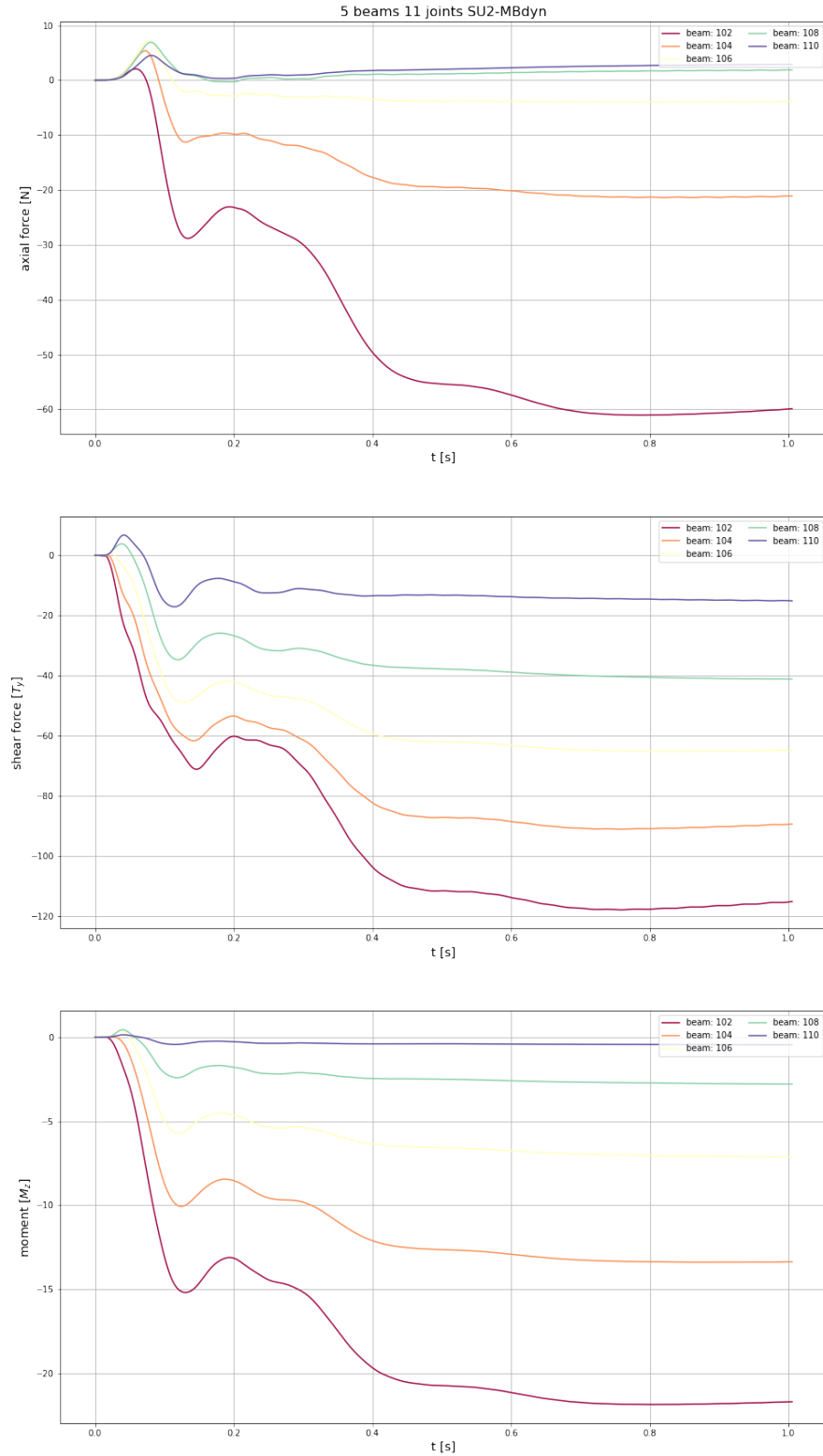


Figure 6.20. vertical flap (compressible): MBDyn internal forces

6.5 Square bluff body Benchmark

The first simple problems aimed at verifying that the complete FSI problem: i.e. the MBDyn model, the mapping with the interface mesh, the coupling adapter and the fluid model (fluid flow and mesh movement performed with different solvers) is working and gives correct results.

After that it is important to verify the performance of the system considering well-known benchmarks, so that the results can be compared with a large number of algorithms and techniques.

6.5.1 Problem description

The first benchmark considered here has been described in [10]. The structural part is composed of a square bluff body with a trailing thin flap, as described in Figure 6.21. The geometrical data are given in Table 6.11.

parameter		value
H	[mm]	10
L	[mm]	40
t	[mm]	0.6

Table 6.11. square bluff body: geometry

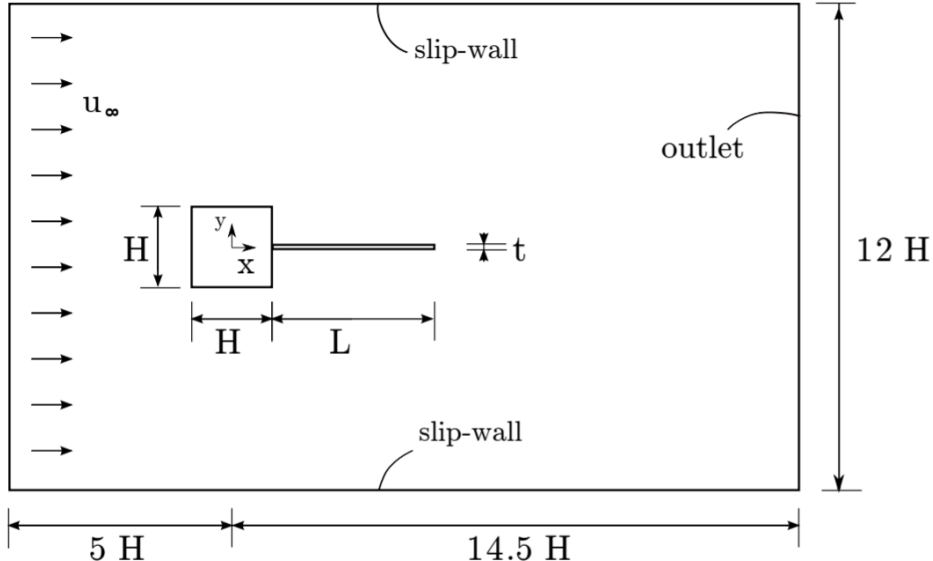


Figure 6.21. square bluff body benchmark: domain

6.5.2 Fluid domain

The fluid domain is represented in Figure 6.21 and has been simulated in OpenFOAM. The inlet is on the left with uniform flow velocity, the outlet is on the right, the external boundaries (top and bottom) are *slip-walls* while all other boundaries (cylinder and flap) are *no-slip* walls.

The fluid domain is discretized in an structured hexaedral mesh as depicted in Figure 6.22. The main fluid and mesh values are given in Table 6.12 and 6.13.

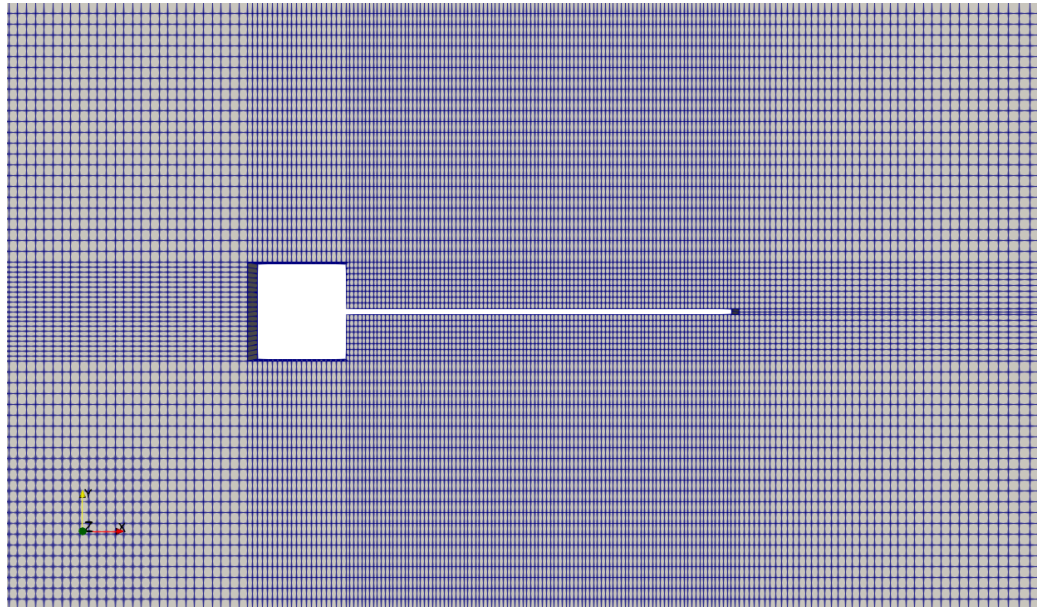


Figure 6.22. square bluff body: fluid mesh

parameter			value
fluid density	ρ	kg m^{-3}	1.18
dynamic viscosity	μ	$\text{kg m}^{-1} \text{s}^{-1}$	$1.82 \cdot 10^{-5}$
Reynolds number	Re		332
flow velocity	\vec{u}_∞	m s^{-1}	0.513
flow type			laminar

Table 6.12. square bluff body: fluid properties

parameter		value
number of mesh points	n_{dof}	59096
number of cells	n_c	29040
number of interface cells	n_{int}	202

Table 6.13. square bluff body: mesh properties

6.5.3 Solid domain

The properties of the solid are reported in Table 6.14.

The MBDyn model is composed of 10 `beam3` elements. The setup resembles the one briefly described in Section 6.2. The structural damping of the beam elements (see Section 4.1.4) has been set to be proportional to stiffness matrix of the element with a coefficient of

parameter	value	
solid density	ρ	kg m^{-3}
Elastic modulus	E	Pa
Poisson coefficient	ν	

Table 6.14. square bluff body: solid properties

$1 \cdot 10^{-2}$. This value appeared to be high enough to give a smooth structural solution without being excessively damping.

The interface mesh is divided into 202 faces and is shown in Figure 6.23.

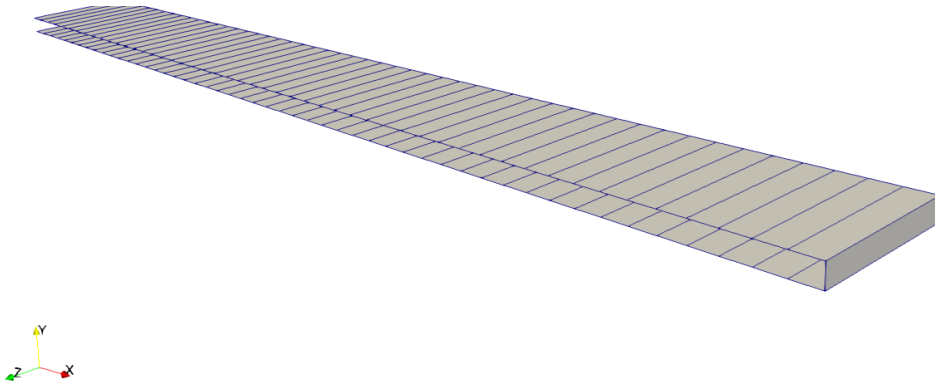


Figure 6.23. square bluff body: structural interface mesh

6.5.4 Coupling parameters

The main coupling data are given in Table 6.15. The particularly short time step is required by fluid mesh movement: as it will be apparent in the results, the thin flexible flap moves quickly and with large displacement. The diffusion algorithm used by OpenFOAM to deform the fluid mesh produced inconsistent cell volumes when using higher time steps.

parameter	value	
simulation time	t	s
step size	Δt	s
coupling scheme		serial implicit $S \rightarrow F$
coupling algorithm		IQN-ILS
displacement rel. convergence limit		10^{-4}
force rel. convergence limit		10^{-3}
interface mesh mapping		RBF

Table 6.15. square bluff body: coupling parameters

Most parameters are similar to the ones used in other examples as they turned out to fit well with most of the experiments.

6.5.5 Results

The problem considered is characterized by the adimensional parameters given in Table 6.16 and its solution is represented in Figure 6.26.

parameter		value
mass number	M	$1.18 \cdot 10^{-2}$
reduced velocity	U_R	$\approx 1 \cdot 10^{-2}$
Cauchy number	C_Y	$1.24 \cdot 10^{-6}$

Table 6.16. square bluff body: adimensional numbers

As in other simulations, fluid forces are applied with a ramp to ease convergence at the beginning of the simulation: during the first 100 ms they are scaled to 10% to reach 100% after another 100 ms.

Alternating vortices begin developing quite rapidly and the structure begins oscillating. After around 2 seconds reaches a vortex lock-in regime (e.g. [61]), as shown in Figure 6.24 (in particular the tip displacement in y direction).

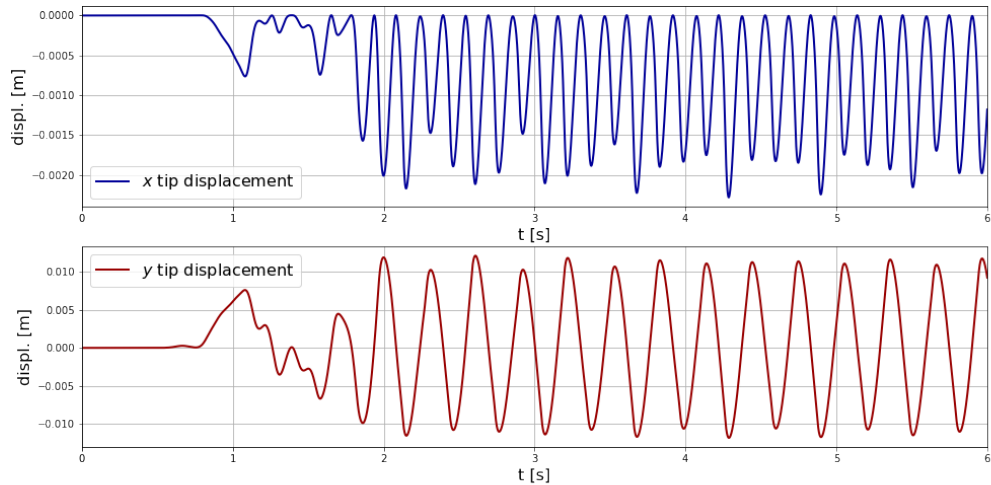


Figure 6.24. square bluff body: tip displacement

Forces are measured on the whole structure on the fluid side, while are measured on the flap in the solid domain. Figure 6.25 shows a detail of 0.5 s of simulation. The difference in x -direction represents the drag force on the cylinder. Differences in lift and moment are almost zero.

Each time step converges with an average of 8 iterations, except for some situations where the coupling algorithm fails in making coupling forces converge. Those situations show a quite distorted fluid mesh that make the overall FSI problem harder to solve.

An higher average number of iterations agrees with the fact that a higher mass number, here in the order of $\mathcal{O}(10^{-2})$, makes the problem strongly coupled.

As in the previous examples, the axial, shear and bending moment in each of the MBDyn elements are plotted in Figure 6.28: in this case a temporal slice of 0.5s has been considered.

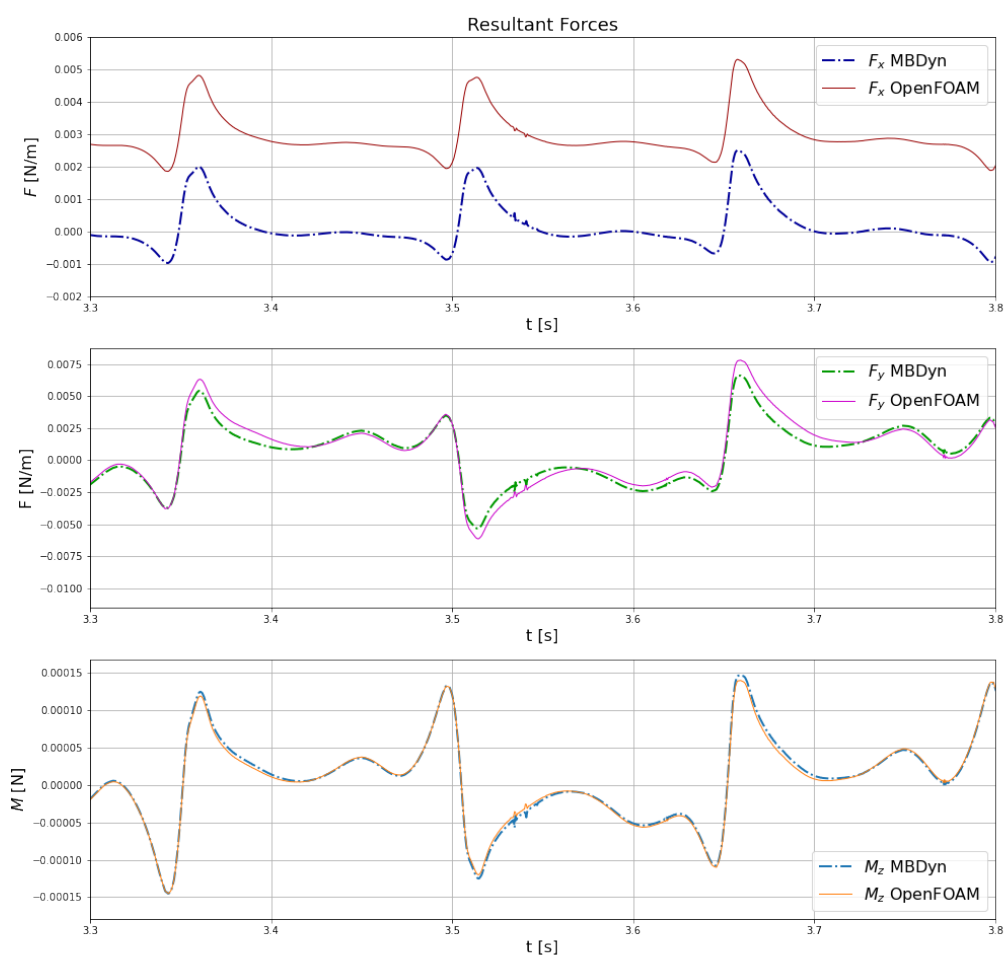


Figure 6.25. square bluff body: resultant forces (detail)

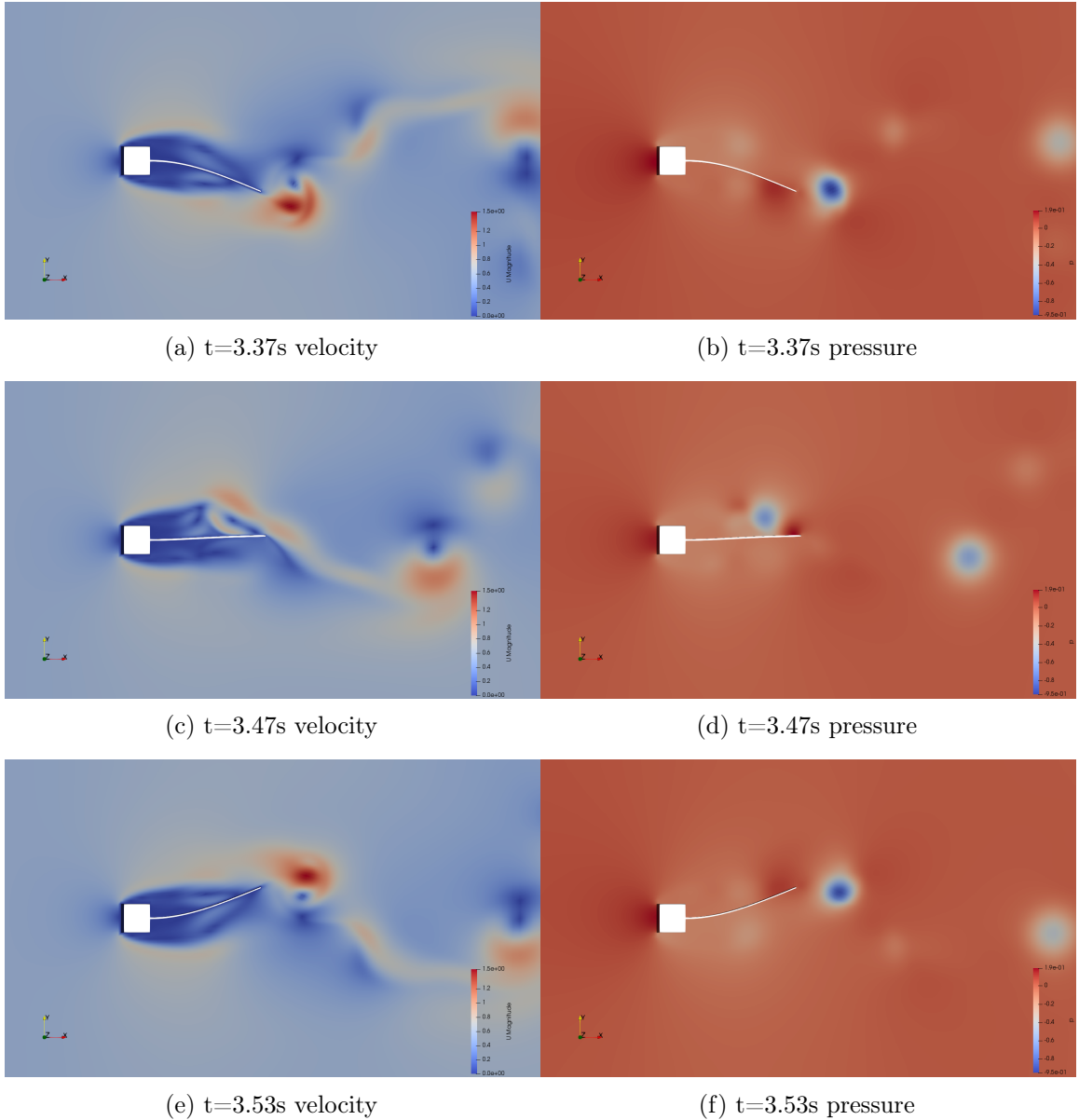


Figure 6.26. square bluff body: fluid solution

6.5.6 Validation

This problem has been used as a benchmark in a great number of studies in literature. The comparison between the studies is generally made on the tip displacement, in term of amplitude and frequency of oscillation. In Table 6.17 some results are given and compared to the present study.

The comparison shows a very good agreement among the studies: considering all the previous simulations, the average tip displacement is 11.2 mm with a standard deviation of 1.06 mm and the average frequency of oscillation is 3.1 Hz with a standard deviation of 0.09 Hz. This study, with a tip displacement of 11.2 mm at a frequency of 3.067 Hz, shows that the implementation of the adapter can give good results.

⁴Fluid Structure Interaction Problems using SU2. First SU2 Annual Developers Meeting. TU Delft, 6 September 2016

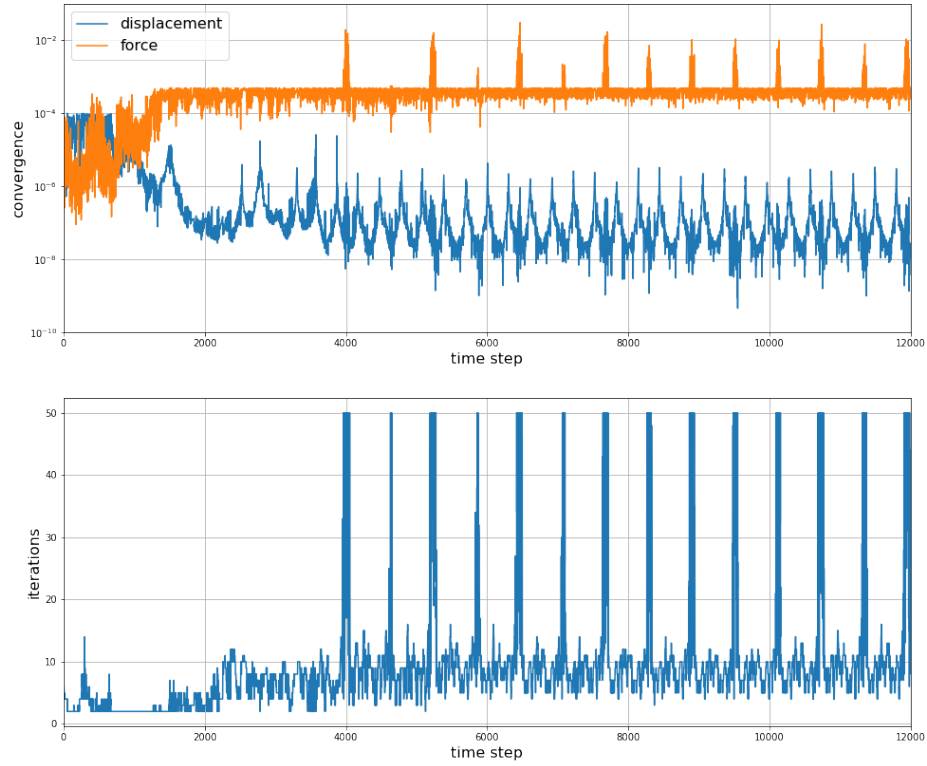


Figure 6.27. square bluff body: convergence and iterations

Study	f [s ⁻¹]	d_{ytip} [mm]
Wall and Ramm [10]	3.08	13.1
Kassiotis et al. [62]	2.98	10.5
Wood et al. [63]	2.94	11.5
Olivier et al. [64]	3.17	9.5
Walhorn et al. [65]	3.14	10.2
Matthies and Steindorf [66]	3.13	11.8
Dettmer and Peric [67]	3.03	12.5
Habchi et al. [68]	3.25	10.2
Froehle and Persson [69]	3.18	11.2
Sanchez et al. ⁴	3.15	11.5
Present study	3.067	11.2

Table 6.17. square bluff body: results

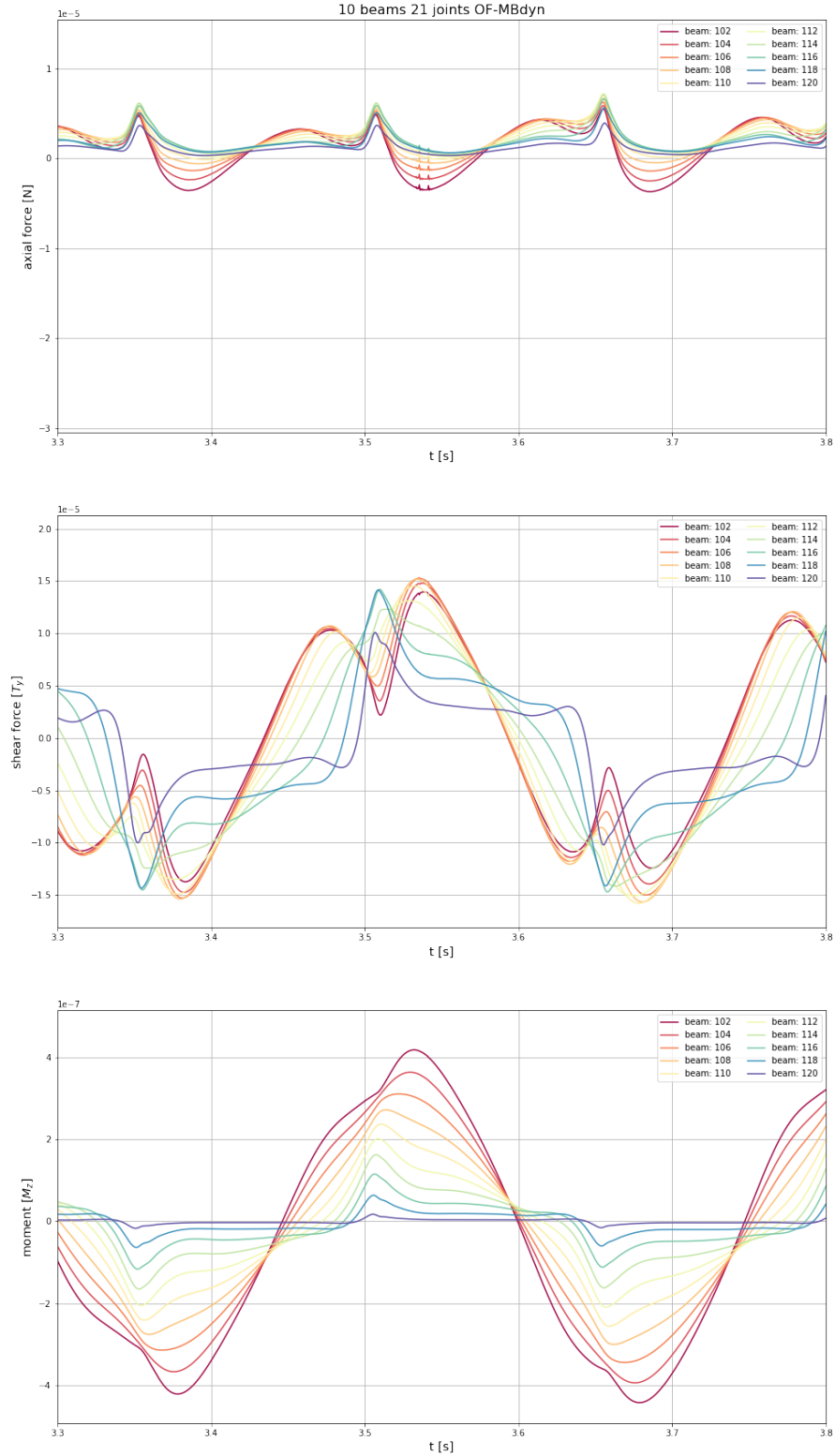


Figure 6.28. square bluff body: MBDyn internal forces (detail)

6.6 Turek-Hron FSI2 Benchmark

Another well known benchmark concerning FSI simulations performed in incompressible flow regime is proposed by Turek and Hron [60]. A very important thing to notice about this study is that it is a proposal for a benchmark, as it is called “Proposal for numerical benchmarking of fluid-structure interaction between an elastic object and laminar incompressible flow”. So the paper gives a specific problem setup which others can contribute.

The fluid domain is similar to the one described in the previous chapter. The domain is again composed by a cylinder and a flap, but different flow velocities and structural properties are considered, so that 3 cases arise, commonly known as FSI1, FSI2 and FSI3.

For reasons that will be apparent in the next section, FSI2 is considered first.

6.6.1 Problem Description

The structural part is composed of a round cylinder with a trailing thin flap, as described in Figure 6.29. The geometrical data are given in Table 6.18.

parameter		value
H	[m]	0.41
L	[m]	2.5
l	[m]	0.35
h	[m]	0.02
C	[m]	(0.2, 0.2)
r	[m]	0.05

Table 6.18. FSI2: geometry

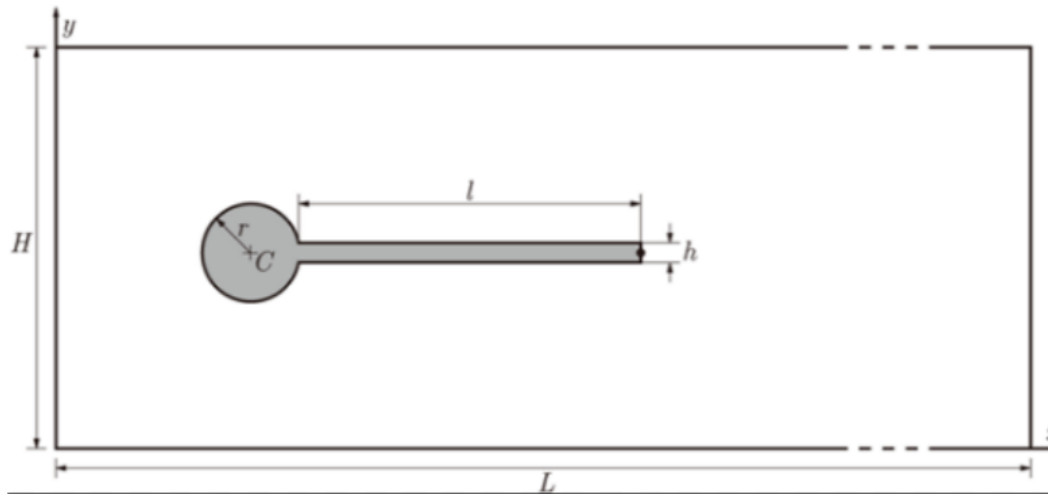


Figure 6.29. FSI2: domain

6.6.2 Fluid domain

The fluid domain is represented in Figure 6.29 and has been simulated in OpenFOAM. The inlet is on the left with *parabolic* flow velocity, the outlet is on the right, while all other

boundaries are *no-slip* walls.

The fluid domain is discretized in an structured hexaedral mesh as depicted in Figure 6.30. The main fluid and mesh values are given in Table 6.19 and 6.20.

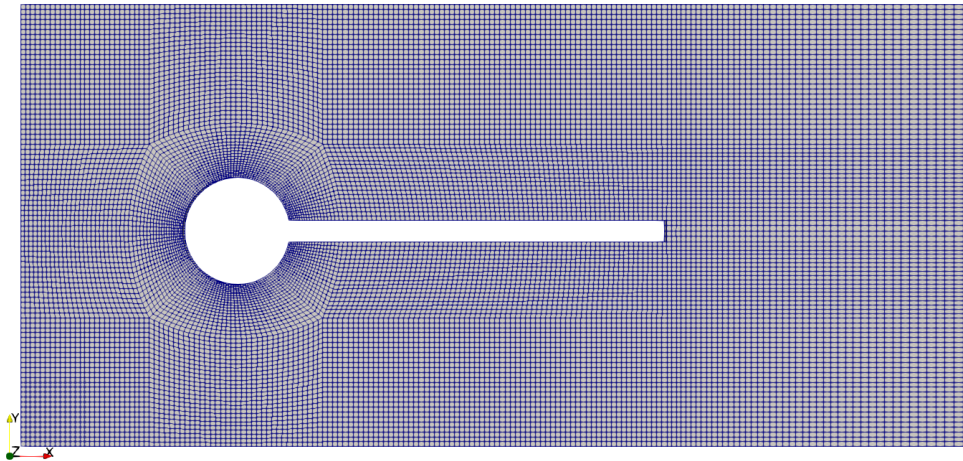


Figure 6.30. FSI2: fluid mesh

parameter			value
fluid density	ρ	kg m^{-3}	1000
kinematic viscosity	ν	$\text{m}^2 \text{s}^{-1}$	$1 \cdot 10^{-3}$
Reynolds number	Re		100
max flow velocity	\vec{u}_{\max}	m s^{-1}	1.5
mean flow velocity	\vec{u}	m s^{-1}	1
flow type			laminar

Table 6.19. FSI2: fluid properties

parameter		value
number of mesh points	n_{dof}	51464
number of cells	n_c	25224
number of interface cells	n_{int}	180

Table 6.20. FSI2: mesh properties

6.6.3 Solid domain

The properties of the solid are reported in Table 6.21.

parameter	value	
solid density	ρ	kg m^{-3}
Elastic modulus	E	Pa
Poisson coefficient	ν	

Table 6.21. FSI2: solid properties

The MBDyn model is the same as the one used in 6.5 and is composed of 10 `beam3` elements, with a structural damping of $1 \cdot 10^{-2}$.

The interface mesh is divided into 90 faces and is shown in Figure 6.31.

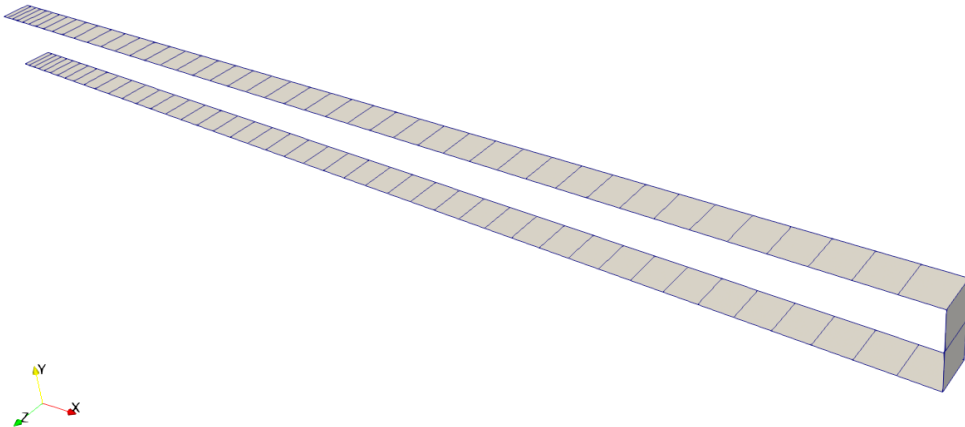


Figure 6.31. FSI2: structural interface mesh

6.6.4 Coupling parameters

The main coupling data are given in Table 6.22. In this case a time step of 1ms is enough for the simulation.

parameter	value	
simulation time	t	s
step size	Δt	s
coupling scheme		serial implicit $S \rightarrow F$
coupling algorithm		IQN-ILS
displacement rel. convergence limit		10^{-4}
force rel. convergence limit		$2 \cdot 10^{-4}$
interface mesh mapping		RBF

Table 6.22. FSI2: coupling parameters

6.6.5 Results

The problem considered is characterized by the adimensional parameters given in Table 6.23 and its solution is represented in Figure 6.34.

parameter		value
mass number	M	0.1
reduced velocity	U_R	$8.45 \cdot 10^{-2}$
Cauchy number	C_Y	$7.14 \cdot 10^{-4}$

Table 6.23. FSI2: adimensional numbers

In this case, the ramp applied to fluid forces at the beginning of the simulation is longer in order to make the fluid and structure settle: during the first 500 ms forces are scaled to 10% and reach 100% after another 500 ms.

Alternating vortices begin developing and the flap begins oscillating with an increasing amplitude. After around 4 seconds reaches a vortex lock-in regime, as shown in Figure 6.32 (in particular the tip displacement in y direction).

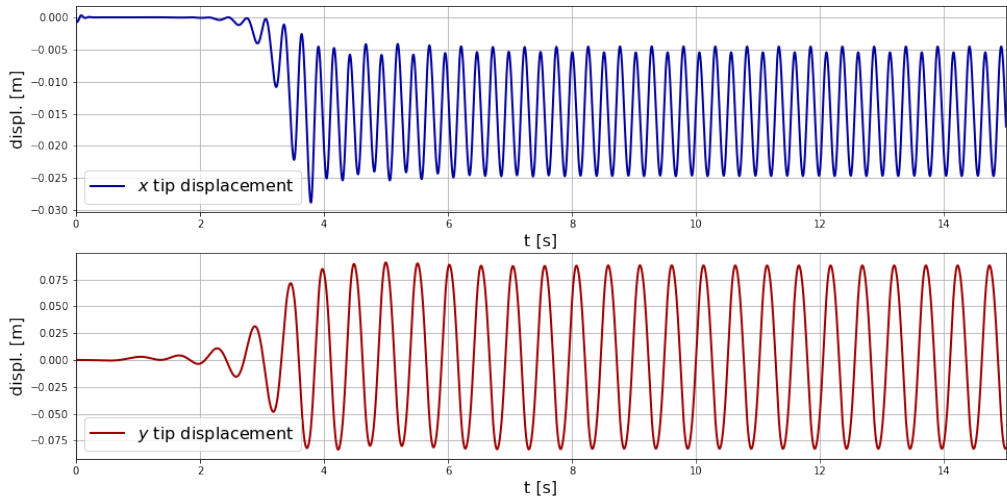


Figure 6.32. FSI2: tip displacement

Forces are measured on the whole structure on the fluid side, while are measured on the flap in the solid domain. Figure 6.33 shows a detail of 2 s of simulation. The difference in x -direction represents the drag force on the cylinder.

Each time step converges with an average of 14.5 iterations, which again confirms the trend of more coupling iterations as the mass number increases.

As in the previous examples, the axial, shear and bending moment in each of the MBDyn elements are plotted in Figure 6.28: in this case a temporal slice of 25s has been considered. The values plotted here consider a beam with 2mm width: i.e. the thickness of the solid and fluid domains considered in this case.

6.6.6 Validation

Turek and Hron benchmarks have been used as a benchmark in many studies considering strongly coupled FSI simulations.

FSI2 is fully oscillating while the same problem, considering the structure rigid (named CFD2 in [60]) is steady: for this reason it is considered an excellent check for interaction mechanisms [70].

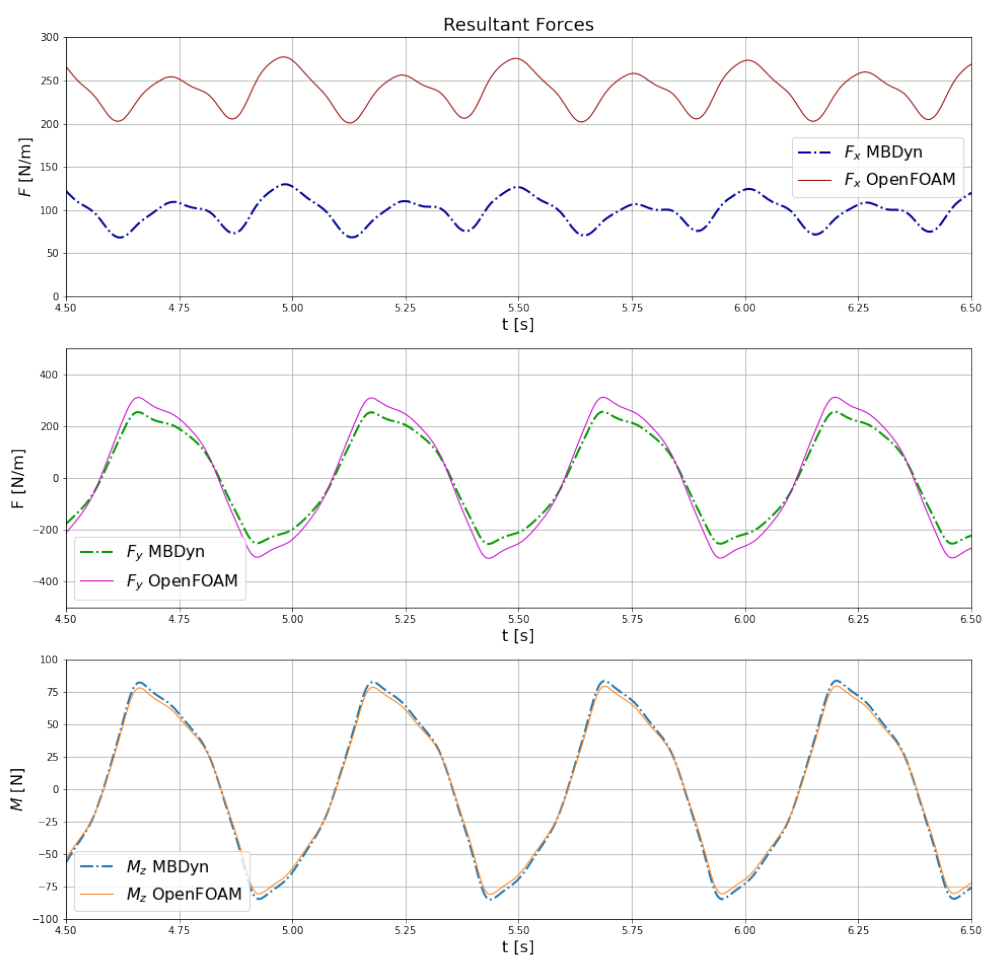


Figure 6.33. FSI2: resultant forces (detail)

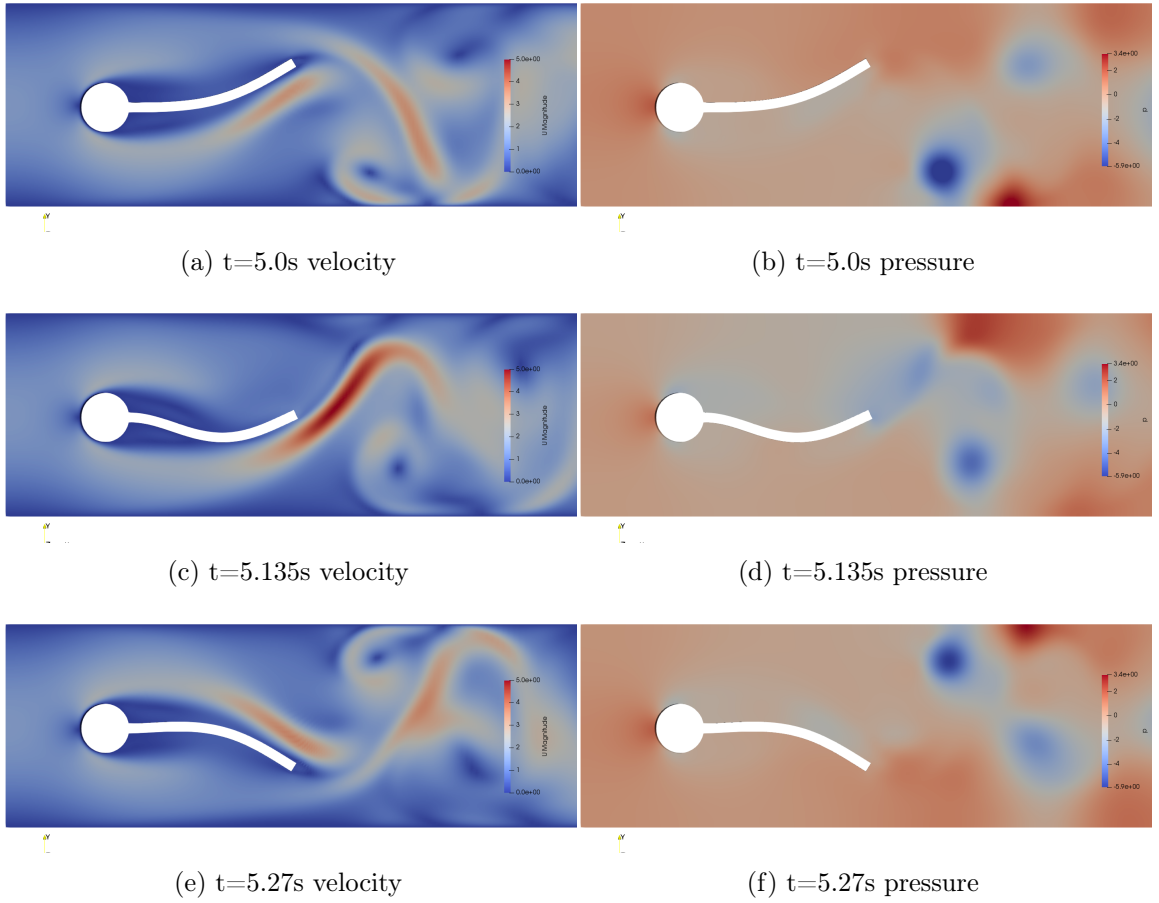


Figure 6.34. FSI2: fluid solution

Besides, FSI2 gives the largest deformation and in some cases it is considered the most difficult of the three benchmarks [71], as it gives deformations 2.5 times greater than the flap height.

The comparison of the results can be done in terms of tip displacement and in terms of lift and drag force applied to the whole structure. The results given in the original paper and in a review made by the same authors, together with other studies found in literature are compared to the present study in Table 6.24 for the data concerning tip displacement, and in Table 6.25 for the forces applied to the structure.

Study	d_{xtip} [mm]	f [Hz]	d_{ytip} [mm]	f [Hz]
Benchmark [60]	-14.58 ± 12.44	3.8	1.23 ± 80.6	2.0
Turek et al. (2010) [70]	-14.85 ± 12.70	3.86	1.30 ± 81.7	1.93
Gjertsen [72]	-14.83 ± 13.11		1.24 ± 81.6	
Degroote [73]	-14.07 ± 12.37	3.7	1.18 ± 76.5	1.9
Present study	-14.95 ± 9.85	3.87	2.78 ± 83.39	1.93

Table 6.24. FSI2: comparison of results (displacements)

The study [70] gives 7 different methods and results for FSI1 and FSI3 test cases. In the numerical results it is stated that “clear differences between the different approaches

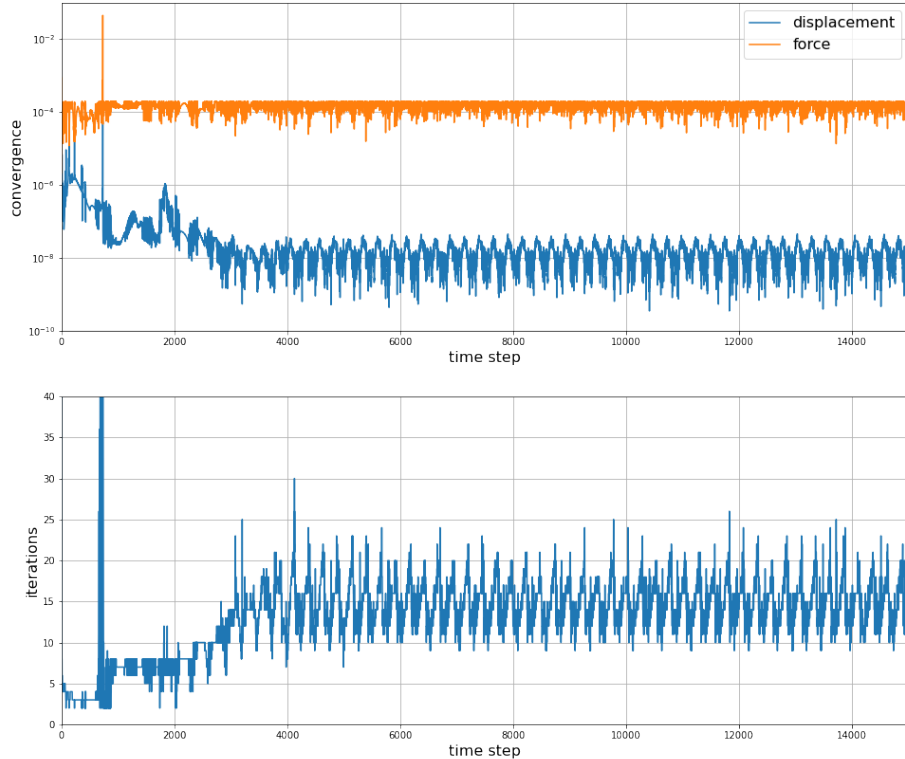


Figure 6.35. FSI2: convergence and iterations

Study	drag [N m ⁻¹]	f [Hz]	lift [N m ⁻¹]	f [Hz]
Benchmark [60]	208.83 ± 73.75	3.8	0.88 ± 234.2	2.0
Turek et al. (2010) [70]	215.06 ± 77.63	3.86	0.61 ± 237.8	1.93
Gjertsen [72]	161.50 ± 73.75		0.88 ± 234.2	
Degroote [73]	217.52 ± 84.65	3.7	-0.74 ± 267.6	1.9
Present study	239.13 ± 31.93	3.87	3.43 ± 308.57	1.93

Table 6.25. FSI2: comparison of results (forces)

with regard to accuracy are visible. Particularly for the drag and lift values, which lead to differences of up to order 50%, and also for the displacement values which are in the range of 10% errors”.

For the FSI2 test case only the results from the initial Hron and Turek paper [60] and a few others are available.

Comparing the results, with previous studies (Table 6.24), mean displacement in x direction is very close to all other results (mainly due to mean pressure applied to the tip face), while mean oscillation is lower of about 3mm. The displacement in y direction is about 2mm higher. It looks like the MBDyn structure is a bit more flexible (as also seen in Section 6.3 for the vertical flap). This also reflects the fact that average drag and lift are higher.

The greatest difference can be seen in the oscillation of drag, which is much smaller than other studies. The data collected during the simulation allow to separate the contribution of the cylinder from the one of the flap (see first graph of Figure 6.33). The cylinder has

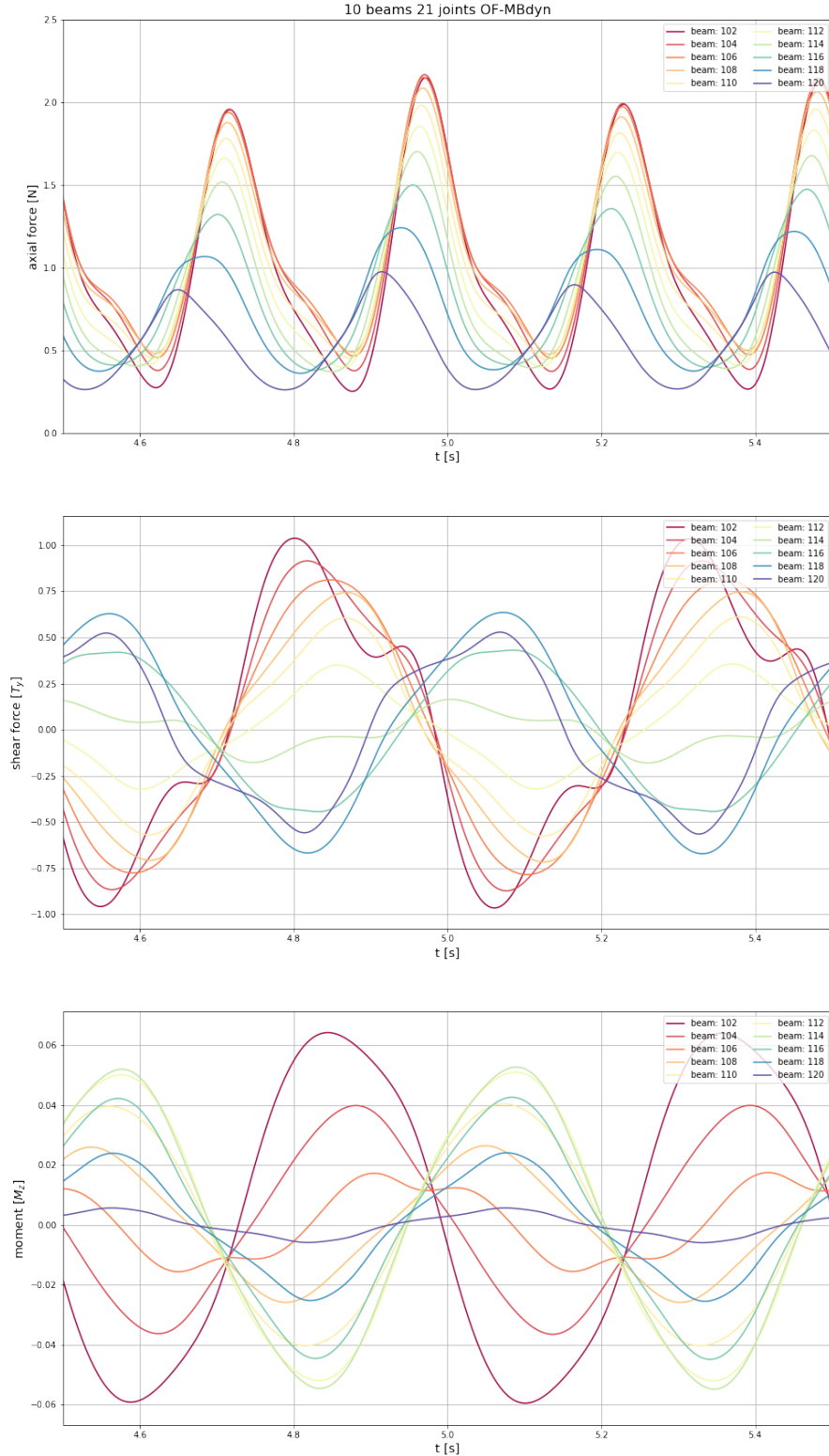


Figure 6.36. FSI2: MBDyn internal forces (detail)

an average drag of 140 N m^{-1} with a standard deviation of $\approx 7 \text{ N m}^{-1}$. Considering that the average C_D of a cylinder at $Re = 100$ is around 1.35 [74], and an average fluid velocity around the cylinder of about 1.4 m s^{-1} , the contribution is as expected. The contribution of the flap seems to be much lower than expected.

As previously stated, the results for the FSI3 case differ by in some cases 50% for Drag and Lift. With this in mind, in the FSI2 case it is reasonable to assume that since there were such differences in the results for different implementations for the FSI3 results, we would expect similar behavior in the FSI2 results.

6.7 Turek-Hron FSI3 Benchmark

Omitting for a while the test case named FSI1 as it is not oscillating, the other benchmark proposed in [60], named FSI3, is very similar to FSI2 with the only different properties shown in Table 6.26. The corresponding adimensional numbers are given in Table 6.27.

parameter			FSI2	FSI3
solid density	ρ	kg m^{-3}	10000	1000
Elastic modulus	E	Pa	$1.4 \cdot 10^6$	$5.6 \cdot 10^6$
max flow velocity	\vec{u}_{\max}	m s^{-1}	1.5	3
mean flow velocity	\vec{u}	m s^{-1}	1	2

Table 6.26. FSI2-FSI3: different parameters

parameter		FSI2	FSI3
mass number	M	0.1	1
reduced velocity	U_R	$8.45 \cdot 10^{-2}$	$2.67 \cdot 10^{-2}$
Cauchy number	C_Y	$7.14 \cdot 10^{-4}$	$7.14 \cdot 10^{-4}$
Reynolds number	Re	100	200

Table 6.27. FSI2-FSI3: adimensional numbers

The simulation of FSI3 using MBDyn and OpenFOAM connected with preCICE proved to be an unfeasible task, at least at the time of writing. This same test case is known to work, giving correct results, coupling OpenFOAM and CalculiX as described in the preCICE website⁵. Nevertheless, substituting CalculiX with MBDyn, all other parameters being equal, makes the simulation diverge.

Different approaches have been experimented, acting on each part of the problem. For example:

- in the fluid domain:
 1. using more strict convergence criteria for the fluid solver
 2. using a linear or parabolic profile of the inlet velocity (tests on FSI2 showed very little difference)
 3. using a ramp also in the fluid velocity
 4. defining a finer ($2\times$ or $3\times$) fluid mesh
 5. considering a different thickness of the fluid and solid domain (which showed that having thicker domain produces a negative impact on the convergence)
- in the solid domain:
 1. considering more or fewer MBDyn nodes (from 5 to 20 nodes)
 2. changing solver (`naive`, `umfpack`, `klu`, ...)

⁵Tutorial-for-FSI-with-OpenFOAM-and-CalculiX

- 3. using different damping coefficients
- in the adapter:
 - 1. using different ramp profiles and times
- in the coupling parameters:
 - 1. changing coupling strategies (serial, parallel)
 - 2. using more strict convergence criteria
 - 3. turning the *extrapolation* parameter on or off (*on* gets a better initial guess for the next time step)
 - 4. changing acceleration algorithm and parameters

None of the simulations carried on allowed to simulate the system correctly. In general every simulation diverged at some point of the ramp phase.

For this reason a sensitivity analysis has been carried out in order to understand better the limits of the current coupling, as described in the following Section.

6.8 Sensitivity analysis of FSI1-FSI3 Benchmarks

It can be interesting to understand what combination of simulation parameters influence most the convergence or divergence of the model. We decided to focus on the FSI3 benchmark and perturb some of the input parameters.

Table 6.27 shows that the two test cases present the same Cauchy Number C_Y . It looks that, at first, it might not be a significant parameter to understand the limits of application of this setup. For that reason we decided to vary the *mass number* M and the *reduced velocity* U_R and observe in which cases the simulation diverges.

We started from the original FSI3 test case with the same configuration parameters given in Section 6.6, and modified the following parameters:

1. ρ_f (fluid density): $100 \rightarrow 1000 \text{ kg m}^{-3}$, so that the mass number is in the range $0. \rightarrow 1$. A mass number of 0.1 has shown to converge (i.e. FSI2 benchmark) while previous tests, characterized by smaller mass number, did not present convergence issues. Solid density ρ_s is kept fixed at 1000 kg m^{-3} .
2. E (structure elastic modulus): $5.6 \cdot 10^6 \rightarrow 2 \cdot 10^{11} \text{ Pa}$, so ranging from the elastic modulus of a soft rubber (used in the benchmark) to the one of steel. The corresponding reduced velocity, at $\vec{u} = 2 \text{ m s}^{-1}$, U_R ranges from $\approx 7 \cdot 10^{-4} \rightarrow 0.13$
3. \vec{u} (mean flow velocity): $0.2 \rightarrow 10 \text{ m s}^{-1}$ so that the Reynolds number Re ranges from 20 (as in FSI1) to 1000.

We were interested in keeping the simulation time short, so each experiment lasted one second: the first 0.5s have been used to ramp up forces on the structure from 10% up to 100%, then the simulation evolves for the remaining 0.5s. A simulation is considered successfully completed if it reaches the final time without non-physical results due to lack of convergence at some time steps.

The results are presented in the following subsections.

6.8.1 FSI3 sensitivity Analysis

The first scenario is a perturbation of the FSI3 test case, i.e. with $\vec{u} = 2\text{m s}^{-1}$ and $Re = 200$. The results are presented in the following table:

U_R	E[MPa]	mass ratio				
		0.1	0.2	0.25	0.5	1
$1.41 \cdot 10^{-4}$	$2 \cdot 10^5$	2.204		2.618	3.126	4.418
$6.32 \cdot 10^{-4}$	$1 \cdot 10^4$		15.024	43.1		
$2 \cdot 10^{-3}$	$1 \cdot 10^3$	23.46		10.78		
$6.32 \cdot 10^{-3}$	$1 \cdot 10^2$		7.592	11.788		
$1.41 \cdot 10^{-2}$	20	11.46		87.675		
$2.67 \cdot 10^{-2}$	5.6	7.216	36.426			FSI3

Table 6.28. FSI3 sensitivity analysis: *green cells* simulation completed with average number of iterations, *red cells* simulation diverged

Table 6.28 shows that there is a limit in the ability of the system to work. It is situated in the range between 0.25 and 0.5. This can improve for stiffer material (and so smaller U_R) and be worse for more flexible material. The lower right corner of the table, which represents the FSI3 setup, appears to be quite far from the actual range of convergence of the system. The table also shows the average number of iterations required for each time step to converge. A trend is visible (even if it does not hold for every case): the higher *mass ratio* the more iterations are needed. The similar trend is visible for U_R .

The empty green cells have not been simulated. It is supposed that, if a simulation completes successfully for a given *mass ratio*, it will complete also for a lower one. Conversely, if a simulation does not work for a given U_R , it will not work for a higher U_R (i.e. for a more flexible material).

6.8.2 FSI1 sensitivity Analysis

The same kind of analysis has been conducted considering a fluid velocity of 0.2m s^{-1} ($Re = 20$), thus replicating FSI1 test case in [60].

U_R	E[MPa]	mass ratio				
		0.1	0.2	0.25	0.5	1
$1.41 \cdot 10^{-5}$	$2 \cdot 10^5$		2.138		2.146	3.064
$6.32 \cdot 10^{-5}$	$1 \cdot 10^4$			2.337		
$2 \cdot 10^{-4}$	$1 \cdot 10^3$		9.83			
$6.32 \cdot 10^{-4}$	$1 \cdot 10^2$	8.688		24.45		
$1.41 \cdot 10^{-3}$	20		18.238	38.398		
$2.67 \cdot 10^{-3}$	5.6	6.314				FSI1

Table 6.29. FSI1 sensitivity analysis

Table 6.29 illustrates the results: as in the previous section, *green cells* indicate that the simulation with the average number of iterations reported, *red cells* indicate that simulation diverged. In this case *yellow cells* indicate that the simulation finished, but at some point

reached the maximum number of iterations, or the progressive loading of the structure is difficult. It can be possible that there exist a better set of coupling parameters that makes the test work better, nevertheless it looks to be a symptom of the fact that the simulation is close to the limits of applicability.

Comparing the results with Table 6.28, it can be seen that the range of feasible parameters becomes smaller. This seems to be in accordance with the idea that a lower fluid velocity the the interaction is stronger, thus making the convergence more difficult.

Similarly, the lower right cell represents test case FSI1 and it seems to be not possible to simulate it with the current setup.

6.8.3 Sensitivity Analysis at higher velocity

In order to have more insight on the influence of the physical parameters on the simulation, also a higher fluid velocity of 10m s^{-1} ($Re = 1000$) has been considered.

($Re=1000$)

U_R	E[MPa]	mass ratio				
		0.1	0.2	0.25	0.5	1
$7.07 \cdot 10^{-4}$	$2 \cdot 10^5$					8.647
$3.16 \cdot 10^{-3}$	$1 \cdot 10^4$					9.713
$1 \cdot 10^{-2}$	$1 \cdot 10^3$		14.101	50.731		36.566
$3.16 \cdot 10^{-2}$	$1 \cdot 10^2$			17.122		
$7.07 \cdot 10^{-2}$	20				35.046	
$1.34 \cdot 10^{-1}$	5.6	11.725				

Table 6.30. Re 1000 sensitivity analysis

Table 6.30 shows a pattern similar to the previous experiments. In this case, more combinations of parameters appear to be feasible.

6.8.4 Conclusions

The current knowledge regarding the setup of coupling parameters does not allow to correctly simulate the benchmark experiments FSI1 and FSI3, characterized by a mass ratio of 1. Perturbing some of the parameters, thus lowering the mass ratio M or the reduced velocity U_R , it is possible to reach feasible configurations.

Tables 6.28 to 6.30 show a similar path: the upper left part of the table contains feasible configurations, while the lower right part the unfeasible ones. If the fluid velocity is lower, more configurations fail.

Those aspects appear to agree with the explanations given in Section 3.5 and in the cited literature. The model considered here shows a clear relationship between mass ratio, structure stiffness and simulation outcome at a prescribed fluid velocity. The same clear path would not hold if we considered reduced velocity U_R only, thus putting all experiments together. For example, row 1 of table 6.30 tells that $U_r \approx 7 \cdot 10^{-4}$ would allow to reach $M = 1$, while row 4 of table 6.29 tells that $U_r \approx 6.3 \cdot 10^{-4}$ would allow to reach only $M \approx 0.2$.

Chapter 7

Conclusions

In this thesis, we developed an adapter for MBDyn to enable fluid-structure interaction simulations with the coupling library preCICE. The adapter has been validated both qualitatively and quantitatively with several test cases. This work gives insights into the basics of FSI simulations and allows to classify the implemented partitioned coupling among the wide variety of coupling strategies.

The adapter that we propose applies to a wider set of OpenFOAM solvers, is more configurable, and can be plugged in at runtime without requiring any modifications to the solver's source code – an extra step that previously raised difficulties for the user.

Our proposed adapter not only allows for higher compatibility, but also makes the preparation stage easier because it can simply be “plugged-in” at runtime. Up to now, this required additional changes in the solver's source code. This was achieved by wrapping the adapter into a function object, a pattern also used by bundled post-processing tools.

Our adapter is also more flexible. The solver-specific parameters are read from the OpenFOAM configuration files (dictionaries) and the user does not need to specify them elsewhere. The boundary conditions on the interfaces are configured through the adapter's configuration file (YAML) and have been extended to support more solvers. The adapter can now directly read any additionally required material properties from the case files, instead of requiring modifications to the solver to read them. In case a solver uses different names for the required fields, these are also configurable.

We validated the proposed adapter with multiple solvers, for two scenarios. The first one was a flow over a heated plate, described in [19.]. In most of the cases, the result files using the proposed adapter were identical to the files that were produced using the previous adapters. In some cases, sporadic errors in the order of the results' precision were observed. In the case of the buoyantBoussinesqPimpleFoam, a problem was discovered and corrected in the previous implementation, which was an example for the need for checkpointing in implicit coupling. The second scenario was a shell-and-tube heat exchanger, a complex

This work makes preCICE compatible with a wide range of OpenFOAM solvers used widely in both academia and industry. This brings preCICE not only closer to users but also to developers. Being designed with extensibility in mind, our proposed adapter could be equipped with additional boundary conditions for mechanical fluid-structure interaction or other computational fields, making multi-physics simulations more accessible. In this direction, the adapter could be ported to older versions and other variants of OpenFOAM. Test cases should be developed, in order to make the continuous development of the adapter for multiple OpenFOAM versions easier. Additionally, tutorials would help to reach new users. In order to convince the OpenFOAM community, examples that highlight the advantages of preCICE over the monolithic OpenFOAM solvers for conjugate heat transfer should

be presented. Developing additional modules for mechanical fluid-structure interaction or acoustics would help to establish preCICE and OpenFOAM as standard components of multi-physics simulations, leading to benefits for both communities

An adapter for linking the CFD solver SU2 with the multiphysics coupling tool preCICE is developed in this work and validated both qualitatively and quantitatively with several testcases. This work gives insights into the basics of FSI simulations and allows to classify the implemented partitioned coupling among the wide variety of solver strategies. The integration of the adapter into the code structure of SU2 is explained, as well as its implementation itself. The coupling approach is validated via generic two- and three-dimensional testcases, and the well-known numerical benchmark scenario FSI3 ([39]). The adapter is capable of handling three-dimensional, real-world examples. This is exemplified by simulating a long, slender cylinder under turbulent flow conditions. The practical background of this simulation is research on brush seals for e.g. gas turbines. However, time did not suffice to obtain meaningful simulation results in the scope of this thesis. Thus, work on this topic will be continued. Once feasible single-cylinder simulation results are achieved, scenarios involving multiple cylinders in a channel should be simulated in order to include possible mutual interactions of these structures. Thereby, the real conditions in brush seals can be approximated more precisely. In its current version, the adapter is limited to a single wet surface in the SU2 mesh file. While it is technically possible to define the surface of multiple cylinders as a single wet surface, it is more accurate to extend the adapter such that an arbitrary number of separate FSI interfaces can be defined. Moreover, it might be useful to integrate a load ramping functionality in the adapter, such that at the beginning of an FSI simulation the forces exerted on the structure are reduced by a factor, which is consequently increased to recover the real force values after a certain number of time steps. This might help to stabilize simulations as the initially occurring, large displacements can be reduced by this method. Recently, several RBF mapping methods have been included in preCICE, which can be used for parallel simulations. Applying these elaborate interpolation procedures instead of NN mapping allows to use finer solid meshes without encountering oscillatory forces at the wet surface, such that simulation results are expected to significantly improve (compared to simulations done with NN mapping). Furthermore, the spatial oscillations at the FSI interface are expected to vanish. Consequently, further testing with the FSI3 benchmark scenario will be done in order to verify this. The adapter is implemented such that it perfectly integrates into SU2, allowing to reuse characteristic functionalities like turbulence modeling, convergence acceleration via dual time stepping and multi-grid functionalities. Moreover, usage of preCICE for coupled FSI simulations can be configured via the native SU2 configuration file. A single executable of SU2 can be used for different FSI scenarios and even fluid-only computations without the need for recompilation. The adapter allows for inter- and intrafield parallel simulations. While no ALE implementation is currently available for the incompressible solver in SU2, the adapter is already prepared for this feature, possibly extending the FSI capabilities to the incompressible regime in the future. Although intrinsic FSI functionalities were recently added to SU2, the coupling with preCICE offers more flexibility, as even commercial partner solvers can be chosen for multiphysics simulations. Moreover, the coupling algorithms and data mapping methods of preCICE are more elaborate. The possibility of running fully-parallel simulations outperforms the intrinsic FSI capabilities with regard to HPC. Another practically very useful outcome of this work is the description of the procedure for integrating the adapter into SU2 and building it with preCICE. Thus, users can easily extend SU2 to FSI via preCICE guided by this thesis, which addresses both SU2 and preCICE communities. The adapter will soon be included in the preCICE repository.

Appendix A

preCICE configuration file

```
1 <?xml version="1.0"?>
2 <precice-configuration>
3 <solver-interface dimensions="3">
4
5   <data:vector name="Forces" />
6   <data:vector name="Displacements" />
7
8   <mesh name="FluidMesh">
9     <use-data name="Forces" />
10    <use-data name="Displacements" />
11  </mesh>
12  <mesh name="StructureMesh">
13    <use-data name="Forces" />
14    <use-data name="Displacements" />
15  </mesh>
16
17  <participant name="FluidSolver">
18    <use-mesh name="FluidMesh" provide="yes" />
19    <use-mesh name="StructureMesh" from="StructureSolver" />
20    <write-data name="Forces" mesh="FluidMesh" />
21    <read-data name="Displacements" mesh="FluidMesh" />
22  </participant>
23  <participant name="StructureSolver">
24    <use-mesh name="StructureMesh" provide="yes"/>
25    <write-data name="Displacements" mesh="StructureMesh" />
26    <read-data name="Forces" mesh="StructureMesh" />
27  </participant>
28
29  <m2n:sockets from="FluidSolver" to="StructureSolver" />
30
31  <coupling-scheme:serial-implicit>
32    <participants first="FluidSolver" second="StructureSolver" />
33    <max-time-windows value="10" />
34    <time-window-size value="1.0" />
35    <max-iterations value="15" />
36    <relative-convergence-measure limit="1e-3" data="Displacements" mesh="
```

Appendix A. preCICE configuration file

```
    StructureSolver"/>
37  <exchange data="Forces" mesh="StructureMesh" from="FluidSolver" to="
      StructureSolver" />
38  <exchange data="Displacements" mesh="StructureMesh" from="
      StructureSolver" to="FluidSolver"/>
39  </coupling-scheme:serial-implicit>
40 </solver-interface>
41 </precice-configuration>
```

Listing A.1. preCICE configuration file example

Appendix B

MBDyn adapter configuration file

```
1 {  
2   "precice-config": "./precice-config.xml",  
3   "readDataName": "Displacements0",  
4   "writeDataName": "Forces0",  
5   "participantName": "Solid",  
6   "meshName": "Solid-Mesh",  
7   "mesh": "./mesh/root0f.dat",  
8   "mbdyn-input": "./map_10n_3x_21j.mbd",  
9   "node-socket": "/tmp/mbdyn.node.sock",  
10  "mbdyn-output": "./out_mbd",  
11  "displacement-delta": false,  
12  "iterstart": 500,  
13  "coeff0": 0.05,  
14  "period": 2000,  
15  "ramp-type": "linear",  
16  "write-interval": 10,  
17  "resultant-file": "./output/resultant.txt",  
18  "root-coords": [0.0, 0.0, 0.0],  
19  "vtk-output": "./output/MBDyn-OF_",  
20  "pre-iteration": 5,  
21  "read-coords": true,  
22  "every-iteration": false  
23 }
```

Listing B.1. MBDyn adapter configuration file example

Appendix C

preCICE API

C.1 preCICE API calls

Each participating solver needs to be modified to link to the preCICE library and call methods from its application programming interface. Usually, the calls to the API are grouped together in a preCICE adapter. While preCICE is written in C++, it provides an API also for C, Fortran and Python. An excerpt from the C++ API is shown in Listing 2.1., as drawn from the preCICE source code documentation

```
1 class SolverInterface
2 {
3 public:
4     SolverInterface(
5         %const std::string& solverName,
6         int solverProcessIndex,
7         int solverProcessSize);
8
9     %void configure(const std::string& configurationFileName);
10
11    double initialize();
12    void initializeData();
13    double advance(double computedTimestepLength);
14    void finalize();
15
16    %int getMeshID(const std::string& meshName);
17    int setMeshVertex(int meshID, const double* position);
18    void setMeshVertices(int meshID, int size, double* positions, int* ids);
19
20    void writeScalarData(int dataID, int valueIndex, double value);
21    void writeVectorData(int dataID, int valueIndex, const double* value);
22    void writeBlockScalarData(
23        int dataID,
24        int size,
25        int* valueIndices,
26        double* values);
27
28    bool isCouplingOngoing();
```

```
29 bool isReadDataAvailable();
30 bool isWriteDataRequired(double computedTimestepLength);
31 bool isTimestepComplete();
32
33 %bool isActionRequired(const std::string& action);
34 %void fulfilledAction(const std::string& action);
35
36 // ...
37 };
```

Listing C.1. preCICE API methods

C.2 preCICE adapter structure

First, a SolverInterface object needs to be created. The constructor expects the rank of the process and the size of the communicator in the parallel execution environment. The configure() method sets the name of the preCICE configuration file, reads and validates it and sets up the communication inside the solver. The methods that follow in Listing 2.1. are called “steering methods”. The initialize() method sets up the data structures and communication channels to other participants. Here the first communication happens, as the participants exchange meshes and, if necessary, re-partition them. It returns the maximum time step size that the solver is allowed to execute next. It is followed by the initializeData(), which is optional and transfers any initial non-zero coupling data values among participants. The equation coupling, the data mapping and the communication are all hidden inside the advance() method. This method also returns the maximum time step size allowed. The last method to call is finalize(), which destroys the data structures and closes the communication channels. The solvers need to define their interface meshes. Only some of the methods for mesh definition are listed in Listing 2.1.. Each mesh and each node on the mesh are assigned an integer ID. The getMeshID() gets the ID of the mesh over which the coupling data of the specific kind are exchanged. The setMeshVertex() creates a vertex on the specified mesh and position and returns the id of the vertex. For performance reasons, multiple vertices can be defined at once with setMeshVertices(). Additionally, topological information, such as edges or triangles can be passed to preCICE with additional methods which are not listed here. After defining the meshes, they need to be assigned data values. This is done by methods with names write*Data(), which fill the “buffers” with data from the solver’s mesh or with methods read*Data(), which read data from the buffers into the solver’s mesh. Since preCICE distinguishes between scalar and vector data, both kinds of methods are available. Again, for performance reasons, blocks of data can be processed together using the respective writeBlock*Data() and readBlock*Data(). Please note that these data are not communicated among participants before the next advance() (or initializeData()). A number of auxiliary methods allow to access information important for the coupling, such as whether the coupled simulation is still running, if writing or reading data is expected or if the current coupling time step has finished successfully. The solver can also inquire if it is required to execute a specific action (e.g. to write or to read a checkpoint) and it can inform preCICE that it fulfilled these tasks [16.]. An example of an adapted solver is shown in Listing 2.2., as published in the presentation article of preCICE [6.]. A more detailed example is presented in the wiki of preCICE6 ..

..

```

1 turnOnSolver(); //e.g. setup and partition mesh
2
3 precice::SolverInterface precice("FluidSolver", "precice-config.xml", rank,
4 size); // constructor
5
6 %const std::string& coric = precice::constants::
7     actionReadIterationCheckpoint();
8 %const std::string& cowic = precice::constants::
9     actionWriteIterationCheckpoint();
10
11 int dim = precice.getDimension();
12 int meshID = precice.getMeshID("FluidMesh");
13 int vertexSize; // number of vertices at wet surface
14 // determine vertexSize
15 double* coords = new double[vertexSize*dim]; // coords of vertices at wet
16     surface
17 // determine coordinates
18 int* vertexIDs = new int[vertexSize];
19 precice.setMeshVertices(meshID, vertexSize, coords, vertexIDs);
20 delete[] coords;
21
22 int displID = precice.getDataID("Displacements", meshID);
23 int forceID = precice.getDataID("Forces", meshID);
24 double* forces = new double[vertexSize*dim];
25 double* displacements = new double[vertexSize*dim];
26
27 double dt; // solver timestep size
28 double precice_dt; // maximum precice timestep size
29
30 precice_dt = precice.initialize();
31 while (precice.isCouplingOngoing()){
32     if(precice.isActionRequired(cowic)){
33         saveOldState(); // save checkpoint
34         precice.markActionFulfilled(cowic);
35     }
36     precice.readBlockVectorData(displID, vertexSize, vertexIDs, displacements)
37         ;
38     setDisplacements(displacements);
39     dt = beginTimeStep(); // e.g. compute adaptive dt
40     dt = min(precice_dt, dt);
41     computeTimeStep(dt);
42     computeForces(forces);
43     precice.writeBlockVectorData(forceID, vertexSize, vertexIDs, forces);
44     precice_dt = precice.advance(dt);
45     if(precice.isActionRequired(coric)){ // timestep not converged
46         reloadOldState(); // set variables back to checkpoint
47         precice.markActionFulfilled(coric);
48     }
49     else{ // timestep converged
50         endTimeStep(); // e.g. update variables, increment time
51     }
52 }

```

```
46     }
47 }
48 precice.finalize(); // frees data structures and closes communication
49 channels
50 delete[] vertexIDs, forces, displacements;
51 turnOffSolver();
```

Listing C.2. preCICE adapter structure

Appendix D

MBDyn input/output file example

D.1 MBDyn input file

Main File

```
1 # $Header: /var/cvs/mbdyn/mbdyn-1.0/tests/forces/strext/socket/
  simplerotor/mapping/simplerotor2_mapping,v 1.7 2017/01/12 15:02:57
  masarati Exp $
2 #
3 # MBDyn (C) is a multibody analysis code.
4 # http://www.mbdyn.org
5 #
6 # Copyright (C) 1996-2017
7 #
8 # Pierangelo Masarati <masarati@aero.polimi.it>
9 # Paolo Mantegazza <mantegazza@aero.polimi.it>
10 #
11 # Dipartimento di Ingegneria Aerospaziale - Politecnico di Milano
12 # via La Masa, 34 - 20156 Milano, Italy
13 # http://www.aero.polimi.it
14 #
15 # Changing this copyright notice is forbidden.
16 #
17 # This program is free software; you can redistribute it and/or modify
18 # it under the terms of the GNU General Public License as published by
19 # the Free Software Foundation (version 2 of the License).
20 #
21 #
22 # This program is distributed in the hope that it will be useful,
23 # but WITHOUT ANY WARRANTY; without even the implied warranty of
24 # MERCHANTABILITY or FITNESS FOR A PARTICULAR PURPOSE. See the
25 # GNU General Public License for more details.
26 #
27 # You should have received a copy of the GNU General Public License
28 # along with this program; if not, write to the Free Software
29 # Foundation, Inc., 59 Temple Place, Suite 330, Boston, MA 02111-1307 USA
30 #
```

Appendix D. MBDyn input/output file example

```
31 # Author: Giuseppe Quaranta <quaranta@aero.polimi.it>
32
33
34 begin: data;
35   problem: initial value;
36 end: data;
37
38 set: real DT = 5e-4;
39 set: real INITIAL_TIME = 0.0;
40 set: real FINAL_TIME = 10.0;
41
42
43 begin: initial value;
44
45   initial time: INITIAL_TIME;
46   final time: FINAL_TIME;
47   time step: DT;
48 # set: const integer TIMESTEP = 1234;
49 # strategy: change, postponed, TIMESTEP; # changes the time step as
      specified by the drive caller labeled TIMESTEP, whose definition is
      postponed (this is simply a placeholder)
50
51   method: ms, .6;
52   nonlinear solver: newton raphson, modified, 5;
53   linear solver: umfpack, colamd, mt, 1;
54 # linear solver: naive, colamd;
55 # linear solver: umfpack;
56
57   tolerance: 1e-6;
58   max iterations: 1000;
59
60   derivatives coefficient: 1e-9;
61   derivatives tolerance: 1e-6;
62   derivatives max iterations: 100;
63
64   output: iterations;
65   output: residual;
66 end: initial value;
67
68 # number of beam3 elements
69 set: integer N = 10;
70
71 begin: control data;
72   structural nodes:
73     +1 # clamped node
74     +2*N # other nodes
75   ;
76   rigid bodies:
77     +2*N # mass of other nodes
78   ;
```

```

79 joints:
80     +1 # clamp
81     +2*N # other total joints on nodes to force 2D
82 ;
83 beams:
84     +N # the whole beam
85 ;
86 forces:
87     +1 # loads the beam
88     +1 # load on last node
89 ;
90 # file drivers:
91 # +1
92 # ;
93 end: control data;
94
95 # root reference
96 set: const integer ROOT = 1;
97 set: const real Xroot = 0.0;
98 set: const real Yroot = 0.0;
99 set: const real Zroot = 0.0;
100 reference: ROOT, Xroot, Yroot, Zroot, eye, null, null;
101
102
103 # material density [kg/m^3]
104 set: real rho = 100.;
105 # beam width (z direction)
106 set: real w = 4.e-3;
107 # beam height (y direction)
108 set: real h = 6.e-4;
109 # beam lenght (x direction)
110 set: real L = 0.04;
111 # lenght of half beam3 element
112 set: real dL = L/(2*N);
113
114 # mass of single chunck
115 set: real m = rho*w*h*dL;
116
117 # elastic properties
118 set: real E = 2.5e5;
119 set: real nu = 0.35;
120 set: real G = E/(2*(1+nu));
121 set: real A = w*h;
122 set: real Jz = 1./12.*w*h^3;
123 set: real Jy = 1./12.*h*w^3;
124 set: real Jp = Jy + Jz;
125 set: real damp = .01;
126
127 set: integer curr_node;
128

```

```

129 begin: nodes;
130   structural: ROOT, static,
131     reference, ROOT, null, # position
132     reference, ROOT, eye, # orientation
133     reference, ROOT, null, # initial velocity
134     reference, ROOT, null; # angular velocity
135
136   set: curr_node = 2;
137   include: "beam.nod";
138   set: curr_node = 4;
139   include: "beam.nod";
140   set: curr_node = 6;
141   include: "beam.nod";
142   set: curr_node = 8;
143   include: "beam.nod";
144   set: curr_node = 10;
145   include: "beam.nod";
146   set: curr_node = 12;
147   include: "beam.nod";
148   set: curr_node = 14;
149   include: "beam.nod";
150   set: curr_node = 16;
151   include: "beam.nod";
152   set: curr_node = 18;
153   include: "beam.nod";
154   set: curr_node = 20;
155   include: "beam.nod";
156 end: nodes;
157
158 #begin: drivers;
159 # set: const integer INPUT = 200;
160 # file: INPUT, stream,
161 #   stream drive name, "TS_DRV", # irrelevant but needed
162 #   create, yes,
163 #   path, "/tmp/mbdyn.ts.sock", # or use port
164 #   1; # one channel: the time step
165 # drive caller: TIMESTEP, file, INPUT, 1; # replace placeholder with file
166   driver
167 #end: drivers;
168
169
170 set: const integer BEAM_NNODES = 2*N+1;
171 set: real da = .005;
172 set: integer CURR_BEAM = 1;
173
174 begin: elements;
175   joint: 500+ROOT, clamp, ROOT, node, node;
176
177   set: curr_node = 2;

```

```

178 include: "beam.elm";
179 include: "joint.elm";
180 set: curr_node = 4;
181 include: "beam.elm";
182 include: "joint.elm";
183 set: curr_node = 6;
184 include: "beam.elm";
185 include: "joint.elm";
186 set: curr_node = 8;
187 include: "beam.elm";
188 include: "joint.elm";
189 set: curr_node = 10;
190 include: "beam.elm";
191 include: "joint.elm";
192 set: curr_node = 12;
193 include: "beam.elm";
194 include: "joint.elm";
195 set: curr_node = 14;
196 include: "beam.elm";
197 include: "joint.elm";
198 set: curr_node = 16;
199 include: "beam.elm";
200 include: "joint.elm";
201 set: curr_node = 18;
202 include: "beam.elm";
203 include: "joint.elm";
204 set: curr_node = 20;
205 include: "beam.elm";
206 include: "joint.elm";
207
208 force: CURR_BEAM, external structural mapping,
209 socket,
210 create, yes,
211 path, "/tmp/mbdyn.node.sock",
212 no signal,
213 coupling,
214 # loose,
215 tight,
216 #reference node, 1,
217 #orientation, euler 123,
218 #use reference node forces, yes,
219 points number, 3* BEAM_NNODES,
220 CURR_BEAM,
221 offset, null,
222 offset, 0., da, 0.,
223 offset, 0., 0., da,
224 CURR_BEAM + 1,
225 offset, null,
226 offset, 0., da, 0.,
227 offset, 0., 0., da,

```

```
228     CURR_BEAM + 2,
229         offset, null,
230         offset, 0.,da, 0.,
231         offset, 0., 0., da,
232     CURR_BEAM + 3,
233         offset, null,
234         offset, 0.,da, 0.,
235         offset, 0., 0., da,
236     CURR_BEAM + 4,
237         offset, null,
238         offset, 0.,da, 0.,
239         offset, 0., 0., da,
240     CURR_BEAM + 5,
241         offset, null,
242         offset, 0.,da, 0.,
243         offset, 0., 0., da,
244     CURR_BEAM + 6,
245         offset, null,
246         offset, 0.,da, 0.,
247         offset, 0., 0., da,
248     CURR_BEAM + 7,
249         offset, null,
250         offset, 0.,da, 0.,
251         offset, 0., 0., da,
252     CURR_BEAM + 8,
253         offset, null,
254         offset, 0.,da, 0.,
255         offset, 0., 0., da,
256     CURR_BEAM + 9,
257         offset, null,
258         offset, 0.,da, 0.,
259         offset, 0., 0., da,
260     CURR_BEAM + 10,
261         offset, null,
262         offset, 0.,da, 0.,
263         offset, 0., 0., da,
264     CURR_BEAM + 11,
265         offset, null,
266         offset, 0.,da, 0.,
267         offset, 0., 0., da,
268     CURR_BEAM + 12,
269         offset, null,
270         offset, 0.,da, 0.,
271         offset, 0., 0., da,
272     CURR_BEAM + 13,
273         offset, null,
274         offset, 0.,da, 0.,
275         offset, 0., 0., da,
276     CURR_BEAM + 14,
277         offset, null,
```

```
278      offset, 0,da, 0.,
279      offset, 0., 0., da,
280      CURR_BEAM + 15,
281      offset, null,
282      offset, 0,da, 0.,
283      offset, 0., 0., da,
284      CURR_BEAM + 16,
285      offset, null,
286      offset, 0,da, 0.,
287      offset, 0., 0., da,
288      CURR_BEAM + 17,
289      offset, null,
290      offset, 0,da, 0.,
291      offset, 0., 0., da,
292      CURR_BEAM + 18,
293      offset, null,
294      offset, 0,da, 0.,
295      offset, 0., 0., da,
296      CURR_BEAM + 19,
297      offset, null,
298      offset, 0,da, 0.,
299      offset, 0., 0., da,
300      CURR_BEAM + 20,
301      offset, null,
302      offset, 0,da, 0.,
303      offset, 0., 0., da,
304      # echo, "flap_points.dat", surface, "flap.dat", output, "flap_H.dat",
305      #           order, 2, basenode, 12, weight, 2, stop;
306      mapped points number, 204,
307      sparse mapping file, "flap_H.dat";
308
309 # constant absolute force in node 11
310     force: 2,absolute,
311     2*N + 1,
312     position, null,
313     0., 1., 0.,
314     # slope, initial time, final time / forever, initial value
315     ramp, .0, 0., 1., 0.;
316 end: elements;
317
318 # vim:ft=mbd
```

Listing D.1. MBDyn input file example

Beam nodes

```
1 # $Header: /var/cvs/mbdyn/mbdyn/mbdyn-web/documentation/examples/beam.nod,v
   1.2 2008/11/05 20:47:14 masarati Exp $
```

```

2
3 structural: curr_node, dynamic,
4   reference, ROOT, (curr_node - 1) * dL, 0.0, 0.0,
5   reference, ROOT, eye,
6   reference, ROOT, null,
7   reference, ROOT, null;
8
9 structural: curr_node + 1,dynamic,
10  reference, ROOT, curr_node * dL, 0.0, 0.0,
11  reference, ROOT, eye,
12  reference, ROOT, null,
13  reference, ROOT, null;

```

Listing D.2. MBDyn beam nodes

Beam elements and Bodies

```

1 # $Header: /var/cvs/mbdyn/mbdyn/mbdyn-web/documentation/examples/beam.elm,v
     1.2 2008/11/05 20:47:14 masarati Exp $
2
3 # body: BODY_LABEL, NODE_LABEL,
4 # mass
5 # reference node offset
6 # inertia tensor
7
8 body: 1000+ curr_node, curr_node,
9   m,
10  null,
11  diag, 1./12.*( $h^2+w^2$ )*m, 1./12.*( $dL^2+w^2$ )*m, 1./12.*( $dL^2+h^2$ )*m;
12
13 body: 1000+ curr_node + 1,curr_node,
14   m,
15  null,
16  diag, 1./12.*( $h^2+w^2$ )*m, 1./12.*( $dL^2+w^2$ )*m, 1./12.*( $dL^2+h^2$ )*m;
17
18
19 # beam 3 nodes
20 # NODE1_LABEL, offset
21 # NODE2_LABEL, offset
22 # NODE3_LABEL, offset
23 # orientation from node
24 # CONSTITUTIVE LAW: EA, GAy, GAz, GJ, EJy, EJz
25 #linear elastic generic, diag,
26 #EA, GAy, GAz, GJ, EJy, EJz,
27
28
29 beam3: 100+curr_node,
30   curr_node - 1,null,
31   curr_node, null,

```

```

32     curr_node + 1,null,
33     eye,
34     linear viscoelastic generic,
35         diag, E*A, G*A*5./6., G*A*5./6., G*Jp, E*Jy, E*Jz,
36             diag, damp*E*A, damp*G*A*5./6., damp*G*A*5./6., damp*G*Jp, damp*E*Jy,
37                 damp*E*Jz,
38 # proportional, damp,
39     same,
39     same;

```

Listing D.3. MBDyn beam elements

Joints

```

1 joint: 500+curr_node, total joint,
2     ROOT,
3     position, null,
4     position orientation, eye,
5     rotation orientation, eye,
6     curr_node,
7     position, null,
8     position orientation, eye,
9     rotation orientation, eye,
10
11    position constraint, 0,0,1,null,
12
13    orientation constraint, 1,1,0,null;
14
15 joint: 500+curr_node+1, total joint,
16     ROOT,
17     position, null,
18     position orientation, eye,
19     rotation orientation, eye,
20     curr_node+1,
21     position, null,
22     position orientation, eye,
23     rotation orientation, eye,
24
25    position constraint, 0,0,1,null,
26
27    orientation constraint, 1,1,0,null;

```

Listing D.4. MBDyn joints

D.2 MBDyn output file structure

.mov file

For each time step the file contains one row for each node whose output is required. The rows contain the following columns:

- 1: the label of the node
- 2–4: the three components of the position of the node
- 5–7: the three Euler angles that define the orientation of the node
- 8–10: the three components of the velocity of the node
- 11–13: the three components of the angular velocity of the node
- 14–16: the three components of the linear acceleration of the dynamic and modal nodes (optional)
- 17–19: the three components of the angular acceleration of the dynamic and modal nodes (optional)

All the quantities are expressed in the global frame, except for the relative frame type of dummy node, whose quantities are, by definition, in the relative frame.

.ine file

This output file refers only to dynamic nodes, and contains their inertia. For each time step, it contains information about the inertia of all the nodes whose output is required. Notice that more than one inertia body can be attached to one node; the information in this file refers to the sum of all the inertia related to the node. The rows contain the following columns:

- 1: the label of the node
- 2–4: item the three components of the momentum in the absolute reference frame
- 5–7: item the three components of the momenta moment in the absolute reference frame, with respect to the coordinates of the node, thus to a moving frame
- 8–10: the three components of the derivative of the momentum
- 11–13: the three components of the derivative of the momentum moment

.frc file

An external structural element writes one line for each connected node at each time step in this file. Each line contains the following columns:

- 1: the label of the element and that of the corresponding node; the format of this field is `element_label@node_label`
- 2–4: the three components of the force
- 5–7: the three components of the moment

If a reference node is defined, a special line is output for the reference node, containing the following columns:

- 1: the label of the element and that of the corresponding node; the format of this field is `element_label#node_label`

- 2–4: the three components of the force applied to the reference node, as received from the peer
- 5–7: the three components of the moment applied to the reference node, as received from the peer
- 8–10: the three components of the force that are actually applied to the reference node, in the global reference frame
- 11–13: the three components of the moment with respect to the reference node that are actually applied to the reference node, in the global reference frame
- 14–16: the three components of the force resulting from the combination of all nodal forces, in the global reference frame
- 17–19: the three components of the moment with respect to the reference node resulting from the combination of all nodal forces and moments, in the global reference frame

.act file

This type of file contains the output related to beam elements. The internal forces and couples are computed from the interpolated strains along the beam by means of the constitutive law, at the two evaluation points. For each time step and for each element, the format of the columns is:

- 1: the label of the beam
- 2–4: the three components of the force at the first evaluation point
- 5–7: the three components of the couple at the first evaluation point
- 8–10: the three components of the force at the second evaluation point
- 11–13: the three components of the couple at the second evaluation point

.jnt file

The output concerning joint elements is generally made of a standard part, plus some extra information depending on the type of joint, which, when available, is described along with the joint description. Here the standard part is described:

- 1: the label of the joint
- 2–4: the three components of the reaction force in a local reference
- 5–7: the three components of the reaction couple in a local frame
- 8–10: the three components of the reaction force in the global frame
- 11–13: the three components of the reaction couple, rotated into the global frame

for total joints:

- 14–16: the three components of the relative displacement in the reference frame of the element

- 17–19: the three components of the relative rotation vector in the reference frame of the element
- 20–22: the three components of the relative velocity in the reference frame of the element
- 23–25: the three components of the relative angular velocity in the reference frame of the element

Acronyms

FSI	Fluid-Structure Interaction
MBDyn	MultiBody Dynamics analysis software
preCICE	precise Code Interaction Coupling Environment
ALE	arbitrary Lagrangian-Eulerian
CFD	Computational Fluid Dynamics
CSM	Computational Solid Mechanics
NSE	Navier Stokes Equations
PDE	Partial Differential Equations
VWP	Virtual Work Principle
FEM	Finite Element Method
AME	added mass effect
FPI	fixed point iteration
IQN-ILS	interface quasi Newton with inverse Jacobian from a least squares model
RBF	Radial Basis Function
API	application programming interface
XML	extensible markup language
MPI	message passing interface
TCP/IP	Transmission Control Protocol/Internet Protocol

Bibliography

- [1] G. L. Ghiringhelli, P. Masarati, M. Morandini, and D. Muffo, “Integrated aeroservoelastic analysis of induced strain rotor blades,” *Mechanics of Advanced Materials and Structures*, vol. 15, no. 3-4, pp. 291–306, 2008.
- [2] B. Uekermann, H.-J. Bungartz, L. Cheung Yau, G. Chourdakis, and A. Rusch, “Official precice adapters for standard open-source solvers,” in *Proceedings of the 7th GACM Colloquium on Computational Mechanics for Young Scientists from Academia*, 2017.
- [3] R. C. Batra, *Elements of continuum mechanics*. Aiaa, 2006.
- [4] J. Cheng, G. Zhao, Z. Jia, Y. Chen, S. Wang, and W. Wen, “Sliding free lagrangian-eulerian finite element method,” in *International Conference on Computational Science*, 2006.
- [5] J. Donea, A. Huerta, J.-P. Ponthot, and A. Rodríguez-Ferran, “Arbitrary lagrangian–eulerian methods,” *Encyclopedia of Computational Mechanics Second Edition*, pp. 1–23, 2017.
- [6] J. T. Xing, “Chapter 3 - fundamentals of continuum mechanics,” in *Fluid-Solid Interaction Dynamics*, J. T. Xing, Ed. Academic Press, 2019, pp. 57 – 101. [Online]. Available: <http://www.sciencedirect.com/science/article/pii/B9780128193525000033>
- [7] S. Lipton, J. A. Evans, Y. Bazilevs, T. Elguedj, and T. J. Hughes, “Robustness of isogeometric structural discretizations under severe mesh distortion,” *Computer Methods in Applied Mechanics and Engineering*, vol. 199, no. 5-8, pp. 357–373, 2010.
- [8] A. Bertram, *Elasticity and plasticity of large deformations*. Springer, 2012.
- [9] A. De Boer, M. Van der Schoot, and H. Bijl, “Mesh deformation based on radial basis function interpolation,” *Computers & structures*, vol. 85, no. 11-14, pp. 784–795, 2007.
- [10] E. Ramm and W. Wall, “Fluid-structure interaction based upon a stabilized (ale) finite element method,” in *4th World Congress on Computational Mechanics: New Trends and Applications, CIMNE, Barcelona*, 1998, pp. 1–20.
- [11] L. Quartapelle and F. Auteri, *Fluidodinamica incomprimibile*. Casa editrice ambrosiana, 2013.
- [12] ——, *Fluidodinamica comprimibile*. Casa editrice ambrosiana, 2013.
- [13] S. B. Pope, “Turbulent flows,” 2001.
- [14] G. Galdi, *An introduction to the mathematical theory of the Navier-Stokes equations: Steady-state problems*. Springer Science & Business Media, 2011.

Bibliography

- [15] R. W. Ogden, *Non-linear elastic deformations*. Courier Corporation, 1997.
- [16] K. D. Hjelmstad, *Fundamentals of structural mechanics*. Springer Science & Business Media, 2007.
- [17] G. L. Ghiringhelli, P. Masarati, and P. Mantegazza, “Multibody implementation of finite volume c beams,” *AIAA journal*, vol. 38, no. 1, pp. 131–138, 2000.
- [18] G. Hou, J. Wang, and A. Layton, “Numerical methods for fluid-structure interaction—a review,” *Communications in Computational Physics*, vol. 12, no. 2, pp. 337–377, 2012.
- [19] H. Hanche-Olsen, “Buckingham’s pi-theorem,” *NTNU*: <http://www.math.ntnu.no/~hanche/notes/buckingham/buckingham-a4.pdf>, 2004.
- [20] J.-D. Hardtke, “On buckingham’s π -theorem,” *arXiv preprint arXiv:1912.08744*, 2019.
- [21] R. W. Fox, A. T. McDonald, and J. W. Mitchell, *Fox and McDonald’s introduction to fluid mechanics*. John Wiley & Sons, 2011.
- [22] S. Longo, *Analisi Dimensionale e Modellistica Fisica: Principi e applicazioni alle scienze ingegneristiche*. Springer Science & Business Media, 2011.
- [23] E. De Langre, *Fluides et solides*. Editions Ecole Polytechnique, 2001.
- [24] B. Hübner, E. Walhorn, and D. Dinkler, “A monolithic approach to fluid–structure interaction using space–time finite elements,” *Computer methods in applied mechanics and engineering*, vol. 193, no. 23-26, pp. 2087–2104, 2004.
- [25] P. Ryzhakov, R. Rossi, S. Idelsohn, and E. Oñate, “A monolithic lagrangian approach for fluid–structure interaction problems,” *Computational mechanics*, vol. 46, no. 6, pp. 883–899, 2010.
- [26] T. Richter, *Fluid-structure interactions: models, analysis and finite elements*. Springer, 2017, vol. 118.
- [27] J. Degroote, K.-J. Bathe, and J. Vierendeels, “Performance of a new partitioned procedure versus a monolithic procedure in fluid–structure interaction,” *Computers & Structures*, vol. 87, no. 11-12, pp. 793–801, 2009.
- [28] C. Farhat, K. G. Van der Zee, and P. Geuzaine, “Provably second-order time-accurate loosely-coupled solution algorithms for transient nonlinear computational aeroelasticity,” *Computer methods in applied mechanics and engineering*, vol. 195, no. 17-18, pp. 1973–2001, 2006.
- [29] M. Mehl, B. Uekermann, H. Bijl, D. Blom, B. Gatzhammer, and A. Van Zuijlen, “Parallel coupling numerics for partitioned fluid–structure interaction simulations,” *Computers & Mathematics with Applications*, vol. 71, no. 4, pp. 869–891, 2016.
- [30] E. H. van Brummelen, “Added mass effects of compressible and incompressible flows in fluid–structure interaction,” *Journal of Applied mechanics*, vol. 76, no. 2, 2009.
- [31] U. Küttler and W. A. Wall, “Fixed-point fluid–structure interaction solvers with dynamic relaxation,” *Computational mechanics*, vol. 43, no. 1, pp. 61–72, 2008.
- [32] B. M. Irons and R. C. Tuck, “A version of the aitken accelerator for computer iteration,” *International Journal for Numerical Methods in Engineering*, vol. 1, no. 3, pp. 275–277, 1969.

- [33] B. W. Uekermann, “Partitioned fluid-structure interaction on massively parallel systems,” Ph.D. dissertation, Technische Universität München, 2016.
- [34] R. Haelterman, J. Degroote, D. Van Heule, and J. Vierendeels, “The quasi-newton least squares method: a new and fast secant method analyzed for linear systems,” *SIAM Journal on numerical analysis*, vol. 47, no. 3, pp. 2347–2368, 2009.
- [35] B. Uekermann, H.-J. Bungartz, B. Gatzhammer, and M. Mehl, “A parallel, black-box coupling algorithm for fluid-structure interaction,” in *Proceedings of 5th International Conference on Computational Methods for Coupled Problems in Science and Engineering*, 2013, pp. 1–12.
- [36] R. Haelterman, A. E. Bogaers, K. Scheufele, B. Uekermann, and M. Mehl, “Improving the performance of the partitioned qn-ils procedure for fluid–structure interaction problems: Filtering,” *Computers & Structures*, vol. 171, pp. 9–17, 2016.
- [37] D. Blom, F. Lindner, M. Mehl, K. Scheufele, B. Uekermann, and A. van Zuijen, “A review on fast quasi-newton and accelerated fixed-point iterations for partitioned fluid–structure interaction simulation,” in *Advances in Computational Fluid-Structure Interaction and Flow Simulation*. Springer, 2016, pp. 257–269.
- [38] F. Lindner, M. Mehl, K. Scheufele, and B. Uekermann, “A comparison of various quasi-newton schemes for partitioned fluid-structure interaction,” in *Proceedings of 6th International Conference on Computational Methods for Coupled Problems in Science and Engineering, Venice*, 2015, pp. 1–12.
- [39] T. Kajishima and K. Taira, “Immersed boundary methods,” in *Computational Fluid Dynamics*. Springer, 2017, pp. 179–205.
- [40] R. van Loon, P. D. Anderson, F. N. van de Vosse, and S. J. Sherwin, “Comparison of various fluid–structure interaction methods for deformable bodies,” *Computers & structures*, vol. 85, no. 11-14, pp. 833–843, 2007.
- [41] C. Degand and C. Farhat, “A three-dimensional torsional spring analogy method for unstructured dynamic meshes,” *Computers & structures*, vol. 80, no. 3-4, pp. 305–316, 2002.
- [42] A. O. González, A. Vallier, and H. Nilsson, “Mesh motion alternatives in openfoam,” *PhD course in CFD with OpenSource software*, 2009.
- [43] H.-J. Bungartz, F. Lindner, B. Gatzhammer, M. Mehl, K. Scheufele, A. Shukaev, and B. Uekermann, “precice—a fully parallel library for multi-physics surface coupling,” *Computers & Fluids*, vol. 141, pp. 250–258, 2016.
- [44] F. Lindner, M. Mehl, and B. Uekermann, “Radial basis function interpolation for black-box multi-physics simulations,” 2017.
- [45] S. Chen, M. t. Wambsganss, and J. Jendrzejczyk, “Added mass and damping of a vibrating rod in confined viscous fluids,” in *asme*, 1976.
- [46] C. Conca, A. Osses, and J. Planchard, “Added mass and damping in fluid-structure interaction,” *Computer methods in applied mechanics and engineering*, vol. 146, no. 3-4, pp. 387–405, 1997.

- [47] J. Gauthier, A. Giroux, S. Etienne, and F. Gosselin, “A numerical method for the determination of flow-induced damping in hydroelectric turbines,” *Journal of Fluids and Structures*, vol. 69, pp. 341–354, 2017.
- [48] G. Ricciardi and E. Boccaccio, “Modelling of the flow induced stiffness of a pwr fuel assembly,” *Nuclear Engineering and Design*, vol. 282, pp. 8–14, 2015.
- [49] P. Causin, J.-F. Gerbeau, and F. Nobile, “Added-mass effect in the design of partitioned algorithms for fluid–structure problems,” *Computer methods in applied mechanics and engineering*, vol. 194, no. 42-44, pp. 4506–4527, 2005.
- [50] J. Degroote, P. Bruggeman, R. Haelterman, and J. Vierendeels, “Stability of a coupling technique for partitioned solvers in fsi applications,” *Computers & Structures*, vol. 86, no. 23-24, pp. 2224–2234, 2008.
- [51] T. Bodnár, G. P. Galdi, and Š. Nečasová, *Fluid-structure interaction and biomedical applications*. Springer, 2014, ch. 13.
- [52] C. Förster, W. A. Wall, and E. Ramm, “The artificial added mass effect in sequential staggered fluid-structure interaction algorithms,” in *ECCOMAS CFD 2006: Proceedings of the European Conference on Computational Fluid Dynamics, Egmond aan Zee, The Netherlands, September 5-8, 2006*. Delft University of Technology; European Community on Computational Methods . . ., 2006.
- [53] B. Gatzhammer, “Efficient and flexible partitioned simulation of fluid-structure interactions,” Ph.D. dissertation, Technische Universität München, 2014.
- [54] A. K. Shukaev, “A fully parallel process-to-process intercommunication technique for precice.” Master’s thesis, Technische Universitt München, Jun. 2015.
- [55] P. Masarati, M. Morandini, and P. Mantegazza, “An efficient formulation for general-purpose multibody/multiphysics analysis,” *Journal of Computational and Nonlinear Dynamics*, vol. 9, no. 4, 2014.
- [56] V. Giavotto, M. Borri, P. Mantegazza, G. Ghiringhelli, V. Carmaschi, G. Maffoli, and F. Mussi, “Anisotropic beam theory and applications,” *Computers & Structures*, vol. 16, no. 1-4, pp. 403–413, 1983.
- [57] D. H. Hodges, “Review of composite rotor blade modeling,” *AIAA journal*, vol. 28, no. 3, pp. 561–565, 1990.
- [58] T. Kim, A. M. Hansen, and K. Branner, “Development of an anisotropic beam finite element for composite wind turbine blades in multibody system,” *Renewable Energy*, vol. 59, pp. 172–183, 2013.
- [59] P. Masarati, “A formulation of kinematic constraints imposed by kinematic pairs using relative pose in vector form,” *Multibody System Dynamics*, vol. 29, no. 2, pp. 119–137, 2013.
- [60] S. Turek and J. Hron, “Proposal for numerical benchmarking of fluid-structure interaction between an elastic object and laminar incompressible flow,” in *Fluid-structure interaction*. Springer, 2006, pp. 371–385.
- [61] J.-H. Hong and N. Arai, “Fluid-structure interaction under the vortex lock-in regime,” in *Computational Fluid Dynamics 2000*. Springer, 2001, pp. 601–606.

- [62] C. Kassiotis, A. Ibrahimbegovic, R. Niekamp, and H. G. Matthies, “Nonlinear fluid–structure interaction problem. part i: implicit partitioned algorithm, nonlinear stability proof and validation examples,” *Computational Mechanics*, vol. 47, no. 3, pp. 305–323, 2011.
- [63] C. Wood, A. Gil, O. Hassan, and J. Bonet, “Partitioned block-gauss–seidel coupling for dynamic fluid–structure interaction,” *Computers & structures*, vol. 88, no. 23-24, pp. 1367–1382, 2010.
- [64] M. Olivier, J.-F. Morissette, and G. Dumas, “A fluid-structure interaction solver for nano-air-vehicle flapping wings,” in *19th AIAA Computational Fluid Dynamics*, 2009, p. 3676.
- [65] E. Walhorn, B. Hübner, and D. Dinkler, “Space-time finite elements for fluid-structure interaction,” in *PAMM: Proceedings in Applied Mathematics and Mechanics*, vol. 1, no. 1. Wiley Online Library, 2002, pp. 81–82.
- [66] H. G. Matthies and J. Steindorf, “Partitioned strong coupling algorithms for fluid–structure interaction,” *Computers & structures*, vol. 81, no. 8-11, pp. 805–812, 2003.
- [67] W. Dettmer and D. Perić, “A computational framework for fluid–rigid body interaction: finite element formulation and applications,” *Computer Methods in Applied Mechanics and Engineering*, vol. 195, no. 13-16, pp. 1633–1666, 2006.
- [68] C. Habchi, S. Russeil, D. Bougeard, J.-L. Harion, T. Lemenand, A. Ghanem, D. Della Valle, and H. Peerhossaini, “Partitioned solver for strongly coupled fluid–structure interaction,” *Computers & Fluids*, vol. 71, pp. 306–319, 2013.
- [69] B. Froehle and P.-O. Persson, “A high-order discontinuous galerkin method for fluid–structure interaction with efficient implicit–explicit time stepping,” *Journal of Computational Physics*, vol. 272, pp. 455–470, 2014.
- [70] S. Turek, J. Hron, and M. Razzaq, “Numerical benchmarking of fluid-structure interaction between elastic object and laminar incompressible *Universitätsbibliothek Dortmund*, 2010.
- [71] T. Richter and T. Wick, “On time discretizations of fluid-structure interactions,” in *Multiple Shooting and Time Domain Decomposition Methods*. Springer, 2015, pp. 377–400.
- [72] S. Gjertsen, “Development of a verified and validated computational framework for fluid–structure interaction: Investigating lifting operators and numerical stability,” Master’s thesis, 2017.
- [73] J. Degroote, R. Haelterman, S. Annerel, A. Swillens, P. Segers, and J. Vierendeels, “An interface quasi-newton algorithm for partitioned simulation of fluid-structure interaction,” in *International Workshop on Fluid-Structure Interaction. Theory, Numerics and Applications*. kassel university press GmbH, 2009, p. 55.
- [74] Z. Qin and J. Suckale, “Direct numerical simulations of gas–solid–liquid interactions in dilute fluids,” *International Journal of Multiphase Flow*, vol. 96, pp. 34–47, 2017.